

Measurement of the inclusive isolated prompt photon cross section in pp collisions at $\sqrt{s} = 7$ TeV with the ATLAS detector

G. Aad *et al.*^{*}

(The ATLAS Collaboration)
(Dated: November 26, 2024)

A measurement of the cross section for the inclusive production of isolated prompt photons in pp collisions at a centre-of-mass energy $\sqrt{s} = 7$ TeV is presented. The measurement covers the pseudorapidity ranges $|\eta^\gamma| < 1.37$ and $1.52 \leq |\eta^\gamma| < 1.81$ in the transverse energy range $15 \leq E_T^\gamma < 100$ GeV. The results are based on an integrated luminosity of 880 nb^{-1} , collected with the ATLAS detector at the Large Hadron Collider. Photon candidates are identified by combining information from the calorimeters and from the inner tracker. Residual background in the selected sample is estimated from data based on the observed distribution of the transverse isolation energy in a narrow cone around the photon candidate. The results are compared to predictions from next-to-leading order perturbative QCD calculations.

PACS numbers: 13.25.Hw, 12.15.Hh, 11.30.Er

I. INTRODUCTION

Prompt photon production at hadron colliders provides a handle for testing perturbative QCD (pQCD) predictions [1, 2]. Photons provide a colorless probe of quarks in the hard partonic interaction and the subsequent parton shower. Their production is directly sensitive to the gluon content of the proton through the $qg \rightarrow q\gamma$ process, which dominates at leading order (LO). The measurement of the prompt photon production cross section can thus be exploited to constrain the gluon density function [3, 4]. Furthermore, photon identification is important for many physics signatures, including searches for Higgs boson [5–7], graviton decays [8] to photon pairs, decays of excited fermions [9], and decays of pairs of supersymmetric particles characterized by the production of two energetic photons and large missing transverse energy [10–12].

Prompt photons include both “direct” photons, which take part in the hard scattering subprocess (mostly quark-gluon Compton scattering, $qg \rightarrow q\gamma$, or quark-antiquark annihilation, $q\bar{q} \rightarrow g\gamma$), and “fragmentation” photons, which are the result of the fragmentation of a high- p_T parton [13, 14]. In this analysis, an isolation criterion is applied based on the amount of transverse energy inside a cone of radius $R = \sqrt{(\eta - \eta^\gamma)^2 + (\phi - \phi^\gamma)^2} = 0.4$ centered around the photon direction in the pseudorapidity (η) and azimuthal angle (ϕ) plane [15]. After the isolation requirement is applied the relative contribution to the total cross section from fragmentation photons decreases, though it remains non-negligible especially at low transverse energies [14].

The isolation requirement also significantly reduces the main background of non-prompt photon candidates from decays of energetic π^0 and η mesons inside jets.

Early studies of prompt photon production were carried out at the ISR collider [16, 17]. Subsequent studies, for example [18–20], further established prompt photons as a useful probe of parton interactions. More recent measurements at hadron colliders were performed at the Tevatron, in $p\bar{p}$ collisions at a centre-of-mass energy $\sqrt{s} = 1.96$ TeV. The measurement by the D0 Collaboration [21] is based on 326 pb^{-1} and covers a pseudorapidity range $|\eta^\gamma| < 0.9$ and a transverse energy range $23 < E_T^\gamma < 300$ GeV, while the measurement by the CDF Collaboration [22] is based on 2.5 fb^{-1} and covers a pseudorapidity range $|\eta^\gamma| < 1.0$ and a transverse energy range $30 < E_T^\gamma < 400$ GeV. Both D0 and CDF measure an isolated prompt photon cross section in agreement with next-to-leading order (NLO) pQCD calculations, with a slight excess seen in the CDF data between 30 and 50 GeV. Measurements of the inclusive prompt photon production cross section have also been performed in ep collisions, both in photoproduction and deep inelastic scattering, by the H1 [23, 24] and ZEUS [25, 26] Collaborations. The most recent measurement of the inclusive isolated prompt photon production was done with 2.9 pb^{-1} at $\sqrt{s} = 7$ TeV by the CMS Collaboration [27]. That measurement, which covers $21 < E_T^\gamma < 300$ GeV and $|\eta^\gamma| < 1.45$, is in good agreement with NLO predictions for the full E_T^γ range.

This paper describes the extraction of a signal of isolated prompt photons using 880 nb^{-1} of data collected with the ATLAS detector at the Large Hadron Collider (LHC). A measurement of the production cross section in pp collisions at $\sqrt{s} = 7$ TeV is presented, in the pseudorapidity ranges $|\eta^\gamma| < 0.6$, $0.6 \leq |\eta^\gamma| < 1.37$ and $1.52 \leq |\eta^\gamma| < 1.81$, for photons with transverse energies

* Full author list given at the end of the article in Appendix C.

between 15 GeV and 100 GeV.

The paper is organized as follows. The detector is described in Section II, followed by a summary of the data and the simulated samples used in the measurement in Section III. Section IV introduces the theoretical predictions to which the measurement is compared. Section V describes the photon reconstruction and identification algorithms; their performance is given in Section VI. Section VII describes the methods used to estimate the residual background in the data and to extract the prompt photon signal, followed by a discussion of the data corrections for the cross section measurement in Section VIII. The sources of systematic uncertainties on the cross section measurement are discussed in Section IX. Section X contains the main experimental results and the comparison of the observed cross sections with the theoretical predictions, followed by the conclusions in Section XI.

II. THE ATLAS DETECTOR

The ATLAS detector is described in detail in Refs. [28] and [29]. For the measurement presented in this paper, the calorimeter, with mainly its electromagnetic section, and the inner detector are of particular relevance.

The inner detector consists of three subsystems: at small radial distance r from the beam axis ($50.5 < r < 150$ mm), pixel silicon detectors are arranged in three cylindrical layers in the barrel and in three disks in each end-cap; at intermediate radii ($299 < r < 560$ mm), double layers of single-sided silicon microstrip detectors are used, organized in four cylindrical layers in the barrel and nine disks in each end-cap; at larger radii ($563 < r < 1066$ mm), a straw tracker with transition radiation detection capabilities divided into one barrel section (with 73 layers of straws parallel to the beam line) and two end-caps (with 160 layers each of straws radial to the beam line) is used. These three systems are immersed in a 2 T axial magnetic field provided by a superconducting solenoid. The inner detector has full coverage in ϕ . The silicon pixel and microstrip subsystems cover the pseudorapidity range $|\eta| < 2.5$, while the transition radiation tracker (TRT) acceptance is limited to the range $|\eta| < 2.0$. The inner detector allows an accurate reconstruction of tracks from the primary proton-proton collision region, and also identifies tracks from secondary vertices, permitting the efficient reconstruction of photon conversions in the inner detector up to a radius of ≈ 80 cm.

The electromagnetic calorimeter is a lead-liquid argon (Pb-LAr) sampling calorimeter with an accordion geometry. It is divided into a barrel section, covering the pseudorapidity region $|\eta| < 1.475$, and two end-cap sections, covering the pseudorapidity regions $1.375 < |\eta| < 3.2$. It consists of three longitudinal layers. The first one, with a thickness between 3 and 5 radiation lengths, is segmented into high granularity strips in the η direction (width between 0.003 and 0.006 depending on η , with the

exception of the regions $1.4 < |\eta| < 1.5$ and $|\eta| > 2.4$), sufficient to provide an event-by-event discrimination between single photon showers and two overlapping showers coming from a π^0 decay. The second layer of the electromagnetic calorimeter, which collects most of the energy deposited in the calorimeter by the photon shower, has a thickness around 17 radiation lengths and a granularity of 0.025×0.025 in $\eta \times \phi$ (corresponding to one cell). A third layer, with thickness varying between 4 and 15 radiation lengths, is used to correct leakage beyond the calorimeter for high energy showers. In front of the accordion calorimeter a thin presampler layer, covering the pseudorapidity interval $|\eta| < 1.8$, is used to correct for energy loss before the calorimeter. The sampling term a of the energy resolution ($\sigma(E)/E \approx a/\sqrt{E}$ [GeV]) varies between 10% and 17% as a function of $|\eta|$ and is the largest contribution to the resolution up to about 200 GeV, where the global constant term, estimated to be 0.7% [30], starts to dominate.

The total amount of material before the first active layer of the electromagnetic calorimeter (including the presampler) varies between 2.5 and 6 radiation lengths as a function of pseudorapidity, excluding the transition region ($1.37 \leq |\eta| < 1.52$) between the barrel and the end-caps, where the material thickness increases to 11.5 radiation lengths. The central region ($|\eta| < 0.6$) has significantly less material than the outer barrel ($0.6 \leq |\eta| < 1.37$), which motivates the division of the barrel into two separate regions in pseudorapidity.

A hadronic sampling calorimeter is located beyond the electromagnetic calorimeter. It is made of steel and scintillating tiles in the barrel section ($|\eta| < 1.7$), with depth around 7.4 interaction lengths, and of two wheels of copper and liquid argon in each end-cap, with depth around 9 interaction lengths.

A three-level trigger system is used to select events containing photon candidates during data taking. The first level trigger (level-1) is hardware based: using a coarser cell granularity (0.1×0.1 in $\eta \times \phi$) than that of the electromagnetic calorimeter, it searches for electromagnetic clusters within a fixed window of size 0.2×0.2 and retains only those whose total transverse energy in two adjacent cells is above a programmable threshold. The second and third level triggers (collectively referred to as the “high-level” trigger) are implemented in software. The high-level trigger exploits the full granularity and precision of the calorimeter to refine the level-1 trigger selection, based on improved energy resolution and detailed information on energy deposition in the calorimeter cells.

III. COLLISION DATA AND SIMULATED SAMPLES

A. Collision Data

The measurement presented here is based on proton-proton collision data collected at a centre-of-mass energy

$\sqrt{s} = 7$ TeV between April and August 2010. Events in which the calorimeters or the inner detector are not fully operational, or show data quality problems, are excluded. Events are triggered using a single-photon high-level trigger with a nominal transverse energy threshold of 10 GeV, seeded by a level-1 trigger with nominal threshold equal to 5 GeV. The selection criteria applied by the trigger on shower shape variables computed from the energy profiles of the showers in the calorimeters are looser than the photon identification criteria applied in the offline analysis, and allow ATLAS to reach a plateau of constant efficiency close to 100% for true prompt photons with $E_T^\gamma > 15$ GeV and pseudorapidity $|\eta^\gamma| < 1.81$. In addition, samples of minimum-bias events, triggered by using two sets of scintillator counters located at $z = \pm 3.5$ m from the collision centre, are used to estimate the single-photon trigger efficiency. The total integrated luminosity of the sample passing data quality and trigger requirements amounts to (880 ± 100) nb $^{-1}$.

In order to reduce non-collision backgrounds, events are required to have at least one reconstructed primary vertex consistent with the average beam spot position and with at least three associated tracks. The efficiency of this requirement is expected to be greater than 99.9% in events containing a prompt photon with $E_T^\gamma > 15$ GeV and lying within the calorimeter acceptance. The total number of selected events in data after this requirement is 9.6 million. The remaining amount of non-collision background is estimated using control samples collected with dedicated, low threshold triggers that are activated in events where either no proton bunch or only one of the two beams crosses the interaction region. The estimated contribution to the final photon sample is less than 0.1% and is therefore neglected.

B. Simulated events

To study the characteristics of signal and background events, Monte Carlo (MC) samples are generated using PYTHIA 6.4.21 [31], a leading-order parton-shower MC generator, with the modified leading order MRST2007 [32] parton distribution functions (PDFs). It accounts for QED radiation emitted off quarks in the initial state (ISR) and in the final state (FSR). PYTHIA simulates the underlying event using the multiple-parton interaction model, and uses the Lund string model for hadronisation [33]. The event generator parameters are set according to the ATLAS MC09 tune [34], and the detector response is simulated using the GEANT4 program [35]. These samples are then reconstructed with the same algorithms used for data. More details on the event generation and simulation infrastructure are provided in Ref. [36]. For the study of systematic uncertainties related to the choice of the event generator and the parton shower model, alternative samples are also generated with HERWIG 6.5 [37]. This generator also uses LO pQCD matrix elements, but has a different parton

shower model (angle-ordered instead of p_T -ordered), a different hadronisation model (the cluster model) and a different underlying event model, which is generated using the JIMMY package [38] with multiple parton interactions enabled. The HERWIG event generation parameters are also set according to the MC09 tune.

To study the main background processes, simulated samples of all relevant 2→2 QCD hard subprocesses involving only partons are used. The prompt photon contribution arising from initial and final state radiation emitted off quarks is removed from these samples in studies of the background.

Two different simulated samples are employed to study the properties of the prompt photon signal. The first sample consists of leading-order γ -jet events, and contains primarily direct photons produced in the hard subprocesses $qg \rightarrow q\gamma$ and $q\bar{q} \rightarrow g\gamma$. The second signal sample includes ISR and FSR photons emitted off quarks in all 2→2 QCD processes involving only quarks and gluons in the hard scatter. This sample is used to study the contribution to the prompt photon signal by photons from fragmentation, or from radiative corrections to the direct process, that are less isolated than those from the LO direct processes.

Finally, a sample of $W \rightarrow e\nu$ simulated events is used for the efficiency and purity studies involving electrons from W decays.

IV. THEORETICAL PREDICTIONS

The expected isolated prompt photon production cross section as a function of the photon transverse energy E_T^γ is calculated with the JETPHOX Monte Carlo program [13], which implements a full NLO QCD calculation of both the direct and the fragmentation contributions to the total cross section. In the calculation performed for this measurement, the total transverse energy carried by the partons inside a cone of radius $R = 0.4$ in the $\eta - \phi$ space around the photon direction is required to be less than 4 GeV. The NLO photon fragmentation function [39] and the CTEQ 6.6 parton density functions [40] provided by the LHAPDF package [41] are used. The nominal renormalization (μ_R), factorization (μ_F) and fragmentation (μ_f) scales are set to the photon transverse energy E_T^γ . Varying the CTEQ PDFs within the 68% C.L. intervals causes the cross section to vary between 5% and 2% as E_T increases between 15 and 100 GeV. The variation of the three scales independently between 0.5 and 2.0 times the nominal scale changes the predicted cross section by 20% at low E_T and 10% at high E_T , while the variation of the isolation requirement between 2 and 6 GeV changes the predicted cross section by no more than 2%. The MSTW 2008 PDFs [42] are used as a cross-check of the choice of PDF. The central values obtained with the MSTW 2008 PDFs are between 3 and 5% higher than those predicted using the CTEQ 6.6 PDFs.

The NLO calculation provided by JETPHOX predicts a

cross section at parton level, which does not include effects of hadronisation nor the underlying event and pileup (*i.e.* multiple proton-proton interactions in the same bunch crossing). The non-perturbative effects on the cross section due to hadronisation are evaluated using the simulated PYTHIA and HERWIG signal samples described in Section III B, by evaluating the ratio of the cross section before and after hadronisation and underlying event simulation. The ratios are estimated to be within 1% (2%) of unity in PYTHIA (HERWIG) for all E_T and η regions under study. To account for the effect of the underlying event and pileup on the measured isolation energy, a correction to the photon transverse isolation energy measured in data is applied, using a procedure described in Section V C.

V. PHOTON RECONSTRUCTION, IDENTIFICATION AND ISOLATION

A. Photon reconstruction and preselection

Photon reconstruction is seeded by clusters in the electromagnetic calorimeter with transverse energies exceeding 2.5 GeV, measured in projective towers of 3×5 cells in $\eta \times \phi$ in the second layer of the calorimeter. An attempt is made to match these clusters with tracks that are reconstructed in the inner detector and extrapolated to the calorimeter. Clusters without matching tracks are directly classified as “unconverted” photon candidates. Clusters with matched tracks are considered as electron candidates. To recover photon conversions, clusters matched to pairs of tracks originating from reconstructed conversion vertices in the inner detector are considered as “converted” photon candidates. To increase the reconstruction efficiency of converted photons, conversion candidates where only one of the two tracks is reconstructed (and does not have any hit in the innermost layer of the pixel detector) are also retained [29, 30].

The final energy measurement, for both converted and unconverted photons, is made using only the calorimeter, with a cluster size that depends on the photon classification. In the barrel, a cluster corresponding to 3×5 ($\eta \times \phi$) cells in the second layer is used for unconverted photons, while a cluster of 3×7 ($\eta \times \phi$) cells is used for converted photon candidates (to compensate for the opening between the conversion products in the ϕ direction due to the magnetic field). In the end-cap, a cluster size of 5×5 is used for all candidates. A dedicated energy calibration [29] is then applied separately for converted and unconverted photon candidates to account for upstream energy loss and both lateral and longitudinal leakage.

Photon candidates with calibrated transverse energies (E_T^γ) above 15 GeV are retained for the successive analysis steps. To minimise the systematic uncertainties related to the efficiency measurement at this early stage of the experiment, the cluster barycenter in the second layer of the electromagnetic calorimeter is required to lie in the

pseudorapidity region $|\eta^\gamma| < 1.37$, or $1.52 \leq |\eta^\gamma| < 1.81$. Photon candidates with clusters containing cells overlapping with few problematic regions of the calorimeter readout are removed. After the above preselection, 1.3 million photon candidates remain in the data sample.

B. Photon identification

Shape variables computed from the lateral and longitudinal energy profiles of the shower in the calorimeters are used to discriminate signal from background. The exact definitions of the discriminating variables are provided in Appendix A. Two sets of selection criteria (denoted “loose” and “tight”) are defined, each based on independent requirements on several shape variables. The selection criteria do not depend on the photon candidate transverse energy, but vary as a function of the photon reconstructed pseudorapidity, to take into account variations in the total thickness of the upstream material and in the calorimeter geometry.

1. Loose identification criteria

A set of loose identification criteria for photons is defined based on independent requirements on three quantities:

- the leakage R_{had} in the first layer of the hadronic compartment beyond the electromagnetic cluster, defined as the ratio between the transverse energy deposited in the first layer of the hadronic calorimeter and the transverse energy of the photon candidate;
- the ratio R_η between the energy deposits in 3×7 and 7×7 cells in the second layer of the electromagnetic calorimeter;
- the RMS width w_2 of the energy distribution along η in the second layer of the electromagnetic calorimeter.

True prompt photons are expected to have small hadronic leakage (typically below 1–2%) and a narrower energy profile in the electromagnetic calorimeter, more concentrated in the core of the cluster, with respect to background photon candidates from jets.

The loose identification criteria on R_{had} , R_η and w_2 are identical for converted and unconverted candidates. They have been chosen, using simulated prompt photon events, in order to obtain a prompt photon efficiency, with respect to reconstruction, rising from 97% at $E_T^\gamma = 20$ GeV to above 99% for $E_T^\gamma > 40$ GeV for both converted and unconverted photons [30]. The number of photon candidates in data passing the preselection and loose photon identification criteria is 0.8 million.

2. Tight identification criteria

To further reject the background, the selection requirements on the quantities used in the loose identification are tightened. In addition, the transverse shape along the ϕ direction in the second layer (the variable R_ϕ , computed from the ratio between the energy deposits in 3×3 and 3×7 cells) and the shower shapes in the first layer of the calorimeter are examined. Several variables that discriminate single photon showers from overlapping nearby showers (in particular those which originate from neutral meson decays to photon pairs) are computed from the energy deposited in the first layer:

- the total RMS width $w_{s,\text{tot}}$ of the energy distribution along η ;
- the asymmetry E_{ratio} between the first and second maxima in the energy profile along η ;
- the energy difference ΔE between the second maximum and the minimum between the two maxima;
- the fraction F_{side} of the energy in seven strips centered (in η) around the first maximum that is not contained in the three core strips;
- the RMS width $w_{s,3}$ of the energy distribution computed with the three core strips.

The first variable rejects candidates with wide showers consistent with jets. The second and third variables provide rejection against cases where two showers give separated energy maxima in the first layer. The last two variables provide rejection against cases where two showers are merged in a wider maximum.

The tight selection criteria are optimised independently for unconverted and converted photons to account for the quite different developments of the showers in each case. They have been determined using samples of simulated signal and background events prior to data taking, aiming to obtain a average efficiency of 85% with respect to reconstruction for true prompt photons with transverse energies greater than 20 GeV [30]. About 0.2 million photon candidates are retained in the data sample after applying the tight identification requirements.

C. Photon transverse isolation energy

An experimental isolation requirement, based on the transverse energy deposited in the calorimeters in a cone around the photon candidate, is used in this measurement to identify isolated prompt photons and to further suppress the main background from π^0 (or other neutral hadrons decaying in two photons), where the π^0 is unlikely to carry the full original jet energy. The transverse isolation energy ($E_{\text{T}}^{\text{iso}}$) is computed using calorimeter cells from both the electromagnetic and hadronic calorimeters, in a cone of radius 0.4 in the $\eta - \phi$ space

around the photon candidate. The contributions from 5×7 electromagnetic calorimeter cells in the $\eta - \phi$ space around the photon barycenter are not included in the sum. The mean value of the small leakage of the photon energy outside this region, evaluated as a function of the photon transverse energy, is subtracted from the measured value of $E_{\text{T}}^{\text{iso}}$. The typical size of this correction is a few percent of the photon transverse energy. After this correction, $E_{\text{T}}^{\text{iso}}$ for truly isolated photons is nominally independent of the photon transverse energy.

In order to make the measurement of $E_{\text{T}}^{\text{iso}}$ directly comparable to parton-level theoretical predictions, such as those described in Section IV, $E_{\text{T}}^{\text{iso}}$ is further corrected by subtracting the estimated contributions from the underlying event and from pileup. This correction is computed on an event-by-event basis using a method suggested in Refs. [43] and [44]. Based on the standard seeds for jet reconstruction, which are noise-suppressed three-dimensional topological clusters [28], and for two different pseudorapidity regions ($|\eta| < 1.5$ and $1.5 < |\eta| < 3.0$), a k_T jet-finding algorithm [45, 46], implemented in FastJet [47], is used to reconstruct all jets without any explicit transverse momentum threshold. During reconstruction, each jet is assigned an area via a Voronoi tessellation [48] of the $\eta - \phi$ space. According to the algorithm, every point within a jet's assigned area is closer to that jet than any other jet. The transverse energy density for each jet is then computed from the ratio between the jet transverse energy and its area. The ambient transverse energy density for the event, from pileup and underlying event, is taken to be the median jet transverse energy density. Finally, this ambient transverse energy density is multiplied by the area of the isolation cone to compute the correction to $E_{\text{T}}^{\text{iso}}$.

The estimated ambient transverse energy fluctuates significantly event-by-event, reflecting the fluctuations in the underlying event and pileup activity in the data. The mean correction to the calorimeter transverse energy in a cone of radius $R = 0.4$ for an event with one pp interaction is around 440 MeV in events simulated with PYTHIA and 550 MeV in HERWIG. In the data, the mean correction is 540 MeV for events containing at least one photon candidate with $E_{\text{T}} > 15$ GeV and exactly one reconstructed primary vertex, and increases by an average of 170 MeV with each additional reconstructed primary vertex. The average number of reconstructed primary vertices for the sample under study is 1.56. The distribution of measured ambient transverse energy densities for photons passing the tight selection criteria is shown in Fig. 1. The impact of this correction on the measured cross section is discussed in Section IX B. For a consistent comparison of this measurement to a theoretical prediction which incorporates an underlying event model, the method described above should be applied to the generated final state in order to evaluate and apply the appropriate event-by-event corrections.

After the leakage and ambient-transverse-energy corrections, the $E_{\text{T}}^{\text{iso}}$ distribution for direct photons in sim-

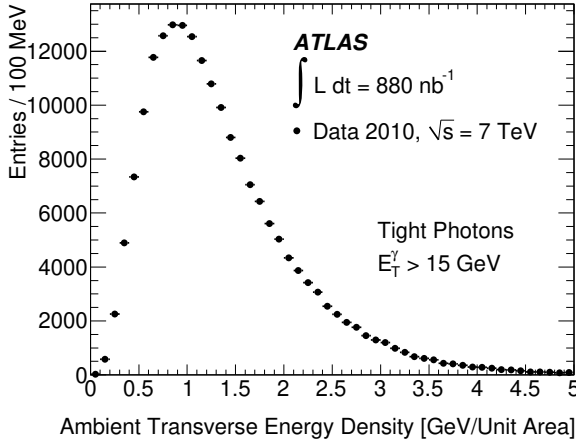


FIG. 1. The measured ambient transverse energy densities, using the jet-area method, for events with at least one tight photon. The ambient transverse energy contains contributions from both the underlying event and pileup. The broad distribution reflects the large event-to-event fluctuations.

ulated events is centered at zero, with an RMS width of around 1.5 GeV (which is dominated by electronic noise in the calorimeter). In the following, all photon candidates with $E_T^{\text{iso}} < 3$ GeV are considered to be experimentally isolated. This criterion can be related to a cut on the transverse isolation energy calculated at the parton level in PYTHIA, in order to mimic the isolation criterion implemented in JETPHOX. This parton-level isolation is the total transverse energy of all partons that lie inside a cone of radius $R = 0.4$ around the photon direction and originated from the same quark emitting the photon in either ISR or FSR. The efficiency of the experimental isolation cut at 3 GeV for photons radiated off partons in PYTHIA is close to the efficiency of a parton-level isolation cut at 4 GeV. This cut on the parton-level isolation is equivalent to the same cut on a particle-level isolation, which measures the transverse energy in a cone of radius $R = 0.4$ around the photon after hadronisation (with the underlying event removed). The experimental isolation criterion is expected to reject roughly 50% of background candidates with transverse energy greater than 15 GeV.

About 110 thousand photon candidates satisfy the tight identification criteria and have $E_T^{\text{iso}} < 3$ GeV: around 74 thousand are reconstructed as unconverted photons and 36 thousand as converted photons. The transverse energy distribution of these candidates is shown in Fig. 2. For comparison, the initial distribution of all photon candidates after the reconstruction and preselection is also shown.

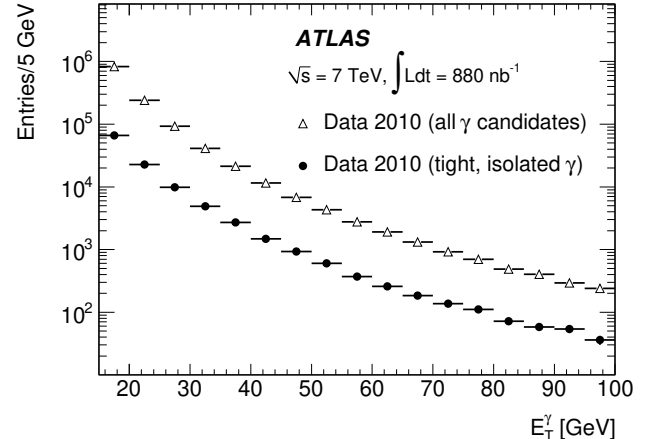


FIG. 2. Transverse energy distribution of photon candidates selected in data, after reconstruction and preselection (open triangles) and after requiring tight identification criteria and transverse isolation energy lower than 3 GeV (full circles). The photon candidates have pseudorapidity $|\eta^\gamma| < 1.37$ or $1.52 \leq |\eta^\gamma| < 1.81$.

VI. SIGNAL EFFICIENCY

A. Reconstruction and preselection efficiency

The reconstruction and preselection efficiency, $\varepsilon_{\text{reco}}$, is computed from simulated events as a function of the true photon transverse energy for each pseudorapidity interval under study. It is defined as the ratio between the number of true prompt photons that are reconstructed – after preselection – in a certain pseudorapidity interval and have reconstructed $E_T^{\text{iso}} < 3$ GeV, and the number of true photons with true pseudorapidity in the same pseudorapidity interval and with particle-level transverse isolation energy lower than 4 GeV. The efficiency of the requirement $E_T^{\gamma} > 15$ GeV for prompt photons of true transverse energy greater than the same threshold is taken into account in Section VIII.

The reconstruction and preselection efficiencies are calculated using a cross-section-weighted mixture of direct photons produced in simulated γ -jet events and of fragmentation photons produced in simulated dijet events. The uncertainty on the reconstruction efficiency due to the difference between the efficiency for direct and fragmentation photons, and the unknown ratio of the two in the final sample of selected signal photons, are taken into account as sources of systematic uncertainty in Section IX A.

The average reconstruction and preselection efficiency for isolated prompt photons with $|\eta_{\text{true}}^\gamma| < 1.37$ or $1.52 \leq |\eta_{\text{true}}^\gamma| < 1.81$ is around 82%; the 18% inefficiency is due to the inefficiency of the reconstruction algorithms at low photon transverse energy (a few %), to the inefficiency of the isolation requirement (5%) and to the acceptance loss from a few inoperative optical links of the calorimeter

readout [49].

B. Identification efficiency

The photon identification efficiency, ε_{ID} , is similarly computed as a function of transverse energy in each pseudorapidity region. It is defined as the efficiency for reconstructed (true) prompt photons, with measured $E_{\text{T}}^{\text{iso}} < 3$ GeV, to pass the tight photon identification criteria described in Section V B. The identification efficiency is determined from simulation after shifting the photon shower shapes by “shower-shape correction factors” that account for the observed average differences between the discriminating variables’ distributions in data and MC. The simulated sample used contains all the main QCD signal and background processes. The average differences between data and simulation are computed after applying the tight identification criteria. The typical size of the correction to the MC efficiency is -3% and is always between -5% and zero. The photon identification efficiency after all selection criteria (including isolation) are applied is shown in Fig. 3 and in Table I, including the systematic uncertainties that are discussed in more detail in Section IX A. The efficiencies for converted photons are, on average, 3-4% lower than for unconverted photons with the same pseudorapidity and transverse energy.

TABLE I. Isolated prompt photon identification efficiency in the intervals of the photon pseudorapidity and transverse energy under study.

E_{T}^{γ} [GeV]	Identification Efficiency [%]		
	$0.00 \leq \eta^{\gamma} < 0.60$	$0.60 \leq \eta^{\gamma} < 1.37$	$1.52 \leq \eta^{\gamma} < 1.81$
[15, 20)	63.3 ± 6.6	63.5 ± 6.9	72.2 ± 8.4
[20, 25)	73.5 ± 6.1	73.5 ± 6.8	81.6 ± 8.3
[25, 30)	80.2 ± 5.4	80.8 ± 5.7	86.7 ± 6.6
[30, 35)	85.5 ± 4.5	85.3 ± 4.8	90.4 ± 5.9
[35, 40)	85.2 ± 3.9	89.3 ± 4.3	92.3 ± 5.0
[40, 50)	89.2 ± 3.3	92.1 ± 3.6	93.5 ± 4.6
[50, 60)	91.3 ± 3.1	94.1 ± 2.8	93.9 ± 3.6
[60, 100)	92.2 ± 2.6	94.8 ± 2.6	94.2 ± 2.9

As a cross-check, photon identification efficiencies are also inferred from the efficiencies of the same identification criteria applied to electrons selected in data from W decays. Events containing $W \rightarrow e\nu$ candidates are selected by requiring: a missing transverse energy greater than 25 GeV (corresponding to the undetected neutrino); an opening azimuthal angle larger than 2.5 radians between the missing transverse energy vector and any energetic jets ($E_{\text{T}} > 15$ GeV) in the event; an electron transverse isolation energy in a cone of radius 0.4 in the $\eta - \phi$ space smaller than 0.3 times the electron transverse momentum; and a track, associated to the electron, that passes track-quality cuts, such as a large amount of transition radiation produced in the TRT and the presence

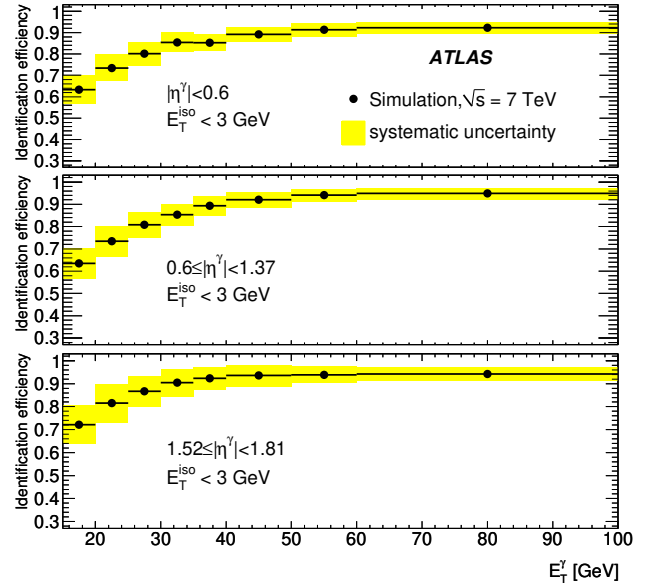


FIG. 3. Efficiency of the tight identification criteria as a function of the reconstructed photon transverse energy for prompt isolated photons. Systematic uncertainties are included.

of hits in the silicon trackers. These selection criteria, which do not rely on the shape of the electron shower in the calorimeter, are sufficient to select a $W \rightarrow e\nu$ sample with a purity greater than 95%. The identification efficiency of converted photons is taken from the efficiency for selected electrons to pass the tight photon selection criteria. This approximation is expected to hold to within 3% from studies of simulated samples of converted isolated prompt photons and of isolated electrons from W decays. For unconverted photons, the electrons in data are used to infer shower-shape corrections. These corrections are then applied to unconverted photons in simulation, in order to calculate the unconverted photon efficiency from Monte Carlo. The results from the electron extrapolation method are consistent with those from the simulation, with worse precision due to the limited statistics of the selected electron sample.

C. Trigger efficiency

The efficiency of the calorimeter trigger, relative to the photon reconstruction and identification selection, is defined as the probability for a true prompt photon, passing the tight photon identification criteria and with $E_{\text{T}}^{\text{iso}} < 3$ GeV, to pass the trigger selection. It is estimated in two steps. First, using a prescaled sample of minimum bias triggers, the efficiency of a lower threshold (≈ 3.5 GeV) level-1 calorimeter trigger is determined. The measured efficiency of this trigger is 100% for all photon candidates with reconstructed $E_{\text{T}}^{\gamma} > 15$ GeV passing tight identification criteria. Then, the efficiency of the high-level trig-

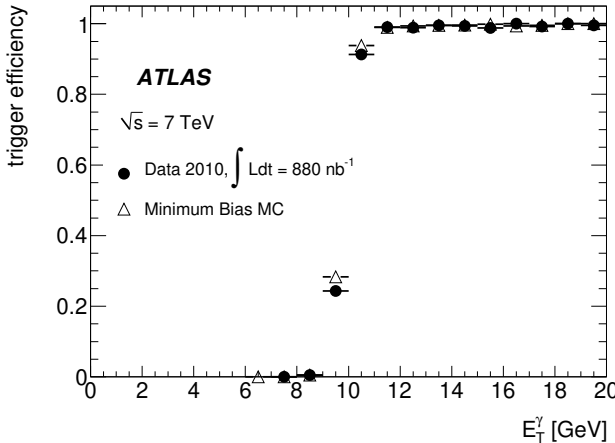


FIG. 4. Photon trigger efficiency, with respect to reconstructed isolated photon passing the tight identification criteria, as measured in data (circles) and simulated background events (triangles).

ger is measured using the sample of events that pass the level-1 calorimeter trigger with the 3.5 GeV threshold.

The trigger efficiency for reconstructed photon candidates passing tight selection criteria, isolated and with $E_T^\gamma > 15$ GeV is found to be $\varepsilon^{\text{trig}} = (99.5 \pm 0.5)\%$, constant within uncertainties over the full E_T and η ranges under study. The quoted uncertainty is obtained from the estimation of the possible bias introduced by using photon candidates from data, which are a mixture of signal and background photon candidates. Using Monte Carlo samples the absolute difference of the trigger efficiency for a pure signal sample and for a pure background sample is found to be smaller than 0.5% for isolated tight photon candidates with $E_T^\gamma > 15$ GeV.

A comparison between the high-level trigger efficiency in data and in the background predicted by the simulation is shown in Fig. 4.

VII. BACKGROUND SUBTRACTION AND SIGNAL YIELD DETERMINATION

A non-negligible residual contribution of background candidates is expected in the selected photon sample, even after the application of the tight identification and isolation requirements. Two methods are used to estimate the background contribution from data and to measure the prompt photon signal yield. The first one is used for the final cross section measurement, while the second one is used as a cross check of the former. All estimates are made separately for each region of pseudorapidity and transverse energy.

A. Isolation vs. identification sideband counting method

The first technique for measuring the prompt photon yield uses the number of photon candidates observed in the sidebands of a two-dimensional distribution to estimate the amount of background in the signal region. The two dimensions are defined by the transverse isolation energy E_T^{iso} on one axis, and the photon identification (γ_{ID}) of the photon candidate on the other axis. On the isolation axis, the signal region contains photon candidates with $E_T^{\text{iso}} < 3$ GeV, while the sideband contains photon candidates with $E_T^{\text{iso}} > 5$ GeV. On the other axis, photon candidates passing the tight identification criteria (“tight” candidates) belong to the γ_{ID} signal region, while those that fail the tight identification criteria but pass a background-enriching selection (“non-tight” candidates) belong to the γ_{ID} sideband. The non-tight selection requires photon candidates to fail at least one of a subset of the photon tight identification criteria, but to pass all criteria not in that subset. All the shower shape variables based on the energy measurement in the first layer of the electromagnetic calorimeter are used to define the background enriching selection, with the exception of $w_{s,\text{tot}}$, since it is found to be significantly correlated with the E_T^{iso} of background photon candidates, while the photon yield measurement relies on the assumption of negligible (or small) correlations between the transverse isolation energy and the shower shape quantities used to define the background enriching selection.

The signal region (region “A”) is therefore defined by photon candidates passing the tight photon identification criteria and having experimental $E_T^{\text{iso}} < 3$ GeV. The three background control regions consist of photon candidates either:

- passing the tight photon identification criteria but having experimental $E_T^{\text{iso}} > 5$ GeV (region “B”)
- having $E_T^{\text{iso}} < 3$ GeV and passing the background-enriching identification criteria (region “C”)
- having $E_T^{\text{iso}} > 5$ GeV and passing the background-enriching identification criteria (region “D”).

A sketch of the two dimensional plane and of the signal and background control region definitions is shown in Fig. 5.

The method assumes that the signal contamination in the three background control regions is small, and that the isolation profile in the non-tight regions is the same as that of the background in the tight regions. If these assumptions hold, then the number of background candidates in the signal region can be calculated by taking the ratio of candidates in the two non-tight regions (N_C/N_D), and multiplying it by the number of candidates in the tight, non-isolated region (N_B). The number of isolated prompt photons passing the tight identifica-

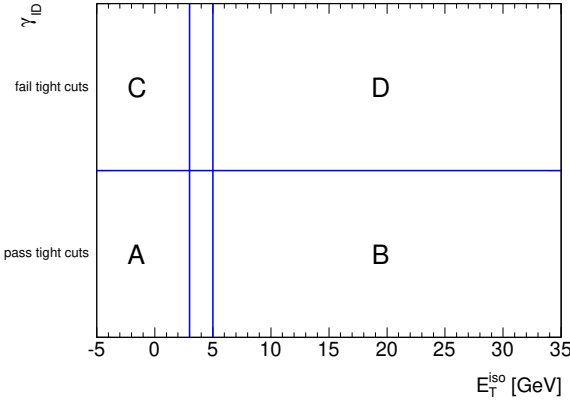


FIG. 5. Illustration of the two-dimensional plane, defined by means of the transverse isolation energy and a subset of the photon identification (ID) variables, used for estimating, from the observed yields in the three control regions (B, C, D), the background yield in the signal region (A).

tion criteria is therefore:

$$N_A^{\text{sig}} = N_A - N_B \frac{N_C}{N_D}, \quad (1)$$

where N_A is the observed number of photon candidates in the signal region.

The assumption that the signal contamination in the background control regions is small is checked using prompt photon MC samples. As the number of signal events in the background control regions is always positive and non-zero, corrections are applied to limit the effects on the final result. For this purpose, Eq. 1 is modified in the following way:

$$N_A^{\text{sig}} = N_A - (N_B - c_B N_A^{\text{sig}}) \frac{(N_C - c_C N_A^{\text{sig}})}{(N_D - c_D N_A^{\text{sig}})}, \quad (2)$$

where $c_K \equiv \frac{N_K^{\text{sig}}}{N_A^{\text{sig}}}$ (for $K \in \{B, C, D\}$) are the signal leakage fractions extracted from simulation. Typical values for c_B are between 3% and 17%, increasing with the photon candidate transverse energy; for c_C , between 2% and 14%, decreasing with E_T^γ . c_D is always less than 2%. The total effect of these corrections on the measured signal photon purities is typically less than 5%.

The isolated prompt photon fraction measured with this method, as a function of the photon reconstructed transverse energy, is shown in Fig. 6. The numbers of isolated prompt photon candidates measured in each pseudorapidity and transverse energy interval are also reported in Table II. The systematic uncertainties on the measured prompt photon yield and fraction in the selected sample are described in Section IX B.

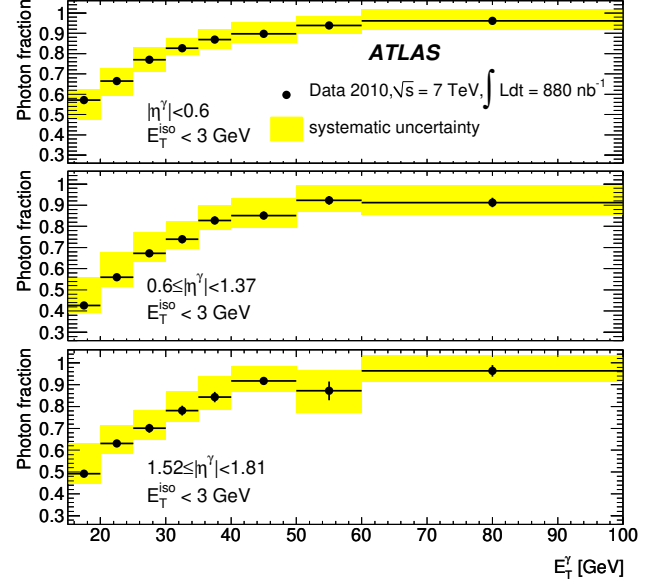


FIG. 6. Fraction of isolated prompt photons as a function of the photon transverse energy, as obtained with the two-dimensional sideband method.

B. Isolation template fit method

The second method relies on a binned maximum likelihood fit to the E_T^{iso} distribution of photon candidates selected in data which pass the tight identification criteria. The distribution is fit to the sum of a signal template and a background template, determined from control samples extracted from data. This is similar to the technique employed in [22], but relies less on simulation for signal and background templates. The signal template is determined from the E_T^{iso} distribution of electrons from W and Z decays, selected using the criteria described in [50]. Electrons from W decays are required to fulfill tight selection criteria on the shapes of their showers in the electromagnetic calorimeter and to pass track-quality requirements, including the presence of transition-radiation hits. They must also be accompanied by $E_T^{\text{miss}} > 25$ GeV, and the electron– E_T^{miss} system must have a transverse mass larger than 40 GeV. Electrons from Z decays are selected with looser criteria, but the pair must have an invariant mass close to the Z mass. A single signal template is constructed for each region in $|\eta|$, exploiting the independence of E_T^{iso} from the transverse energy of the object (after applying the corrections described in Section V C) to maximize the available statistics. A small bias is expected due to differences between the electron and photon E_T^{iso} distributions, especially in regions where there is significant material upstream of the calorimeter. A shift of the signal template is applied to the electron distributions extracted from data to compensate for the differences between electrons and photons seen in simulation. This shift, computed using simulated photon and

TABLE II. Observed number of isolated prompt photons in the photon transverse energy and pseudorapidity intervals under study. The first uncertainty is statistical, the second is the systematic uncertainty, evaluated as described in Section IX B.

Isolated prompt photon yield			
E_T^γ [GeV]	$0.00 \leq \eta^\gamma < 0.60$	$0.60 \leq \eta^\gamma < 1.37$	$1.52 \leq \eta^\gamma < 1.81$
[15, 20)	$(119 \pm 3 \pm 12) \times 10^2$	$(130 \pm 4 \pm 40) \times 10^2$	$(72 \pm 2 \pm 20) \times 10^2$
[20, 25)	$(501 \pm 12 \pm 47) \times 10^1$	$(578 \pm 18 \pm 125) \times 10^1$	$(304 \pm 10 \pm 40) \times 10^1$
[25, 30)	$(260 \pm 7 \pm 20) \times 10^1$	$(306 \pm 10 \pm 46) \times 10^1$	$(135 \pm 6 \pm 16) \times 10^1$
[30, 35)	$(146 \pm 5 \pm 9) \times 10^1$	$(160 \pm 6 \pm 19) \times 10^1$	$(73 \pm 4 \pm 8) \times 10^1$
[35, 40)	$(82 \pm 4 \pm 5) \times 10^1$	$(102 \pm 4 \pm 9) \times 10^1$	$(44 \pm 3 \pm 5) \times 10^1$
[40, 50)	$(77 \pm 3 \pm 5) \times 10^1$	$(98 \pm 4 \pm 9) \times 10^1$	$(38 \pm 2 \pm 3) \times 10^1$
[50, 60)	$(329 \pm 20 \pm 17) \times 10^0$	$(420 \pm 20 \pm 30) \times 10^0$	$(147 \pm 16 \pm 16) \times 10^0$
[60, 100)	$(329 \pm 20 \pm 19) \times 10^0$	$(370 \pm 20 \pm 30) \times 10^0$	$(154 \pm 12 \pm 12) \times 10^0$

electron samples, increases from 100 MeV to 600 MeV with increasing $|\eta^\gamma|$. The background template is extracted from data for each $(E_T, |\eta|)$ bin, using the same reverse-cuts procedure as in the two-dimensional sideband technique. A simulation-based correction, typically of the order of 3-4%, is applied to the final photon fraction to account for signal which leaks into the background template. The fit is performed in each region of $|\eta^\gamma|$ for the individual bins in transverse energy, and the signal yield and fraction are extracted. An example of such a fit is shown in Fig. 7. The results from this alternative technique are in good agreement with those from the simpler counting method described in the previous subsection, with differences typically smaller than 2% and within the systematic uncertainties that are uncorrelated between the two methods.

C. Electron background subtraction

The background of prompt electrons misidentified as photons needs also to be considered. The dominant electron production mechanisms are semileptonic hadron decays (mostly from hadrons containing heavy flavor quarks) and decays of electroweak bosons (the largest contribution being from W decays). Electrons from the former are often produced in association with jets, and have E_T^{iso} profiles similar to the dominant backgrounds from light mesons. They are therefore taken into account and subtracted using the two-dimensional sideband technique described in Section VII A. Conversely, electrons from W and Z decays have E_T^{iso} profiles that are similar to those of signal photons. The contribution of this background to the signal yield computed in Section VII A needs therefore to be removed before the final measurement of the cross section.

The fraction of electrons reconstructed as photon candidates is estimated from the data, as a function of the electron transverse energy and pseudorapidity, using a control sample of $Z \rightarrow e^+e^-$ decays. The average electron misidentification probability is around 8%. Using

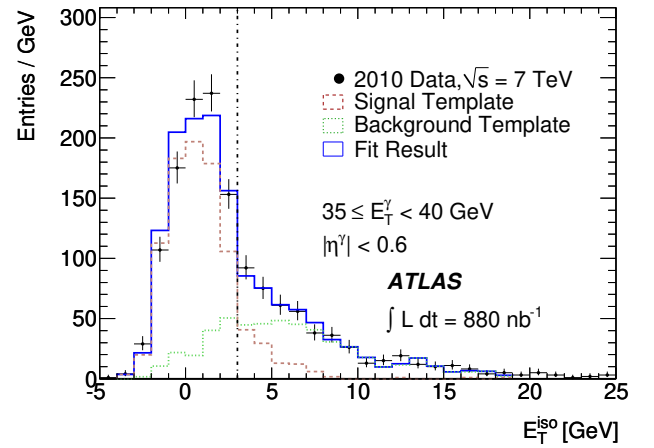


FIG. 7. Example of a fit to extract the fraction of prompt photons using the isolation template technique in the region $0 \leq |\eta| < 0.6$ and $35 \leq E_T^\gamma < 40$ GeV. The signal template is derived from electrons selected from W or Z decays, and is shown with a dashed line. The background template is derived from a background-enriched sample, and is represented by a dotted line. The estimated photon fraction is 0.85 and its statistical uncertainty is 0.01.

the $W \rightarrow e\nu$ and $Z \rightarrow ee$ cross section times branching ratio measured by ATLAS in pp collisions at $\sqrt{s} = 7$ TeV [50], the estimated fraction of photon candidates due to isolated electrons is found to be on average $\sim 0.5\%$, varying significantly with transverse energy. A maximum contamination of $(2.5\% \pm 0.8\%)$ is estimated for transverse energies between 40 and 50 GeV, due to the kinematic distribution of electrons from W and Z decays. The uncertainties on these estimates are less than 1% of the photon yield.

VIII. CROSS SECTION MEASUREMENT

The differential cross section is measured by computing:

$$\frac{d\sigma}{dE_T^\gamma} = \frac{N_{\text{yield}} U}{(\int \mathcal{L} dt) \Delta E_T^\gamma \varepsilon_{\text{trigger}} \varepsilon_{\text{reco}} \varepsilon_{\text{ID}}} . \quad (3)$$

The observed signal yield (N_{yield}) is divided by the widths of the E_T -intervals (ΔE_T^γ) and by the product of the photon identification efficiency (ε_{ID} , determined in Section VI B) and of the trigger efficiency relative to photon candidates passing the identification criteria ($\varepsilon_{\text{trigger}}$, determined in Section VI C). The spectrum obtained this way, which depends on the reconstructed transverse energy of the photon candidates, is then corrected for detector energy resolution and energy scale effects using bin-by-bin correction factors (the “unfolding coefficients” U) evaluated using simulated samples. The corrected spectrum, which is then a function of the true photon energy, is divided by the photon reconstruction efficiency $\varepsilon_{\text{reco}}$ (Section VI A) and by the integrated luminosity of the data sample, $\int \mathcal{L} dt$.

The unfolding coefficients are evaluated from the ratio of the true to reconstructed E_T distributions of photon candidates, using PYTHIA isolated prompt photon simulated samples. This procedure is justified by the small bin-to-bin migrations (typically of the order of a few %) that are expected, given the good electromagnetic calorimeter energy resolution compared to the width of the transverse energy intervals used in this analysis (between 5 and 40 GeV). The values of the unfolding coefficients are slightly higher than 1 and decrease as a function of E_T , approaching 1. They differ from 1 by less than 2% in the $|\eta^\gamma|$ region between 0.0 and 0.6, and by less than 5-7% in the other two $|\eta^\gamma|$ regions, where more material upstream of the electromagnetic calorimeter is present.

IX. SYSTEMATIC UNCERTAINTIES

Several sources of systematic uncertainties on the cross section are identified and evaluated as described in the following sections. The total systematic uncertainty is obtained by combining the various contributions, taking into account their correlations: uncorrelated uncertainties are summed in quadrature while a linear sum of correlated uncertainties is performed.

A. Reconstruction, identification, trigger efficiencies

The systematic uncertainty on the reconstruction efficiency from the experimental isolation requirement is evaluated from the prompt photon simulation varying the

value of the isolation criterion by the average difference (of the order of 500 MeV) observed for electrons between simulation and data control samples. It is 2.5% in the pseudorapidity regions covered by the barrel calorimeter and 4.5% in the end-caps.

The systematic uncertainty on the identification efficiency due to the photon shower-shape corrections is divided into two parts. The first term evaluates the impact of treating the differences between the distributions of the shower shape variables in data and simulation as an average shift. This uncertainty is evaluated in the following way:

- A modified description of the detector material is used to produce a second sample of simulated photon candidates. These candidates have different shower-shape distributions, due to the different amount of material upstream of and within the calorimeter. This alternative model contains an additional 10% of material in the inactive volumes of the inner detector and 10% of radiation length in front of the electromagnetic calorimeter. This model is estimated to represent a conservative upper limit of the additional detector material that is not accounted for by the nominal simulation.
- The correction procedure is applied to the nominal simulation to estimate the differences between the nominal and the alternative simulation. The shifts between the discriminating variable distributions in the nominal and the alternative simulation are evaluated, and are used to correct the shower shape variable distributions of the nominal simulation.
- The photon efficiency from the nominal simulation is recomputed after applying these corrections, and compared with the efficiency obtained from the alternative simulation.

The difference between the efficiency estimated from the nominal simulation (after applying the corrections) and the efficiency measured directly in the alternative sample (with no corrections) ranges from 3% at $E_T^\gamma \sim 20$ GeV to less than 1% at $E_T^\gamma \sim 80$ GeV.

The second part of the systematic uncertainty on the identification efficiency accounts for the uncertainty on the extracted shower-shape correction factors. The correction factors were extracted by comparing tight photons in data and simulation; to evaluate the uncertainty associated with this choice, the same correction factors are extracted using loose photons. The difference in the final efficiency when applying the tight corrections and the loose corrections is then taken as the uncertainty. This uncertainty drops from 4% to 1% with increasing E_T^γ .

Additional systematic uncertainties that may affect both the reconstruction and the identification efficiencies are evaluated simultaneously for the product of the two, to take into account possible correlations. These

sources of uncertainty include the amount of material upstream of the calorimeter; the impact of pile-up; the relative fraction of direct and fragmentation photons in data with respect to simulation; the misidentification of a converted photon as unconverted; the difference between the PYTHIA and HERWIG simulation models; the impact of a sporadic faulty calibration of the cell energies in the electromagnetic calorimeter; and the imperfect simulation of acceptance losses due to inoperative readout links in the calorimeter.

Of all the uncertainties which contribute to this measurement, the largest ones come from the uncertainty on the amount of material upstream of the calorimeter (absolute uncertainties ranging between 1% and 8% and are larger at low E_T^γ), and from the uncertainty on the identification efficiency due to the photon shower-shape corrections (the absolute uncertainties are in the range 1–5%, and are larger at low E_T^γ).

The uncertainty on the trigger efficiency, evaluated as described in Section VI C, is 0.5% and is nearly negligible compared to all other sources.

B. Signal yield estimates

The following sources of systematic uncertainties affecting the accuracy of the signal yield measurement using the two-dimensional sideband technique are considered.

1. Background isolation control region definition

The signal yield is evaluated after changing the isolation control region definition. The minimum value of E_T^{iso} required for candidates in the non-isolated control regions, which is set to 5 GeV in the nominal measurement, is changed to 4 and 6 GeV. This check is sensitive to uncertainties in the contribution of prompt photons from QED radiation from quarks: these photons are less isolated than those originating from the hard process. Alternative measurements are also performed where a maximum value of E_T^{iso} is set to 10 or 15 GeV for candidates in the non-isolated control regions, in order to reduce the correlation between the isolation variable and the shower shape distributions seen in simulated events for candidates belonging to the upper tail of the isolation distribution. The largest positive and negative variations of the signal yield with respect to the nominal result are taken as systematic uncertainties. The signal photon fraction changes by at most $\pm 2\%$ in all the transverse energy and pseudorapidity intervals.

2. Background photon identification control region definition

The measurement is repeated reversing the tight identification criteria on a number of strip variables ranging between two (only F_{side} and w_{s3}) and five (all the variables based on the first layer of the electromagnetic calorimeter). The largest positive and negative variations of the signal yield (with respect to the nominal result) from these three alternative measurements are taken as systematic uncertainties. The effect on the signal photon fraction decreases with increasing photon transverse energy, and is around 10% for E_T^γ between 15 and 20 GeV.

3. Signal leakage into the photon identification background control region

From the photon identification efficiency studies, an upper limit of 5% is set on the uncertainty on the fraction c_C of signal photons passing all the tight photon identification criteria except those used to define the photon identification control region. The signal yields in each $E_T^\gamma, |\eta^\gamma|$ interval are thus measured again after varying the estimated signal contamination in the photon identification control regions (c_C and c_D/c_B) by this uncertainty, and the difference with the nominal result is taken as a systematic uncertainty. The signal fraction variations are always below 6%.

4. Signal leakage into the isolation background control region

The fractions c_B and c_D of signal photons contaminating the isolation control regions depend on the relative amount of direct and fragmentation photons in the signal selected in a certain $E_T^\gamma, |\eta^\gamma|$ interval, since the latter are characterized by larger nearby activity, and therefore usually have slightly larger transverse isolation energies. In the nominal measurement, the values of c_B and c_D are computed with the relative fractions of direct and fragmentation photons predicted by PYTHIA. A systematic uncertainty is assigned by repeating the measurement after varying these fractions between 0% and 100%. The measured signal photon fraction varies by less than 5%.

5. Signal photon simulation

The signal yield is estimated using samples of prompt photons simulated with HERWIG instead of PYTHIA to determine the fraction of signal leaking into the three background control regions. The variations of the signal photon fractions in each $E_T^\gamma, |\eta^\gamma|$ interval are below 2%.

6. Correlations between the isolation and the photon identification variables for background candidates

Non-negligible correlations between the isolation variable and the photon identification quantities would affect Eq. 2: the true number of isolated tight prompt photon candidates would be

$$N_A^{\text{sig}} = N_A - R^{\text{bkg}}(N_B - c_B N_A^{\text{sig}}) \frac{(N_C - c_C N_A^{\text{sig}})}{(N_D - c_D N_A^{\text{sig}})} \quad (4)$$

where $R^{\text{bkg}} \equiv \frac{N_A^{\text{bkg}} N_D^{\text{bkg}}}{N_B^{\text{bkg}} N_C^{\text{bkg}}}$ would then be different from unity. The simulation of background events shows a small but non-negligible correlation between the isolation and the discriminating shower shape variables used to define the photon identification signal and background control regions. The signal yields are therefore recomputed with the formula in Eq. 4, using for R^{bkg} the value predicted by the PYTHIA background simulation, and compared with the nominal results. The effect is smaller than 0.6% in the $|\eta^\gamma| < 1.37$ intervals and around 3.6% for $1.52 \leq |\eta^\gamma| < 1.81$.

7. Transverse isolation energy corrections

The effects of the $E_{\text{T}}^{\text{iso}}$ correction for the underlying event on the estimated signal yield are also investigated. As this is an event-by-event correction, it cannot be unfolded from the observed cross section. The impact of this correction is evaluated by estimating the signal yield, with and without the correction applied, for events with only one reconstructed primary vertex (to eliminate any effects of pileup). The estimated signal yields using the uncorrected values of $E_{\text{T}}^{\text{iso}}$, normalized to the yields derived using the corrected values, show no trend in E_{T}^{γ} or η . Furthermore, the impact on the cross section of the event-by-event corrections is equivalent to that of an average correction of 540 MeV applied to the transverse isolation energies of all photon candidates. Similar studies in PYTHIA and HERWIG MC yield identical results.

C. Unfolding coefficients

The unfolding coefficients used to correct the measured cross section for E_{T} bin-by-bin migrations are computed using simulated samples. There are three sources of uncertainties on these coefficients.

1. Energy scale uncertainty

The uncertainty on the energy scale was estimated to be $\pm 3\%$ in test beam studies [51], and is confirmed to be below this value from the comparison of the $Z \rightarrow e^+e^-$

invariant mass peak in data and Monte Carlo. The unfolding coefficients are thus recomputed using simulated signal events where the true photon energy is shifted by $\pm 3\%$. The coefficients change by $\pm 10\%$. This uncertainty introduces a relative uncertainty of about 10% on the measured cross section which is fully correlated between the different E_{T}^{γ} intervals within each pseudorapidity range.

2. Energy resolution uncertainty

The uncertainty on the energy resolution may affect bin-by-bin migrations between adjacent E_{T} bins. Test beam studies indicate agreement between the sampling term of the resolution between data simulation within 20% relative. Furthermore, studies of the $Z \rightarrow e^+e^-$ invariant mass distribution in data indicate that the constant term of the calorimeter energy resolution is below 1.5% in the barrel and 3.0% in the end-cap (it is 0.7% in the simulation). The unfolding coefficients are thus recomputed after the reconstructed energy of simulated photons smearing to take into account a 20% relative increase of the sampling term and a constant term of 1.5% in the barrel and 3.0% in the end-cap. The resulting variation of the unfolding coefficients is always less than 1%. The uncertainty arising from non-gaussian tails of the energy resolution function is estimated by recomputing the coefficients using a prompt photon simulation where a significant amount of material is added to the detector model. The variations of the unfolding coefficients are smaller than 1% in all the pseudorapidity and transverse energy intervals under study.

3. Simulated photon transverse energy distribution

The unfolding coefficients, computed in E_{T}^{γ} intervals of non-negligible size, depend on the initial E_{T}^{γ} distribution predicted by PYTHIA. An alternative unfolding technique [52] is therefore used, which relies on the repeated application of Bayes' theorem to iteratively obtain an improved estimate of the unfolded spectrum. This technique relies less on the simulated original E_{T} distribution of the prompt photons. The differences between the cross-sections estimated using the bin-by-bin unfolding and the iterative Bayesian unfolding are within 2%, and are taken into account as an additional systematic uncertainty.

D. Luminosity

The integrated luminosity is determined for each run by measuring interaction rates using several ATLAS sub-detectors at small angles to the beam line, with the absolute calibration obtained from beam position scans [53]. The relative systematic uncertainty on the luminosity

measurement is estimated to be 11% and translates directly into a 11% relative uncertainty on the cross section.

X. RESULTS AND DISCUSSION

The measured inclusive isolated prompt photon production cross sections $d\sigma/dE_T^\gamma$ are shown in Fig. 8, 9, and 10. They are presented as a function of the photon transverse energy, for each of the three considered pseudorapidity intervals. They are also presented in tabular form in Appendix B. The measurements extend from $E_T^\gamma = 15$ GeV to $E_T^\gamma = 100$ GeV spanning almost three orders of magnitude. The data are compared to NLO pQCD calculations, obtained with the JETPHOX program as described in Section IV. The error bars on the data points represent the combination of the statistical and systematic uncertainties (summed in quadrature): systematic uncertainties dominate over the whole considered kinematic range. The contribution from the luminosity uncertainty (11%) is shown separately (dotted bands) as it represents a possible global offset of all the measurements. The total systematic uncertainties on the theoretical predictions are represented with a solid band. They are obtained by summing in quadrature the contributions from the scale uncertainty, the PDF uncertainty (at 68% C.L.) and the uncertainty associated with the choice of the parton-level isolation criterion. The same quantities are also shown, in the bottom panels of Fig. 8, 9, and 10, after having been normalized to the expected NLO pQCD cross sections.

In general, the theoretical predictions agree with the measured cross sections for $E_T^\gamma > 25$ GeV. For lower E_T^γ and in the two pseudorapidity regions $|\eta^\gamma| < 0.6$ and $0.6 \leq |\eta^\gamma| < 1.37$, the cross section predicted by JETPHOX is larger than that measured in data. Such low transverse energies at the LHC correspond to extremely small values of $x_T = 2E_T^\gamma/\sqrt{s}$, where NLO theoretical predictions are less accurate. In such a regime the appropriate values of the different scales are not clearly defined, and the uncertainties associated with these scales in the theoretical predictions may not be well modeled by simple variations of any one scale about the default value of E_T^γ [54]. As the low- E_T^γ region is where the fragmentation component has the most significant contribution to the total cross section, the total uncertainty associated with the NLO predictions at low E_T^γ may be underestimated.

XI. CONCLUSION

The inclusive isolated prompt photon production cross section in pp collisions at a center-of-mass energy $\sqrt{s} = 7$ TeV has been measured using 880 nb^{-1} of pp collision data collected by the ATLAS detector at the Large Hadron Collider.

The differential cross section has been measured as a function of the prompt photon transverse energy between

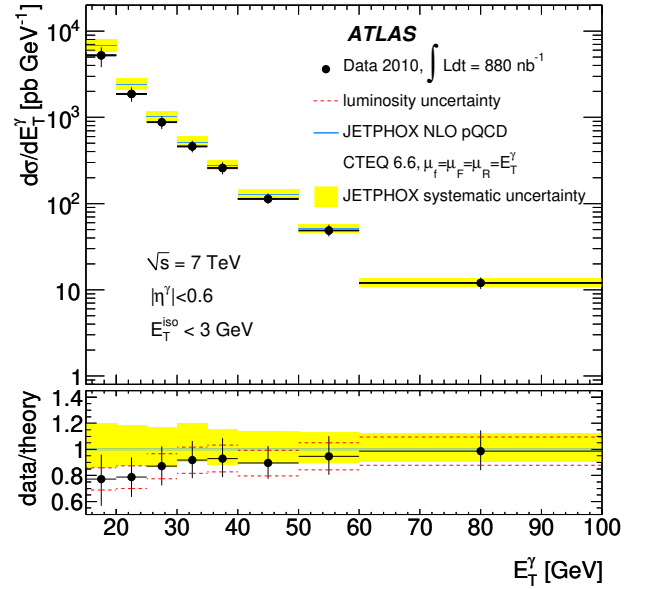


FIG. 8. Measured (dots) and expected (full line) inclusive prompt photon production cross sections, as a function of the photon transverse energies above 15 GeV and in the pseudorapidity range $|\eta^\gamma| < 0.6$. The bottom panel shows the ratio between the measurement and the theoretical prediction.

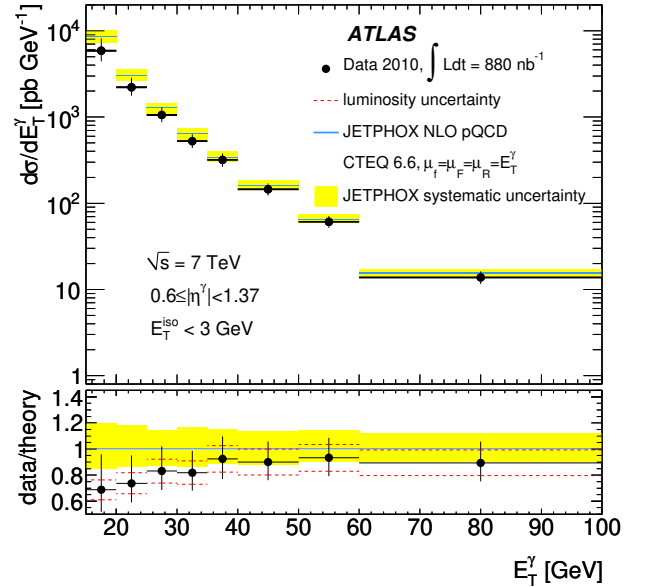


FIG. 9. Measured (dots) and expected (full line) inclusive prompt photon production cross sections, as a function of the photon transverse energies above 15 GeV and in the pseudorapidity range $0.6 \leq |\eta^\gamma| < 1.37$. The bottom panel shows the ratio between the measurement and the theoretical prediction.

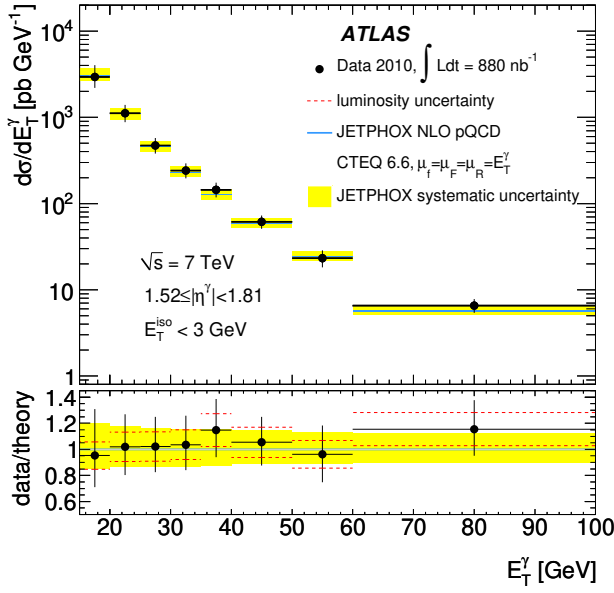


FIG. 10. Measured (dots) and expected (full line) inclusive prompt photon production cross sections, as a function of the photon transverse energies above 15 GeV and in the pseudorapidity range $1.52 \leq |\eta^\gamma| < 1.81$. The bottom panel shows the ratio between the measurement and the theoretical prediction.

15 and 100 GeV, in the three pseudorapidity intervals $|\eta^\gamma| < 0.6$, $0.6 \leq |\eta^\gamma| < 1.37$ and $1.52 \leq |\eta^\gamma| < 1.81$, estimating the background from the selected photon sample and using the photon identification efficiency measurement described in this paper. The photon identification using the fine granularity of the calorimeters. A photon isolation criterion is used, after an *in situ* subtraction of the effects of the underlying event that may also be applied to theoretical predictions.

The observed cross sections rapidly decrease as a function of the increasing photon transverse energy, spanning almost three orders of magnitude. The precision of the measurement is limited by its systematic uncertainty, which receives important contributions from the energy scale uncertainty, the luminosity, the photon identification efficiency, and the uncertainty on the residual background contamination in the selected photon sample.

The NLO pQCD predictions agree with the observed cross sections for transverse energies greater than 25 GeV, while for transverse energies below 25 GeV the cross sections predicted by JETPHOX are higher than measured. However, the precision of this comparison below 25 GeV is limited by large systematic uncertainties on the mea-

surement and on the theoretical predictions at such low values of $x_T = 2E_T^\gamma/\sqrt{s}$.

The measured prompt photon production cross section is more than a factor of thirty larger than that measured at the Tevatron, and a factor of 10^4 larger than for photo-production at HERA, assuming a similar kinematic range in transverse energy and pseudorapidity. This will allow the extension of the measurement up to energies in the TeV range after only a few years of data taking at the LHC.

XII. ACKNOWLEDGEMENTS

We wish to thank CERN for the efficient commissioning and operation of the LHC during this initial high-energy data-taking period as well as the support staff from our institutions without whom ATLAS could not be operated efficiently.

We acknowledge the support of ANPCyT, Argentina; YerPhI, Armenia; ARC, Australia; BMWF, Austria; ANAS, Azerbaijan; SSTC, Belarus; CNPq and FAPESP, Brazil; NSERC, NRC and CFI, Canada; CERN; CONICYT, Chile; CAS, MOST and NSFC, China; COLCIENCIAS, Colombia; MSMT CR, MPO CR and VSC CR, Czech Republic; DNRF, DNSRC and Lundbeck Foundation, Denmark; ARTEMIS, European Union; IN2P3-CNRS, CEA-DSM/IRFU, France; GNAS, Georgia; BMBF, DFG, HGF, MPG and AvH Foundation, Germany; GSRT, Greece; ISF, MINERVA, GIF, DIP and Benoziyo Center, Israel; INFN, Italy; MEXT and JSPS, Japan; CNRST, Morocco; FOM and NWO, Netherlands; RCN, Norway; MNiSW, Poland; GRICES and FCT, Portugal; MERYS (MECTS), Romania; MES of Russia and ROSATOM, Russian Federation; JINR; MSTD, Serbia; MSSR, Slovakia; ARRS and MVZT, Slovenia; DST/NRF, South Africa; MICINN, Spain; SRC and Wallenberg Foundation, Sweden; SER, SNSF and Cantons of Bern and Geneva, Switzerland; NSC, Taiwan; TAEK, Turkey; STFC, the Royal Society and Leverhulme Trust, United Kingdom; DOE and NSF, United States of America.

The crucial computing support from all WLCG partners is acknowledged gratefully, in particular from CERN and the ATLAS Tier-1 facilities at TRIUMF (Canada), NDGF (Denmark, Norway, Sweden), CC-IN2P3 (France), KIT/GridKA (Germany), INFN-CNAF (Italy), NL-T1 (Netherlands), PIC (Spain), ASGC (Taiwan), RAL (UK) and BNL (USA) and in the Tier-2 facilities worldwide.

[1] A. L. S. Angelis *et al.* (CERN-Columbia-Oxford-Rockefeller), *Phys. Lett.* **B94**, 106 (1980).

[2] P. Aurenche, R. Baier, M. Fontannaz, and D. Schiff, *Nucl. Phys.* **B297**, 661 (1988).

- [3] T. Akesson *et al.* (Axial Field Spectrometer), *Z. Phys. C***34**, 293 (1987).
- [4] P. Aurenche, R. Baier, M. Fontannaz, J. F. Owens, and M. Werlen, *Phys. Rev. D***39**, 3275 (1989).
- [5] P. W. Higgs, *Phys. Lett. A***12**, 132 (1964).
- [6] F. Englert and R. Brout, *Phys. Rev. Lett. A***13**, 321 (1964).
- [7] G. S. Guralnik, C. R. Hagen, and T. W. B. Kibble, *Phys. Rev. Lett. A***13**, 585 (1964).
- [8] L. Randall and R. Sundrum, *Phys. Rev. Lett. A***83**, 3370 (1999).
- [9] S. Weinberg, *Phys. Rev. D***19**, 1277 (1979).
- [10] M. Dine, W. Fischler, and M. Srednicki, *Nucl. Phys. B***189**, 575 (1981).
- [11] S. Dimopoulos and S. Raby, *Nucl. Phys. B***192**, 353 (1981).
- [12] C. R. Nappi and B. A. Ovrut, *Phys. Lett. B***113**, 175 (1982).
- [13] S. Catani *et al.*, *JHEP* **05**, 028 (2002).
- [14] P. Aurenche *et al.*, *Phys. Rev. D***73**, 094007 (2006).
- [15] The ATLAS reference system is a Cartesian right-handed coordinate system, with the nominal collision point at the origin. The anticlockwise beam direction defines the positive z -axis, while the positive x -axis is defined as pointing from the collision point to the centre of the LHC ring and the positive y -axis points upwards. The azimuthal angle ϕ is measured around the beam axis, and the polar angle θ is measured with respect to the z -axis. Pseudorapidity is defined as $\eta = -\ln \tan(\theta/2)$.
- [16] E. Anassontzis *et al.*, *Z. Phys. C***13**, 277 (1982).
- [17] A. L. S. Angelis *et al.* (CMOR), *Nucl. Phys. B***327**, 541 (1989).
- [18] J. A. Appel *et al.* (UA2), *Phys. Lett. B***176**, 239 (1986).
- [19] C. Albajar *et al.* (UA1), *Phys. Lett. B***209**, 385 (1988).
- [20] M. Werlen *et al.* (UA6), *Phys. Lett. B***452**, 201 (1999).
- [21] V. M. Abazov *et al.* (D0), *Phys. Lett. B***639**, 151 (2006).
- [22] T. Aaltonen *et al.* (CDF), *Phys. Rev. D***80**, 111106(R) (2009).
- [23] D. Aaron *et al.* (H1), *Eur. Phys. J. C***66**, 17 (2010).
- [24] F. D. Aaron *et al.* (H1), *Eur. Phys. J. C***54**, 371 (2008).
- [25] J. Breitweg *et al.* (ZEUS), *Phys. Lett. B***472**, 175 (2000).
- [26] S. Chekanov *et al.* (ZEUS), *Phys. Lett. B***687**, 16 (2010).
- [27] CMS Collaboration(2010), arXiv:1012.0799 [hep-ex].
- [28] G. Aad *et al.* (ATLAS), *JINST* **3**, S08003 (2008).
- [29] G. Aad *et al.* (ATLAS) arXiv:0901.0512.
- [30] ATLAS Collaboration, ATLAS-CONF-2010-005(2010), <http://cdsweb.cern.ch/record/1273197>.
- [31] T. Sjöstrand *et al.*, *Computer Phys. Commun.* **135**, 238 (2001).
- [32] A. Sherstnev and R. S. Thorne, *Eur. Phys. J. C***55**, 553 (2008).
- [33] B. Andersson, G. Gustafson, G. Ingelman, and T. Sjöstrand, *Phys. Rept.* **97**, 31 (1983).
- [34] G. Aad *et al.* (ATLAS), ATL-PHYS-PUB-2010-002(2010), <http://cdsweb.cern.ch/record/1247375>.
- [35] S. Agostinelli *et al.* (GEANT4), *Nucl. Instrum. Methods A***506**, 250 (2003).
- [36] G. Aad *et al.* (ATLAS), *Eur. Phys. J. C***70**, 823 (2010).
- [37] G. Corcella *et al.*, *JHEP* **01**, 010 (2001).
- [38] J. M. Butterworth, J. R. Forshaw, and M. H. Seymour, *Z. Phys. C***72**, 637 (1996).
- [39] L. Bourhis, M. Fontannaz, J. P. Guillet, and M. Werlen, *Eur. Phys. J. C***19**, 89 (2001).
- [40] J. Pumplin *et al.*, *JHEP* **07**, 012 (2002).
- [41] R. M. Whalley, D. Bourilkov, and R. Group arXiv:hep-ph/0508110.
- [42] A. D. Martin, W. J. Stirling, R. S. Thorne, and G. Watt, *Eur. Phys. J. C***63**, 189 (2009).
- [43] M. Cacciari, G. P. Salam, and G. Soyez, *JHEP* **04**, 005 (2008).
- [44] M. Cacciari, G. P. Salam, and S. Sapeta, *JHEP* **04**, 065 (2010).
- [45] S. D. Ellis and D. E. Soper, *Phys. Rev. D***48**, 3160 (1993).
- [46] S. Catani, Y. L. Dokshitzer, M. H. Seymour, and B. R. Webber, *Nucl. Phys. B***406**, 187 (1993).
- [47] M. Cacciari and G. P. Salam, *Phys. Lett. B***641**, 57 (2006).
- [48] G. Voronoi, *Journal für die Reine und Angewandte Mathematik* **133**, 97 (1907).
- [49] This inefficiency will be recovered in future data collected by ATLAS, as the faulty optical transmitters will be replaced during the LHC shutdown at the end of the 2010 run.
- [50] G. Aad *et al.* (ATLAS) accepted for publication by JHEP, arXiv:1010.2130.
- [51] M. Alekxa *et al.*, ATL-LARG-PUB-2006-003(2006), <http://cdsweb.cern.ch/record/942528>.
- [52] G. D'Agostini, *Nucl. Instrum. Methods A***362**, 487 (1995).
- [53] ATLAS Collaboration, ATLAS-CONF-2010-060(2010), <http://cdsweb.cern.ch/record/1281333>.
- [54] J. P. Guillet and E. Pilon, private communication (2010).

Appendix A: Definition of photon identification discriminating variables

In this Appendix, the quantities used in the selection of photon candidates, based on the reconstructed energy deposits in the ATLAS calorimeters, are summarized.

• Leakage in the hadronic calorimeter

The following discriminating variable is defined, based on the energy deposited in the hadronic calorimeter:

– Normalized hadronic leakage

$$R_{\text{had}} = \frac{E_{\text{T}}^{\text{had}}}{E_{\text{T}}} \quad (\text{A1})$$

is the total transverse energy $E_{\text{T}}^{\text{had}}$ deposited in the hadronic calorimeter, normalized to the total transverse energy E_{T} of the photon candidate.

In the $|\eta|$ interval between 0.8 and 1.37 the energy deposited in the whole hadronic calorimeter is used, while in the other pseudorapidity intervals only the leakage in the first layer of the hadronic calorimeter is used.

• Variables using the second (“middle”) layer of the electromagnetic calorimeter

The discriminating variables based on the energy deposited in the second layer of the electromagnetic calorimeter are the following:

– Middle η energy ratio

$$R_\eta = \frac{E_{3 \times 7}^{S2}}{E_{7 \times 7}^{S2}} \quad (\text{A2})$$

is the ratio between the sum $E_{3 \times 7}^{S2}$ of the energies of the second layer cells of the electromagnetic calorimeter contained in a 3×7 rectangle in $\eta \times \phi$ (measured in cell units), and the sum $E_{7 \times 7}^{S2}$ of the energies in a 7×7 rectangle, both centered around the cluster seed.

– Middle ϕ energy ratio

$$R_\phi = \frac{E_{3 \times 3}^{S2}}{E_{3 \times 7}^{S2}} \quad (\text{A3})$$

is defined similarly to R_η . R_ϕ behaves very differently for unconverted and converted photons, since the electrons and positrons generated by the latter bend in different directions in ϕ because of the solenoid magnetic field, producing larger showers in the ϕ direction than the unconverted photons.

– Middle lateral width

$$w_2 = \sqrt{\frac{\sum E_i \eta_i^2}{\sum E_i} - \left(\frac{\sum E_i \eta_i}{\sum E_i} \right)^2} \quad (\text{A4})$$

measures the shower lateral width in the second layer of the electromagnetic calorimeter, using all cells in a window $\eta \times \phi = 3 \times 5$ measured in cell units.

- Variables using the first (“front”) layer of the electromagnetic calorimeter

The discriminating variables based on the energy deposited in the first layer of the electromagnetic calorimeter are the following:

– Front side energy ratio

$$F_{\text{side}} = \frac{E(\pm 3) - E(\pm 1)}{E(\pm 1)} \quad (\text{A5})$$

measures the lateral containment of the shower, along the η direction. $E(\pm n)$ is the energy in the $\pm n$ strip cells around the one with the largest energy.

– Front lateral width (3 strips)

$$w_{s,3} = \sqrt{\frac{\sum E_i (i - i_{\max})^2}{\sum E_i}} \quad (\text{A6})$$

measures the shower width along η in the first layer of the electromagnetic calorimeter, using two strip cells around the maximal energy deposit. The index i is the strip identification number, i_{\max} identifies the strip cells with the greatest energy, E_i is the energy deposit in each strip cell.

– Front lateral width (total)

$w_{s,\text{tot}}$ measures the shower width along η in the first layer of the electromagnetic calorimeter using all cells in a window $\Delta\eta \times \Delta\phi = 0.0625 \times 0.2$, corresponding approximately to 20×2 strip cells in $\eta \times \phi$, and is computed as $w_{s,3}$.

– Front second maximum difference.

$$\Delta E = [E_{2^{\text{nd}} \max}^{S1} - E_{\min}^{S1}] \quad (\text{A7})$$

is the difference between the energy of the strip cell with the second greatest energy $E_{2^{\text{nd}} \max}^{S1}$, and the energy in the strip cell with the least energy found between the greatest and the second greatest energy E_{\min}^{S1} ($\Delta E = 0$ when there is no second maximum).

– Front maxima relative ratio

$$E_{\text{ratio}} = \frac{E_{1^{\text{st}} \max}^{S1} - E_{2^{\text{nd}} \max}^{S1}}{E_{1^{\text{st}} \max}^{S1} + E_{2^{\text{nd}} \max}^{S1}} \quad (\text{A8})$$

measures the relative difference between the energy of the strip cell with the greatest energy $E_{1^{\text{st}} \max}^{S1}$ and the energy in the strip cell with second greatest energy $E_{2^{\text{nd}} \max}^{S1}$ (1 when there is no second maximum).

Appendix B: Cross Section Measurements

Table III, IV and V list the values of the measured isolated prompt photon production cross sections, for the $0.00 \leq |\eta^\gamma| < 0.60$, $0.60 \leq |\eta^\gamma| < 1.37$ and $1.52 \leq |\eta^\gamma| < 1.81$ regions, respectively. The various systematic uncertainties originating from the purity measurement, the photon selection and identification efficiency, the photon energy scale and the luminosity are shown. The total uncertainty includes both the statistical and all systematic uncertainties, except for the uncertainty on the luminosity.

TABLE III. The measured isolated prompt photon production cross section, for $0.00 \leq |\eta^\gamma| < 0.60$. The systematic uncertainties originating from the purity measurement, the photon selection, the photon energy scale, the unfolding procedure and the luminosity are shown. The total uncertainty includes both the statistical and all systematic uncertainties, except for the uncertainty on the luminosity.

E_T^γ	$\frac{d\sigma}{dE_T^\gamma}$	Measured								JETPHOX	
		stat	syst (purity)	syst (efficiency)	syst (en. scale)	syst (unfolding)	syst (luminosity)	total uncertainty	$\frac{d\sigma}{dE_T^\gamma}$	total uncertainty	
		[GeV]	[nb/GeV]	[nb/GeV]	[nb/GeV]	[nb/GeV]	[nb/GeV]	[nb/GeV]	[nb/GeV]	[nb/GeV]	
[15, 20)	5.24	± 0.11	$+0.52$ -0.88	± 0.81	$+0.51$ -0.46	± 0.11	± 0.58	$+1.3$ -1.4	6.8	$+1.4$ -0.9	
[20, 25)	1.88	± 0.05	$+0.18$ -0.20	± 0.21	$+0.14$ -0.14	± 0.04	± 0.21	± 0.36	2.38	$+0.45$ -0.30	
[25, 30)	0.88	± 0.03	± 0.07	± 0.08	$+0.09$ -0.08	± 0.02	± 0.10	$+0.16$ -0.15	1.01	$+0.17$ -0.13	
[30, 35)	0.461	± 0.016	$+0.029$ -0.019	± 0.035	$+0.045$ -0.046	± 0.009	± 0.05	± 0.07	0.50	$+0.10$ -0.04	
[35, 40)	0.254	± 0.011	$+0.017$ -0.015	± 0.019	$+0.027$ -0.025	± 0.005	± 0.028	± 0.04	0.28	$+0.04$ -0.03	
[40, 50)	0.115	± 0.005	$+0.008$ -0.006	± 0.007	$+0.009$ -0.009	± 0.0023	± 0.013	$+0.017$ -0.016	0.127	$+0.018$ -0.014	
[50, 60)	0.050	± 0.003	$+0.003$ -0.002	± 0.003	$+0.006$ -0.005	± 0.001	± 0.005	$+0.008$ -0.007	0.052	$+0.007$ -0.006	
[60, 100)	0.0120	± 0.0007	$+0.0007$ -0.0005	± 0.0006	$+0.0013$ -0.0012	± 0.0002	± 0.0013	$+0.0019$ -0.0018	0.0121	$+0.0014$ -0.0012	

TABLE IV. The measured isolated prompt photon production cross section, for $0.60 \leq |\eta^\gamma| < 1.37$. The systematic uncertainties originating from the purity measurement, the photon selection, the photon energy scale, the unfolding procedure and the luminosity are shown. The total uncertainty includes both the statistical and all systematic uncertainties, except for the uncertainty on the luminosity.

E_T^γ	$\frac{d\sigma}{dE_T^\gamma}$	Measured								JETPHOX	
		stat	syst (purity)	syst (efficiency)	syst (en. scale)	syst (unfolding)	syst (luminosity)	total uncertainty	$\frac{d\sigma}{dE_T^\gamma}$	total uncertainty	
		[GeV]	[nb/GeV]	[nb/GeV]	[nb/GeV]	[nb/GeV]	[nb/GeV]	[nb/GeV]	[nb/GeV]	[nb/GeV]	
[15, 20)	5.9	± 0.2	$+1.8$ -0.5	± 1.0	$+0.6$ -0.5	± 0.1	± 0.6	$+2.3$ -1.4	8.5	$+1.7$ -1.3	
[20, 25)	2.23	± 0.07	$+0.49$ -0.18	± 0.28	$+0.16$ -0.16	± 0.04	± 0.24	$+0.6$ -0.4	3.0	$+0.5$ -0.4	
[25, 30)	1.05	± 0.03	$+0.16$ -0.06	± 0.10	$+0.10$ -0.10	± 0.021	± 0.12	$+0.24$ -0.19	1.28	$+0.18$ -0.16	
[30, 35)	0.52	± 0.02	$+0.06$ -0.03	± 0.04	$+0.05$ -0.05	± 0.011	± 0.06	$+0.11$ -0.09	0.64	$+0.11$ -0.09	
[35, 40)	0.313	± 0.014	$+0.029$ -0.021	± 0.024	$+0.035$ -0.032	± 0.006	± 0.034	$+0.06$ -0.05	0.344	$+0.052$ -0.039	
[40, 50)	0.146	± 0.006	$+0.014$ -0.011	± 0.009	$+0.013$ -0.013	± 0.003	± 0.016	$+0.025$ -0.022	0.161	$+0.022$ -0.019	
[50, 60)	0.062	± 0.004	$+0.005$ -0.004	± 0.003	$+0.006$ -0.006	± 0.001	± 0.007	$+0.010$ -0.009	0.065	$+0.009$ -0.007	
[60, 100)	0.0138	± 0.0008	$+0.0013$ -0.0009	± 0.0007	$+0.0016$ -0.0014	± 0.0003	± 0.0015	$+0.0025$ -0.0022	0.0154	$+0.0019$ -0.0015	

TABLE V. The measured isolated prompt photon production cross section, for $1.52 \leq |\eta^\gamma| < 1.81$. The systematic uncertainties originating from the purity measurement, the photon selection, the photon energy scale, the unfolding procedure and the luminosity are shown. The total uncertainty includes both the statistical and all systematic uncertainties, except for the uncertainty on the luminosity.

E_T^γ	$\frac{d\sigma}{dE_T^\gamma}$	Measured							JETPHOX		
		stat	syst (purity)	syst (efficiency)	syst (en. scale)	syst (unfolding)	syst (luminosity)	total uncertainty	$\frac{d\sigma}{dE_T^\gamma}$	total uncertainty	
		[GeV]	[nb/GeV]	[nb/GeV]	[nb/GeV]	[nb/GeV]	[nb/GeV]	[nb/GeV]	[nb/GeV]	[nb/GeV]	
[15, 20)	2.9	± 0.1	$+0.8$ -0.3	± 0.5	$+0.3$ -0.3	± 0.1	± 0.3	$+1.1$ -0.7	3.1	$+0.6$ -0.5	
[20, 25)	1.12	± 0.04	$+0.15$ -0.08	± 0.16	$+0.08$ -0.08	± 0.02	± 0.12	$+0.27$ -0.24	1.10	$+0.20$ -0.15	
[25, 30)	0.47	± 0.02	$+0.06$ -0.04	± 0.05	$+0.05$ -0.04	± 0.01	± 0.05	$+0.11$ -0.09	0.46	$+0.07$ -0.06	
[30, 35)	0.240	± 0.013	$+0.028$ -0.016	± 0.023	$+0.025$ -0.026	± 0.005	± 0.026	$+0.052$ -0.045	0.233	$+0.037$ -0.030	
[35, 40)	0.142	± 0.009	$+0.018$ -0.010	± 0.012	$+0.014$ -0.013	± 0.0032	± 0.016	$+0.030$ -0.026	0.126	$+0.020$ -0.015	
[40, 50)	0.062	± 0.004	$+0.005$ -0.004	± 0.005	$+0.006$ -0.006	± 0.0013	± 0.007	$+0.011$ -0.010	0.058	$+0.008$ -0.007	
[50, 60)	0.0237	± 0.0025	$+0.0026$ -0.0028	± 0.0019	$+0.0024$ -0.0022	± 0.0005	± 0.003	± 0.005	0.0243	$+0.0033$ -0.0027	
[60, 100)	0.0066	± 0.0005	$+0.0005$ -0.0003	± 0.0005	$+0.0008$ -0.0007	± 0.0002	± 0.0007	$+0.0013$ -0.0012	0.0057	$+0.0007$ -0.0006	

Appendix C: The ATLAS Collaboration

The ATLAS Collaboration

G. Aad⁴⁸, B. Abbott¹¹¹, J. Abdallah¹¹, A.A. Abdelalim⁴⁹, A. Abdesselam¹¹⁸, O. Abdinov¹⁰, B. Abi¹¹², M. Abolins⁸⁸, H. Abramowicz¹⁵³, H. Abreu¹¹⁵, E. Acerbi^{89a,89b}, B.S. Acharya^{164a,164b}, M. Ackers²⁰, D.L. Adams²⁴, T.N. Addy⁵⁶, J. Adelman¹⁷⁵, M. Aderholz⁹⁹, S. Adomeit⁹⁸, P. Adragna⁷⁵, T. Adye¹²⁹, S. Aefsky²², J.A. Aguilar-Saavedra^{124b,a}, M. Aharrouche⁸¹, S.P. Ahlen²¹, F. Ahles⁴⁸, A. Ahmad¹⁴⁸, M. Ahsan⁴⁰, G. Aielli^{133a,133b}, T. Akdogan^{18a}, T.P.A. Åkesson⁷⁹, G. Akimoto¹⁵⁵, A.V. Akimov⁹⁴, M.S. Alam¹, M.A. Alam⁷⁶, S. Albrand⁵⁵, M. Aleksa²⁹, I.N. Aleksandrov⁶⁵, M. Aleppo^{89a,89b}, F. Alessandria^{89a}, C. Alexa^{25a}, G. Alexander¹⁵³, G. Alexandre⁴⁹, T. Alexopoulos⁹, M. Alhoob²⁰, M. Aliev¹⁵, G. Alimonti^{89a}, J. Alison¹²⁰, M. Aliyev¹⁰, P.P. Allport⁷³, S.E. Allwood-Spiers⁵³, J. Almond⁸², A. Aloisio^{102a,102b}, R. Alon¹⁷¹, A. Alonso⁷⁹, J. Alonso¹⁴, M.G. Alviggi^{102a,102b}, K. Amako⁶⁶, P. Amaral²⁹, C. Amelung²², V.V. Ammosov¹²⁸, A. Amorim^{124a,b}, G. Amorós¹⁶⁷, N. Amram¹⁵³, C. Anastopoulos¹³⁹, N. Andari¹¹⁵, T. Andeen³⁴, C.F. Anders²⁰, K.J. Anderson³⁰, A. Andreazza^{89a,89b}, V. Andrei^{58a}, M-L. Andrieux⁵⁵, X.S. Anduaga⁷⁰, A. Angerami³⁴, F. Anghinolfi²⁹, N. Anjos^{124a}, A. Annovi⁴⁷, A. Antonaki⁸, M. Antonelli⁴⁷, S. Antonelli^{19a,19b}, J. Antos^{144b}, F. Anulli^{132a}, S. Aoun⁸³, L. Aperio Bella⁴, R. Apolle¹¹⁸, G. Arabidze⁸⁸, I. Aracena¹⁴³, Y. Arai⁶⁶, A.T.H. Arce⁴⁴, J.P. Archambault²⁸, S. Arfaoui^{29,c}, J-F. Arguin¹⁴, E. Arik^{18a,*}, M. Arik^{18a}, A.J. Armbruster⁸⁷, K.E. Arms¹⁰⁹, S.R. Armstrong²⁴, O. Arnaez⁸¹, C. Arnault¹¹⁵, A. Artamonov⁹⁵, G. Artoni^{132a,132b}, D. Arutinov²⁰, S. Asai¹⁵⁵, R. Asfandiyarov¹⁷², S. Ask²⁷, B. Åsman^{146a,146b}, L. Asquith⁵, K. Assamagan²⁴, A. Astbury¹⁶⁹, A. Astvatsaturov⁵², G. Atoian¹⁷⁵, B. Aubert⁴, B. Auerbach¹⁷⁵, E. Auge¹¹⁵, K. Augsten¹²⁷, M. Aurousseau⁴, N. Austin⁷³, R. Avramidou⁹, D. Axen¹⁶⁸, C. Ay⁵⁴, G. Azuelos^{93,d}, Y. Azuma¹⁵⁵, M.A. Baak²⁹, G. Baccaglioni^{89a}, C. Bacci^{134a,134b}, A.M. Bach¹⁴, H. Bachacou¹³⁶, K. Bachas²⁹, G. Bachy²⁹, M. Backes⁴⁹, E. Badescu^{25a}, P. Bagnaia^{132a,132b}, S. Bahinipati², Y. Bai^{32a}, D.C. Bailey¹⁵⁸, T. Bain¹⁵⁸, J.T. Baines¹²⁹, O.K. Baker¹⁷⁵, S. Baker⁷⁷, F. Baltasar Dos Santos Pedrosa²⁹, E. Banas³⁸, P. Banerjee⁹³, Sw. Banerjee¹⁶⁹, D. Banfi^{89a,89b}, A. Bangert¹³⁷, V. Bansal¹⁶⁹, H.S. Bansil¹⁷, L. Barak¹⁷¹, S.P. Baranov⁹⁴, A. Barashkou⁶⁵, A. Barbaro Galtieri¹⁴, T. Barber²⁷, E.L. Barberio⁸⁶, D. Barberis^{50a,50b}, M. Barbero²⁰, D.Y. Bardin⁶⁵, T. Barillari⁹⁹, M. Barisonzi¹⁷⁴, T. Barklow¹⁴³, N. Barlow²⁷, B.M. Barnett¹²⁹, R.M. Barnett¹⁴, A. Baroncelli^{134a}, A.J. Barr¹¹⁸, F. Barreiro⁸⁰, J. Barreiro Guimarães da Costa⁵⁷, P. Barrillon¹¹⁵, R. Bartoldus¹⁴³, A.E. Barton⁷¹, D. Bartsch²⁰, R.L. Bates⁵³, L. Batkova^{144a}, J.R. Batley²⁷, A. Battaglia¹⁶, M. Battistin²⁹, G. Battistoni^{89a}, F. Bauer¹³⁶, H.S. Bawa¹⁴³, B. Beare¹⁵⁸, T. Beau⁷⁸, P.H. Beauchemin¹¹⁸, R. Beccerle^{50a}, P. Bechtle⁴¹, H.P. Beck¹⁶, M. Beckingham⁴⁸, K.H. Becks¹⁷⁴, A.J. Beddall^{18c}, A. Beddall^{18c}, V.A. Bednyakov⁶⁵, C. Bee⁸³, M. Begel²⁴, S. Behar Harpaz¹⁵², P.K. Behera⁶³, M. Beimforde⁹⁹, C. Belanger-Champagne¹⁶⁶, B. Belhorma⁵⁵, P.J. Bell⁴⁹, W.H. Bell⁴⁹, G. Bella¹⁵³, L. Bellagamba^{19a}, F. Bellina²⁹, G. Bellomo^{89a,89b}, M. Bellomo^{119a}, A. Belloni⁵⁷, K. Belotskiy⁹⁶, O. Beltramello²⁹, S. Ben Ami¹⁵², O. Benary¹⁵³, D. Benchekroun^{135a}, C. Benchouk⁸³, M. Bendel⁸¹, B.H. Benedict¹⁶³, N. Benekos¹⁶⁵, Y. Benhammou¹⁵³, D.P. Benjamin⁴⁴, M. Benoit¹¹⁵, J.R. Bensinger²², K. Benslama¹³⁰, S. Bentvelsen¹⁰⁵, D. Berge²⁹, E. Bergeaas Kuutmann⁴¹, N. Berger⁴, F. Berghaus¹⁶⁹, E. Berglund⁴⁹, J. Beringer¹⁴, K. Bernardet⁸³, P. Bernat¹¹⁵, R. Bernhard⁴⁸, C. Bernius²⁴, T. Berry⁷⁶, A. Bertin^{19a,19b}, F. Bertinelli²⁹, F. Bertolucci^{122a,122b}, M.I. Besana^{89a,89b}, N. Besson¹³⁶, S. Bethke⁹⁹, W. Bhimji⁴⁵, R.M. Bianchi²⁹, M. Bianco^{72a,72b}, O. Biebel⁹⁸, J. Biesiada¹⁴, M. Biglietti^{132a,132b}, H. Bilokon⁴⁷, M. Bindi^{19a,19b}, A. Bingul^{18c}, C. Bini^{132a,132b}, C. Biscarat¹⁷⁷, R. Bischof⁶², U. Bitenc⁴⁸, K.M. Black²¹, R.E. Blair⁵, J.-B. Blanchard¹¹⁵, G. Blanchot²⁹, C. Blocker²², J. Blocki³⁸, A. Blondel⁴⁹, W. Blum⁸¹, U. Blumenschein⁵⁴, C. Boaretto^{132a,132b}, G.J. Bobbink¹⁰⁵, V.B. Bobrovnikov¹⁰⁷, A. Bocci⁴⁴, R. Bock²⁹, C.R. Boddy¹¹⁸, M. Boehler⁴¹, J. Boek¹⁷⁴, N. Boelaert³⁵, S. Böser⁷⁷, J.A. Bogaerts²⁹, A. Bogdanchikov¹⁰⁷, A. Bogouch^{90,*}, C. Bohm^{146a}, V. Boisvert⁷⁶, T. Bold^{163,e}, V. Boldea^{25a}, M. Bona⁷⁵, M. Boonekamp¹³⁶, G. Boorman⁷⁶, C.N. Booth¹³⁹, P. Booth¹³⁹, J.R.A. Booth¹⁷, S. Bordoni⁷⁸, C. Borer¹⁶, A. Borisov¹²⁸, G. Borissov⁷¹, I. Borjanovic^{12a}, S. Borroni^{132a,132b}, K. Bos¹⁰⁵, D. Boscherini^{19a}, M. Bosman¹¹, H. Boterenbrood¹⁰⁵, D. Botterill¹²⁹, J. Bouchami⁹³, J. Boudreau¹²³, E.V. Bouhouva-Thacker⁷¹, C. Boulahouache¹²³, C. Bourdarios¹¹⁵, N. Bousson⁸³, A. Boveia³⁰, J. Boyd²⁹, I.R. Boyko⁶⁵, N.I. Bozhko¹²⁸, I. Bozovic-Jelisavcic^{12b}, S. Braccini⁴⁷, J. Bracinik¹⁷, A. Braem²⁹, E. Brambilla^{72a,72b}, P. Branchini^{134a}, G.W. Brandenburg⁵⁷, A. Brandt⁷, G. Brandt⁴¹, O. Brandt⁵⁴, U. Bratzler¹⁵⁶, B. Brau⁸⁴, J.E. Brau¹¹⁴, H.M. Braun¹⁷⁴, B. Brelier¹⁵⁸, J. Bremer²⁹, R. Brenner¹⁶⁶, S. Bressler¹⁵², D. Breton¹¹⁵, N.D. Brett¹¹⁸, P.G. Bright-Thomas¹⁷, D. Britton⁵³, F.M. Brochu²⁷, I. Brock²⁰, R. Brock⁸⁸, T.J. Brodbeck⁷¹, E. Brodet¹⁵³, F. Broggi^{89a}, C. Bromberg⁸⁸, G. Brooijmans³⁴, W.K. Brooks^{31b}, G. Brown⁸², E. Brubaker³⁰, P.A. Bruckman de Renstrom³⁸, D. Bruncko^{144b}, R. Bruneliere⁴⁸, S. Brunet⁶¹, A. Bruni^{19a}, G. Bruni^{19a}, M. Bruschi^{19a}, T. Buanes¹³, F. Bucci⁴⁹, J. Buchanan¹¹⁸, N.J. Buchanan², P. Buchholz¹⁴¹, R.M. Buckingham¹¹⁸, A.G. Buckley⁴⁵, S.I. Buda^{25a}, I.A. Budagov⁶⁵, B. Budick¹⁰⁸, V. Büscher⁸¹, L. Bugge¹¹⁷, D. Buira-Clark¹¹⁸, E.J. Buis¹⁰⁵, O. Bulekov⁹⁶, M. Bunse⁴², T. Buran¹¹⁷, H. Burckhart²⁹, S. Burdin⁷³, T. Burgess¹³, S. Burke¹²⁹, E. Busato³³, P. Bussey⁵³, C.P. Buszello¹⁶⁶, F. Butin²⁹, B. Butler¹⁴³, J.M. Butler²¹, C.M. Buttar⁵³, J.M. Butterworth⁷⁷, W. Buttlinger²⁷, T. Byatt⁷⁷, S. Cabrera Urbán¹⁶⁷, M. Caccia^{89a,89b}, D. Caforio^{19a,19b},

- O. Cakir^{3a}, P. Calafiura¹⁴, G. Calderini⁷⁸, P. Calfayan⁹⁸, R. Calkins¹⁰⁶, L.P. Caloba^{23a}, R. Caloi^{132a,132b}, D. Calvet³³, S. Calvet³³, A. Camard⁷⁸, P. Camarri^{133a,133b}, M. Cambiaghi^{119a,119b}, D. Cameron¹¹⁷, J. Cammin²⁰, S. Campana²⁹, M. Campanelli⁷⁷, V. Canale^{102a,102b}, F. Canelli³⁰, A. Canepa^{159a}, J. Cantero⁸⁰, L. Capasso^{102a,102b}, M.D.M. Capeans Garrido²⁹, I. Caprini^{25a}, M. Caprini^{25a}, M. Caprio^{102a,102b}, D. Capriotti⁹⁹, M. Capua^{36a,36b}, R. Caputo¹⁴⁸, C. Caramarcu^{25a}, R. Cardarelli^{133a}, T. Carli²⁹, G. Carlino^{102a}, L. Carminati^{89a,89b}, B. Caron^{159a}, S. Caron⁴⁸, C. Carpentieri⁴⁸, G.D. Carrillo Montoya¹⁷², S. Carron Montero¹⁵⁸, A.A. Carter⁷⁵, J.R. Carter²⁷, J. Carvalho^{124a,f}, D. Casadei¹⁰⁸, M.P. Casado¹¹, M. Casella^{122a,122b}, C. Caso^{50a,50b,*}, A.M. Castaneda Hernandez¹⁷², E. Castaneda-Miranda¹⁷², V. Castillo Gimenez¹⁶⁷, N.F. Castro^{124b,a}, G. Cataldi^{72a}, F. Cataneo²⁹, A. Catinaccio²⁹, J.R. Catmore⁷¹, A. Cattai²⁹, G. Cattani^{133a,133b}, S. Caugron⁸⁸, A. Cavallari^{132a,132b}, P. Cavalleri⁷⁸, D. Cavalli^{89a}, M. Cavalli-Sforza¹¹, V. Cavasinni^{122a,122b}, A. Cazzato^{72a,72b}, F. Ceradini^{134a,134b}, C. Cerna⁸³, A.S. Cerqueira^{23a}, A. Cerri²⁹, L. Cerrito⁷⁵, F. Cerutti⁴⁷, M. Cervetto^{50a,50b}, S.A. Cetin^{18b}, F. Cevenini^{102a,102b}, A. Chafaq^{135a}, D. Chakraborty¹⁰⁶, K. Chan², B. Chapleau⁸⁵, J.D. Chapman²⁷, J.W. Chapman⁸⁷, E. Chareyre⁷⁸, D.G. Charlton¹⁷, V. Chavda⁸², S. Cheatham⁷¹, S. Chekanov⁵, S.V. Chekulaev^{159a}, G.A. Chelkov⁶⁵, H. Chen²⁴, L. Chen², S. Chen^{32c}, T. Chen^{32c}, X. Chen¹⁷², S. Cheng^{32a}, A. Cheplakov⁶⁵, V.F. Chepurnov⁶⁵, R. Cherkaoui El Moursli^{135d}, V. Chernyatin²⁴, E. Cheu⁶, S.L. Cheung¹⁵⁸, L. Chevalier¹³⁶, F. Chevallier¹³⁶, G. Chiefari^{102a,102b}, L. Chikovani⁵¹, J.T. Childers^{58a}, A. Chilingarov⁷¹, G. Chiodini^{72a}, M.V. Chizhov⁶⁵, G. Choudalakis³⁰, S. Chouridou¹³⁷, I.A. Christidi⁷⁷, A. Christov⁴⁸, D. Chromeck-Burckhart²⁹, M.L. Chu¹⁵¹, J. Chudoba¹²⁵, G. Ciapetti^{132a,132b}, A.K. Ciftci^{3a}, R. Ciftci^{3a}, D. Cinca³³, V. Cindro⁷⁴, M.D. Ciobotaru¹⁶³, C. Ciocca^{19a,19b}, A. Ciocio¹⁴, M. Cirilli⁸⁷, M. Ciubancan^{25a}, A. Clark⁴⁹, P.J. Clark⁴⁵, W. Cleland¹²³, J.C. Clemens⁸³, B. Clement⁵⁵, C. Clement^{146a,146b}, R.W. Cliff¹²⁹, Y. Coadou⁸³, M. Cobal^{164a,164c}, A. Coccato^{50a,50b}, J. Cochran⁶⁴, P. Coe¹¹⁸, J.G. Cogan¹⁴³, J. Coggshall¹⁶⁵, E. Cogneras¹⁷⁷, C.D. Cojocaru²⁸, J. Colas⁴, A.P. Colijn¹⁰⁵, C. Collard¹¹⁵, N.J. Collins¹⁷, C. Collins-Tooth⁵³, J. Collot⁵⁵, G. Colon⁸⁴, R. Coluccia^{72a,72b}, G. Comune⁸⁸, P. Conde Muñoz^{124a}, E. Coniavitis¹¹⁸, M.C. Conidi¹¹, M. Consonni¹⁰⁴, S. Constantinescu^{25a}, C. Conta^{119a,119b}, F. Conventi^{102a,g}, J. Cook²⁹, M. Cooke¹⁴, B.D. Cooper⁷⁵, A.M. Cooper-Sarkar¹¹⁸, N.J. Cooper-Smith⁷⁶, K. Copic³⁴, T. Cornelissen^{50a,50b}, M. Corradi^{19a}, S. Correard⁸³, F. Corriveau^{85,h}, A. Cortes-Gonzalez¹⁶⁵, G. Cortiana⁹⁹, G. Costa^{89a}, M.J. Costa¹⁶⁷, D. Costanzo¹³⁹, T. Costin³⁰, D. Côté²⁹, R. Coura Torres^{23a}, L. Courneyea¹⁶⁹, G. Cowan⁷⁶, C. Cowden²⁷, B.E. Cox⁸², K. Cranmer¹⁰⁸, M. Cristinziani²⁰, G. Crosetti^{36a,36b}, R. Crupi^{72a,72b}, S. Crépé-Renaudin⁵⁵, C. Cuenza Almenar¹⁷⁵, T. Cuhadar Donszelmann¹³⁹, S. Cunedo^{50a,50b}, M. Curatolo⁴⁷, C.J. Curtis¹⁷, P. Cwetanski⁶¹, H. Czirr¹⁴¹, Z. Czyczula¹⁷⁵, S. D'Auria⁵³, M. D'Onofrio⁷³, A. D'Orazio^{132a,132b}, A. Da Rocha Gesualdi Mello^{23a}, P.V.M. Da Silva^{23a}, C. Da Via⁸², W. Dabrowski³⁷, A. Dahlhoff⁴⁸, T. Dai⁸⁷, C. Dallapiccola⁸⁴, S.J. Dallison^{129,*}, M. Dam³⁵, M. Dameri^{50a,50b}, D.S. Damiani¹³⁷, H.O. Danielsson²⁹, R. Dankers¹⁰⁵, D. Dannheim⁹⁹, V. Dao⁴⁹, G. Darbo^{50a}, G.L. Darlea^{25b}, C. Daum¹⁰⁵, J.P. Dauvergne²⁹, W. Davey⁸⁶, T. Davidek¹²⁶, N. Davidson⁸⁶, R. Davidson⁷¹, M. Davies⁹³, A.R. Davison⁷⁷, E. Dawe¹⁴², I. Dawson¹³⁹, J.W. Dawson^{5,*}, R.K. Daya³⁹, K. De⁷, R. de Asmundis^{102a}, S. De Castro^{19a,19b}, S. De Cecco⁷⁸, J. de Graat⁹⁸, N. De Groot¹⁰⁴, P. de Jong¹⁰⁵, E. De La Cruz-Burelo⁸⁷, C. De La Taille¹¹⁵, B. De Lotto^{164a,164c}, L. De Mora⁷¹, L. De Nooij¹⁰⁵, M. De Oliveira Branco²⁹, D. De Pidis^{132a}, P. de Saintignon⁵⁵, A. De Salvo^{132a}, U. De Sanctis^{164a,164c}, A. De Santo¹⁴⁹, J.B. De Vivie De Regie¹¹⁵, S. Dean⁷⁷, G. Dedes⁹⁹, D.V. Dedovich⁶⁵, J. Degenhardt¹²⁰, M. Dehchar¹¹⁸, M. Deile⁹⁸, C. Del Papa^{164a,164c}, J. Del Peso⁸⁰, T. Del Prete^{122a,122b}, A. Dell'Acqua²⁹, L. Dell'Asta^{89a,89b}, M. Della Pietra^{102a,g}, D. della Volpe^{102a,102b}, M. Delmastro²⁹, P. Delpierre⁸³, N. Delruelle²⁹, P.A. Delsart⁵⁵, C. Deluca¹⁴⁸, S. Demers¹⁷⁵, M. Demichev⁶⁵, B. Demirkoz¹¹, J. Deng¹⁶³, S.P. Denisov¹²⁸, C. Dennis¹¹⁸, D. Derendarz³⁸, J.E. Derkaoui^{135c}, F. Derue⁷⁸, P. Dervan⁷³, K. Desch²⁰, E. Devetak¹⁴⁸, P.O. Deviveiros¹⁵⁸, A. Dewhurst¹²⁹, B. De Wilde¹⁴⁸, S. Dhaliwal¹⁵⁸, R. Dhullipudi^{24,i}, A. Di Ciaccio^{133a,133b}, L. Di Ciaccio⁴, A. Di Girolamo²⁹, B. Di Girolamo²⁹, S. Di Luise^{134a,134b}, A. Di Mattia⁸⁸, R. Di Nardo^{133a,133b}, A. Di Simone^{133a,133b}, R. Di Sipio^{19a,19b}, M.A. Diaz^{31a}, M.M. Diaz Gomez⁴⁹, F. Diblen^{18c}, E.B. Diehl⁸⁷, H. Dietl⁹⁹, J. Dietrich⁴⁸, T.A. Dietzsch^{58a}, S. Diglio¹¹⁵, K. Dindar Yagci³⁹, J. Dingfelder²⁰, C. Dionisi^{132a,132b}, P. Dita^{25a}, S. Dita^{25a}, F. Dittus²⁹, F. Djama⁸³, R. Djilkibaev¹⁰⁸, T. Djobava⁵¹, M.A.B. do Vale^{23a}, A. Do Valle Wemans^{124a}, T.K.O. Doan⁴, M. Dobbs⁸⁵, R. Dobinson^{29,*}, D. Dobos⁴², E. Dobson²⁹, M. Dobson¹⁶³, J. Dodd³⁴, O.B. Dogan^{18a,*}, C. Doglioni¹¹⁸, T. Doherty⁵³, Y. Doi⁶⁶, J. Dolejsi¹²⁶, I. Dolenc⁷⁴, Z. Dolezal¹²⁶, B.A. Dolgoshein⁹⁶, T. Dohmae¹⁵⁵, M. Donadelli^{23b}, M. Donega¹²⁰, J. Donini⁵⁵, J. Dopke¹⁷⁴, A. Doria^{102a}, A. Dos Anjos¹⁷², M. Dosil¹¹, A. Dotti^{122a,122b}, M.T. Dova⁷⁰, J.D. Dowell¹⁷, A.D. Doxiadis¹⁰⁵, A.T. Doyle⁵³, Z. Drasal¹²⁶, J. Drees¹⁷⁴, N. Dressnandt¹²⁰, H. Drevermann²⁹, C. Driouichi³⁵, M. Dris⁹, J.G. Drohan⁷⁷, J. Dubbert⁹⁹, T. Dubbs¹³⁷, S. Dube¹⁴, E. Duchovni¹⁷¹, G. Duckeck⁹⁸, A. Dudarev²⁹, F. Dudziak¹¹⁵, M. Dührssen²⁹, I.P. Duerdoh⁸², L. Duflot¹¹⁵, M-A. Dufour⁸⁵, M. Dunford²⁹, H. Duran Yildiz^{3b}, R. Duxfield¹³⁹, M. Dwuznik³⁷, F. Dydak²⁹, D. Dzahini⁵⁵, M. Düren⁵², J. Ebke⁹⁸, S. Eckert⁴⁸, S. Eckweiler⁸¹, K. Edmonds⁸¹, C.A. Edwards⁷⁶, I. Efthymiopoulos⁴⁹, W. Ehrenfeld⁴¹, T. Ehrlich⁹⁹, T. Eifert²⁹, G. Eigen¹³, K. Einsweiler¹⁴, E. Eisenhandler⁷⁵, T. Ekelof¹⁶⁶, M. El Kacimi⁴, M. Ellert¹⁶⁶, S. Elles⁴, F. Ellinghaus⁸¹, K. Ellis⁷⁵, N. Ellis²⁹, J. Elmsheuser⁹⁸, M. Elsing²⁹, R. Ely¹⁴, D. Emeliyanov¹²⁹, R. Engelmann¹⁴⁸, A. Engl⁹⁸, B. Epp⁶², A. Eppig⁸⁷, J. Erdmann⁵⁴,

- A. Ereditato¹⁶, D. Eriksson^{146a}, J. Ernst¹, M. Ernst²⁴, J. Ernwein¹³⁶, D. Errede¹⁶⁵, S. Errede¹⁶⁵, E. Ertel⁸¹, M. Escalier¹¹⁵, C. Escobar¹⁶⁷, X. Espinal Curull¹¹, B. Esposito⁴⁷, F. Etienne⁸³, A.I. Etienvre¹³⁶, E. Etzion¹⁵³, D. Evangelakou⁵⁴, H. Evans⁶¹, L. Fabbri^{19a,19b}, C. Fabre²⁹, K. Facius³⁵, R.M. Fakhrutdinov¹²⁸, S. Falciano^{132a}, A.C. Falou¹¹⁵, Y. Fang¹⁷², M. Fanti^{89a,89b}, A. Farbin⁷, A. Farilla^{134a}, J. Farley¹⁴⁸, T. Farooque¹⁵⁸, S.M. Farrington¹¹⁸, P. Farthouat²⁹, D. Fasching¹⁷², P. Fassnacht²⁹, D. Fassouliotis⁸, B. Fatholahzadeh¹⁵⁸, A. Favareto^{89a,89b}, L. Fayard¹¹⁵, S. Fazio^{36a,36b}, R. Febbraro³³, P. Federic^{144a}, O.L. Fedin¹²¹, I. Fedorko²⁹, W. Fedorko⁸⁸, M. Fehling-Kaschek⁴⁸, L. Feligioni⁸³, D. Fellmann⁵, C.U. Felzmann⁸⁶, C. Feng^{32d}, E.J. Feng³⁰, A.B. Fenyuk¹²⁸, J. Ferencei^{144b}, D. Ferguson¹⁷², J. Ferland⁹³, B. Fernandes^{124a,j}, W. Fernando¹⁰⁹, S. Ferrag⁴⁹, J. Ferrando¹¹⁸, V. Ferrara⁴¹, A. Ferrari¹⁶⁶, P. Ferrari¹⁰⁵, R. Ferrari^{119a}, A. Ferrer¹⁶⁷, M.L. Ferrer⁴⁷, D. Ferrere⁴⁹, C. Ferretti⁸⁷, A. Ferretto Parodi^{50a,50b}, F. Ferro^{50a,50b}, M. Fiascaris³⁰, F. Fiedler⁸¹, A. Filipič⁷⁴, A. Filippas⁹, F. Filthaut¹⁰⁴, M. Fincke-Keeler¹⁶⁹, M.C.N. Fiolhais^{124a,f}, L. Fiorini¹¹, A. Firan³⁹, G. Fischer⁴¹, P. Fischer²⁰, M.J. Fisher¹⁰⁹, S.M. Fisher¹²⁹, J. Flammer²⁹, M. Flechl⁴⁸, I. Flechl¹⁴¹, J. Fleckner⁸¹, P. Fleischmann¹⁷³, S. Fleischmann²⁰, T. Flick¹⁷⁴, L.R. Flores Castillo¹⁷², M.J. Flowerdew⁹⁹, F. Föhlsch^{58a}, M. Fokitis⁹, T. Fonseca Martin¹⁶, D.A. Forbush¹³⁸, A. Formica¹³⁶, A. Forti⁸², D. Fortin^{159a}, J.M. Foster⁸², D. Fournier¹¹⁵, A. Foussat²⁹, A.J. Fowler⁴⁴, K. Fowler¹³⁷, H. Fox⁷¹, P. Francavilla^{122a,122b}, S. Franchino^{119a,119b}, D. Francis²⁹, T. Frank¹⁷¹, M. Franklin⁵⁷, S. Franz²⁹, M. Fraternali^{119a,119b}, S. Fratina¹²⁰, S.T. French²⁷, R. Froeschl²⁹, D. Froidevaux²⁹, J.A. Frost²⁷, C. Fukunaga¹⁵⁶, E. Fullana Torregrosa²⁹, J. Fuster¹⁶⁷, C. Gabaldon²⁹, O. Gabizon¹⁷¹, T. Gadfort²⁴, S. Gadomski⁴⁹, G. Gagliardi^{50a,50b}, P. Gagnon⁶¹, C. Galea⁹⁸, E.J. Gallas¹¹⁸, M.V. Gallas²⁹, V. Gallo¹⁶, B.J. Gallop¹²⁹, P. Gallus¹²⁵, E. Galyaev⁴⁰, K.K. Gan¹⁰⁹, Y.S. Gao^{143,k}, V.A. Gapienko¹²⁸, A. Gaponenko¹⁴, F. Garberson¹⁷⁵, M. Garcia-Sciveres¹⁴, C. García¹⁶⁷, J.E. García Navarro⁴⁹, R.W. Gardner³⁰, N. Garelli²⁹, H. Garitaonandia¹⁰⁵, V. Garonne²⁹, J. Garvey¹⁷, C. Gatti⁴⁷, G. Gaudio^{119a}, O. Gaumer⁴⁹, B. Gaur¹⁴¹, L. Gauthier¹³⁶, I.L. Gavrilenco⁹⁴, C. Gay¹⁶⁸, G. Gaycken²⁰, J-C. Gayde²⁹, E.N. Gazis⁹, P. Ge^{32d}, C.N.P. Gee¹²⁹, Ch. Geich-Gimbel²⁰, K. Gellerstedt^{146a,146b}, C. Gemme^{50a}, A. Gemmell⁵³, M.H. Genest⁹⁸, S. Gentile^{132a,132b}, F. Georgatos⁹, S. George⁷⁶, P. Gerlach¹⁷⁴, A. Gershon¹⁵³, C. Geweniger^{58a}, H. Ghazlane^{135d}, P. Ghez⁴, N. Ghodbane³³, B. Giacobbe^{19a}, S. Giagu^{132a,132b}, V. Giakoumopoulou⁸, V. Giangiobbe^{122a,122b}, F. Gianotti²⁹, B. Gibbard²⁴, A. Gibson¹⁵⁸, S.M. Gibson²⁹, G.F. Gieraltowski⁵, L.M. Gilbert¹¹⁸, M. Gilchriese¹⁴, O. Gildemeister²⁹, V. Gilewsky⁹¹, D. Gillberg²⁸, A.R. Gillman¹²⁹, D.M. Gingrich^{2,d}, J. Ginzburg¹⁵³, N. Giokaris⁸, R. Giordano^{102a,102b}, F.M. Giorgi¹⁵, P. Giovannini⁹⁹, P.F. Giraud¹³⁶, D. Giugni^{89a}, P. Giusti^{19a}, B.K. Gjelsten¹¹⁷, L.K. Gladilin⁹⁷, C. Glasman⁸⁰, J. Glatzer⁴⁸, A. Glazov⁴¹, K.W. Glitza¹⁷⁴, G.L. Glonti⁶⁵, J. Godfrey¹⁴², J. Godlewski²⁹, M. Goebel⁴¹, T. Göpfert⁴³, C. Goeringer⁸¹, C. Gössling⁴², T. Göttfert⁹⁹, S. Goldfarb⁸⁷, D. Goldin³⁹, T. Golling¹⁷⁵, N.P. Gollub²⁹, S.N. Golovnia¹²⁸, A. Gomes^{124a,l}, L.S. Gomez Fajardo⁴¹, R. Gonçalo⁷⁶, L. Gonella²⁰, C. Gong^{32b}, A. Gonidec²⁹, S. Gonzalez¹⁷², S. González de la Hoz¹⁶⁷, M.L. Gonzalez Silva²⁶, S. Gonzalez-Sevilla⁴⁹, J.J. Goodson¹⁴⁸, L. Goossens²⁹, P.A. Gorbounov⁹⁵, H.A. Gordon²⁴, I. Gorelov¹⁰³, G. Gorfine¹⁷⁴, B. Gorini²⁹, E. Gorini^{72a,72b}, A. Gorišek⁷⁴, E. Gornicki³⁸, S.A. Gorokhov¹²⁸, B.T. Gorski²⁹, V.N. Goryachev¹²⁸, B. Gosdzik⁴¹, M. Gosselink¹⁰⁵, M.I. Gostkin⁶⁵, M. Gouanère⁴, I. Gough Eschrich¹⁶³, M. Gouighri^{135a}, D. Goujdami^{135a}, M.P. Goulette⁴⁹, A.G. Goussiou¹³⁸, C. Goy⁴, I. Grabowska-Bold^{163,e}, V. Grabski¹⁷⁶, P. Grafström²⁹, C. Grah¹⁷⁴, K-J. Grahn¹⁴⁷, F. Grancagnolo^{72a}, S. Grancagnolo¹⁵, V. Grassi¹⁴⁸, V. Gratchev¹²¹, N. Grau³⁴, H.M. Gray^{34,m}, J.A. Gray¹⁴⁸, E. Graziani^{134a}, O.G. Grebenyuk¹²¹, D. Greenfield¹²⁹, T. Greenshaw⁷³, Z.D. Greenwood^{24,i}, I.M. Gregor⁴¹, P. Grenier¹⁴³, E. Griesmayer⁴⁶, J. Griffiths¹³⁸, N. Grigalashvili⁶⁵, A.A. Grillo¹³⁷, K. Grimm¹⁴⁸, S. Grinstein¹¹, P.L.Y. Gris³³, Y.V. Grishkevich⁹⁷, J.-F. Grivaz¹¹⁵, J. Grognuz²⁹, M. Groh⁹⁹, E. Gross¹⁷¹, J. Grosse-Knetter⁵⁴, J. Groth-Jensen⁷⁹, M. Gruwe²⁹, K. Grybel¹⁴¹, V.J. Guarino⁵, C. Guicheney³³, A. Guida^{72a,72b}, T. Guillemin⁴, S. Guindon⁵⁴, H. Guler^{85,n}, J. Gunther¹²⁵, B. Guo¹⁵⁸, J. Guo³⁴, A. Gupta³⁰, Y. Gusakov⁶⁵, V.N. Gushchin¹²⁸, A. Gutierrez⁹³, P. Gutierrez¹¹¹, N. Guttman¹⁵³, O. Gutzwiller¹⁷², C. Guyot¹³⁶, C. Gwenlan¹¹⁸, C.B. Gwilliam⁷³, A. Haas¹⁴³, S. Haas²⁹, C. Haber¹⁴, R. Hackenburg²⁴, H.K. Hadavand³⁹, D.R. Hadley¹⁷, P. Haefner⁹⁹, F. Hahn²⁹, S. Haider²⁹, Z. Hajduk³⁸, H. Hakobyan¹⁷⁶, J. Haller⁵⁴, K. Hamacher¹⁷⁴, A. Hamilton⁴⁹, S. Hamilton¹⁶¹, H. Han^{32a}, L. Han^{32b}, K. Hanagaki¹¹⁶, M. Hance¹²⁰, C. Handel⁸¹, P. Hanke^{58a}, C.J. Hansen¹⁶⁶, J.R. Hansen³⁵, J.B. Hansen³⁵, J.D. Hansen³⁵, P.H. Hansen³⁵, P. Hansson¹⁴³, K. Hara¹⁶⁰, G.A. Hare¹³⁷, T. Harenberg¹⁷⁴, D. Harper⁸⁷, R. Harper¹³⁹, R.D. Harrington²¹, O.M. Harris¹³⁸, K. Harrison¹⁷, J.C. Hart¹²⁹, J. Hartert⁴⁸, F. Hartjes¹⁰⁵, T. Haruyama⁶⁶, A. Harvey⁵⁶, S. Hasegawa¹⁰¹, Y. Hasegawa¹⁴⁰, S. Hassani¹³⁶, M. Hatch²⁹, D. Hauff⁹⁹, S. Haug¹⁶, M. Hauschild²⁹, R. Hauser⁸⁸, M. Havranek¹²⁵, B.M. Hawes¹¹⁸, C.M. Hawkes¹⁷, R.J. Hawkings²⁹, D. Hawkins¹⁶³, T. Hayakawa⁶⁷, D. Hayden⁷⁶, H.S. Hayward⁷³, S.J. Haywood¹²⁹, E. Hazen²¹, M. He^{32d}, S.J. Head¹⁷, V. Hedberg⁷⁹, L. Heelan²⁸, S. Heim⁸⁸, B. Heinemann¹⁴, S. Heisterkamp³⁵, L. Helary⁴, M. Heldmann⁴⁸, M. Heller¹¹⁵, S. Hellman^{146a,146b}, C. Helsens¹¹, R.C.W. Henderson⁷¹, P.J. Hendriks¹⁰⁵, M. Henke^{58a}, A. Henrichs⁵⁴, A.M. Henriques Correia²⁹, S. Henrot-Versille¹¹⁵, F. Henry-Couannier⁸³, C. Hensel⁵⁴, T. Henß¹⁷⁴, Y. Hernández Jiménez¹⁶⁷, R. Herrberg¹⁵, A.D. Hershenhorn¹⁵², G. Herten⁴⁸, R. Hertenberger⁹⁸, L. Hervas²⁹, N.P. Hessey¹⁰⁵, A. Hidvegi^{146a}, E. Higón-Rodriguez¹⁶⁷, D. Hill^{5,*}, J.C. Hill²⁷, N. Hill⁵, K.H. Hiller⁴¹, S. Hillert²⁰, S.J. Hillier¹⁷, I. Hinchliffe¹⁴, D. Hindson¹¹⁸, E. Hines¹²⁰, M. Hirose¹¹⁶, F. Hirsch⁴², D. Hirschbuehl¹⁷⁴, J. Hobbs¹⁴⁸, N. Hod¹⁵³, M.C. Hodgkinson¹³⁹, P. Hodgson¹³⁹, A. Hoecker²⁹, M.R. Hoeferkamp¹⁰³, J. Hoffman³⁹,

- D. Hoffmann⁸³, M. Hohlfeld⁸¹, M. Holder¹⁴¹, T.I. Hollins¹⁷, A. Holmes¹¹⁸, S.O. Holmgren^{146a}, T. Holy¹²⁷, J.L. Holzbauer⁸⁸, R.J. Homer¹⁷, Y. Homma⁶⁷, T. Horazdovsky¹²⁷, C. Horn¹⁴³, S. Horner⁴⁸, K. Horton¹¹⁸, J-Y. Hostachy⁵⁵, T. Hott⁹⁹, S. Hou¹⁵¹, M.A. Houlden⁷³, A. Hoummada^{135a}, J. Howarth⁸², D.F. Howell¹¹⁸, I. Hristova⁴¹, J. Hrvnac¹¹⁵, I. Hruska¹²⁵, T. Hryna'ova⁴, P.J. Hsu¹⁷⁵, S.-C. Hsu¹⁴, G.S. Huang¹¹¹, Z. Hubacek¹²⁷, F. Hubaut⁸³, F. Huegging²⁰, T.B. Huffman¹¹⁸, E.W. Hughes³⁴, G. Hughes⁷¹, R.E. Hughes-Jones⁸², M. Huhtinen²⁹, P. Hurst⁵⁷, M. Hurwitz¹⁴, U. Husemann⁴¹, N. Huseynov^{65,o}, J. Huston⁸⁸, J. Huth⁵⁷, G. Iacobucci^{102a}, G. Iakovidis⁹, M. Ibbotson⁸², I. Ibragimov¹⁴¹, R. Ichimiya⁶⁷, L. Iconomidou-Fayard¹¹⁵, J. Idarraga¹¹⁵, M. Idzik³⁷, P. Iengo⁴, O. Igonkina¹⁰⁵, Y. Ikegami⁶⁶, M. Ikeno⁶⁶, Y. Ilchenko³⁹, D. Iliadis¹⁵⁴, D. Imbault⁷⁸, M. Imhaeuser¹⁷⁴, M. Imori¹⁵⁵, T. Ince²⁰, J. Inigo-Golfin²⁹, P. Ioannou⁸, M. Iodice^{134a}, G. Ionescu⁴, A. Irles Quiles¹⁶⁷, K. Ishii⁶⁶, A. Ishikawa⁶⁷, M. Ishino⁶⁶, R. Ishmukhametov³⁹, T. Isobe¹⁵⁵, C. Issever¹¹⁸, S. Istin^{18a}, Y. Itoh¹⁰¹, A.V. Ivashin¹²⁸, W. Iwanski³⁸, H. Iwasaki⁶⁶, J.M. Izen⁴⁰, V. Izzo^{102a}, B. Jackson¹²⁰, J.N. Jackson⁷³, P. Jackson¹⁴³, M.R. Jaekel²⁹, V. Jain⁶¹, K. Jakobs⁴⁸, S. Jakobsen³⁵, J. Jakubek¹²⁷, D.K. Jana¹¹¹, E. Jankowski¹⁵⁸, E. Jansen⁷⁷, A. Jantsch⁹⁹, M. Janus²⁰, G. Jarlskog⁷⁹, L. Jeanty⁵⁷, K. Jelen³⁷, I. Jen-La Plante³⁰, P. Jenni²⁹, A. Jeremie⁴, P. Jež³⁵, S. Jézéquel⁴, H. Ji¹⁷², W. Ji⁸¹, J. Jia¹⁴⁸, Y. Jiang^{32b}, M. Jimenez Belenguer²⁹, G. Jin^{32b}, S. Jin^{32a}, O. Jinmouchi¹⁵⁷, M.D. Joergensen³⁵, D. Joffe³⁹, L.G. Johansen¹³, M. Johansen^{146a,146b}, K.E. Johansson^{146a}, P. Johansson¹³⁹, S. Johnert⁴¹, K.A. Johns⁶, K. Jon-And^{146a,146b}, G. Jones⁸², M. Jones¹¹⁸, R.W.L. Jones⁷¹, T.W. Jones⁷⁷, T.J. Jones⁷³, O. Jonsson²⁹, K.K. Joo¹⁵⁸, C. Joram²⁹, P.M. Jorge^{124a,b}, S. Jorgensen¹¹, J. Joseph¹⁴, X. Ju¹³⁰, V. Juraneck¹²⁵, P. Jussel⁶², V.V. Kabachenko¹²⁸, S. Kabana¹⁶, M. Kaci¹⁶⁷, A. Kaczmarska³⁸, P. Kadlecik³⁵, M. Kado¹¹⁵, H. Kagan¹⁰⁹, M. Kagan⁵⁷, S. Kaiser⁹⁹, E. Kajomovitz¹⁵², S. Kalinin¹⁷⁴, L.V. Kalinovskaya⁶⁵, S. Kama³⁹, N. Kanaya¹⁵⁵, M. Kaneda¹⁵⁵, T. Kanno¹⁵⁷, V.A. Kantserov⁹⁶, J. Kanzaki⁶⁶, B. Kaplan¹⁷⁵, A. Kapliy³⁰, J. Kaplon²⁹, D. Kar⁴³, M. Karagoz¹¹⁸, M. Karnevskiy⁴¹, K. Karr⁵, V. Kartvelishvili⁷¹, A.N. Karyukhin¹²⁸, L. Kashif⁵⁷, A. Kasmi³⁹, R.D. Kass¹⁰⁹, A. Kastanas¹³, M. Kataoka⁴, Y. Kataoka¹⁵⁵, E. Katsoufis⁹, J. Katzy⁴¹, V. Kaushik⁶, K. Kawagoe⁶⁷, T. Kawamoto¹⁵⁵, G. Kawamura⁸¹, M.S. Kayl¹⁰⁵, V.A. Kazanin¹⁰⁷, M.Y. Kazarinov⁶⁵, S.I. Kazi⁸⁶, J.R. Keates⁸², R. Keeler¹⁶⁹, R. Kehoe³⁹, M. Keil⁵⁴, G.D. Kekelidze⁶⁵, M. Kelly⁸², J. Kennedy⁹⁸, C.J. Kenney¹⁴³, M. Kenyon⁵³, O. Kepka¹²⁵, N. Kerschen²⁹, B.P. Kerševan⁷⁴, S. Kersten¹⁷⁴, K. Kessoku¹⁵⁵, C. Ketterer⁴⁸, M. Khakzad¹²⁸, F. Khalil-zada¹⁰, H. Khandanyan¹⁶⁵, A. Khanov¹¹², D. Kharchenko⁶⁵, A. Khodinov¹⁴⁸, A.G. Kholodenko¹²⁸, A. Khomich^{58a}, T.J. Khoo²⁷, G. Khoriauli²⁰, N. Khovanskiy⁶⁵, V. Khovanskiy⁹⁵, E. Khramov⁶⁵, J. Khubua⁵¹, G. Kilvington⁷⁶, H. Kim⁷, M.S. Kim², P.C. Kim¹⁴³, S.H. Kim¹⁶⁰, N. Kimura¹⁷⁰, O. Kind¹⁵, B.T. King⁷³, M. King⁶⁷, R.S.B. King¹¹⁸, J. Kirk¹²⁹, G.P. Kirsch¹¹⁸, L.E. Kirsch²², A.E. Kiryunin⁹⁹, D. Kisielewska³⁷, T. Kittelmann¹²³, A.M. Kiver¹²⁸, H. Kiyamura⁶⁷, E. Kladiva^{144b}, J. Klaiber-Lodewigs⁴², M. Klein⁷³, U. Klein⁷³, K. Kleinknecht⁸¹, M. Klemetti⁸⁵, A. Klier¹⁷¹, A. Klimentov²⁴, R. Klingenberg⁴², E.B. Klinkby³⁵, T. Klioutchnikova²⁹, P.F. Klok¹⁰⁴, S. Klous¹⁰⁵, E.-E. Kluge^{58a}, T. Kluge⁷³, P. Kluit¹⁰⁵, S. Kluth⁹⁹, E. Kneringer⁶², J. Knobloch²⁹, A. Knue⁵⁴, B.R. Ko⁴⁴, T. Kobayashi¹⁵⁵, M. Kobel⁴³, B. Koblitz²⁹, M. Kocian¹⁴³, A. Kocnar¹¹³, P. Kodys¹²⁶, K. Köneke²⁹, A.C. König¹⁰⁴, S. Koenig⁸¹, S. König⁴⁸, L. Köpke⁸¹, F. Koetsveld¹⁰⁴, P. Koevesarki²⁰, T. Koffas²⁹, E. Koffeman¹⁰⁵, F. Kohn⁵⁴, Z. Kohout¹²⁷, T. Kohriki⁶⁶, T. Koi¹⁴³, T. Kokott²⁰, G.M. Kolachev¹⁰⁷, H. Kolanoski¹⁵, V. Kolesnikov⁶⁵, I. Koletsou^{89a,89b}, J. Koll⁸⁸, D. Kollar²⁹, M. Kollefrath⁴⁸, S.D. Kolya⁸², A.A. Komar⁹⁴, J.R. Komaragiri¹⁴², T. Kondo⁶⁶, T. Kono^{41,p}, A.I. Kononov⁴⁸, R. Konoplich^{108,q}, N. Konstantinidis⁷⁷, A. Kootz¹⁷⁴, S. Koperny³⁷, S.V. Kopikov¹²⁸, K. Korcyl³⁸, K. Kordas¹⁵⁴, V. Koreshev¹²⁸, A. Korn¹⁴, A. Korol¹⁰⁷, I. Korolkov¹¹, E.V. Korolkova¹³⁹, V.A. Korotkov¹²⁸, O. Kortner⁹⁹, S. Kortner⁹⁹, V.V. Kostyukhin²⁰, M.J. Kotämäki²⁹, S. Kotov⁹⁹, V.M. Kotov⁶⁵, C. Kourkoumelis⁸, A. Koutsman¹⁰⁵, R. Kowalewski¹⁶⁹, T.Z. Kowalski³⁷, W. Kozanecki¹³⁶, A.S. Kozhin¹²⁸, V. Kral¹²⁷, V.A. Kramarenko⁹⁷, G. Kramberger⁷⁴, O. Krasel⁴², M.W. Krasny⁷⁸, A. Krasznahorkay¹⁰⁸, J. Kraus⁸⁸, A. Kreisel¹⁵³, F. Krejci¹²⁷, J. Kretzschmar⁷³, N. Krieger⁵⁴, P. Krieger¹⁵⁸, G. Krobath⁹⁸, K. Kroeninger⁵⁴, H. Kroha⁹⁹, J. Kroll¹²⁰, J. Kroseberg²⁰, J. Krstic^{12a}, U. Kruchonak⁶⁵, H. Krüger²⁰, Z.V. Krumshteyn⁶⁵, A. Kruth²⁰, T. Kubota¹⁵⁵, S. Kuehn⁴⁸, A. Kugel^{58c}, T. Kuhl¹⁷⁴, D. Kuhn⁶², V. Kukhtin⁶⁵, Y. Kulchitsky⁹⁰, S. Kuleshov^{31b}, C. Kummer⁹⁸, M. Kuna⁸³, N. Kundu¹¹⁸, J. Kunkle¹²⁰, A. Kupco¹²⁵, H. Kurashige⁶⁷, M. Kurata¹⁶⁰, Y.A. Kurochkin⁹⁰, V. Kus¹²⁵, W. Kuykendall¹³⁸, M. Kuze¹⁵⁷, P. Kuzhir⁹¹, O. Kvasnicka¹²⁵, R. Kwee¹⁵, A. La Rosa²⁹, L. La Rotonda^{36a,36b}, L. Labarga⁸⁰, J. Labbe⁴, C. Lacasta¹⁶⁷, F. Lacava^{132a,132b}, H. Lacker¹⁵, D. Lacour⁷⁸, V.R. Lacuesta¹⁶⁷, E. Ladygin⁶⁵, R. Lafaye⁴, B. Laforge⁷⁸, T. Lagouri⁸⁰, S. Lai⁴⁸, E. Laisne⁵⁵, M. Lamanna²⁹, M. Lambacher⁹⁸, C.L. Lampen⁶, W. Lampl⁶, E. Lancon¹³⁶, U. Landgraf⁴⁸, M.P.J. Landon⁷⁵, H. Landsman¹⁵², J.L. Lane⁸², C. Lange⁴¹, A.J. Lankford¹⁶³, F. Lanni²⁴, K. Lantzsch²⁹, V.V. Lapin^{128,*}, S. Laplace⁴, C. Lapoire²⁰, J.F. Laporte¹³⁶, T. Lari^{89a}, A.V. Larionov¹²⁸, A. Larner¹¹⁸, C. Lasseur²⁹, M. Lassnig²⁹, W. Lau¹¹⁸, P. Laurelli⁴⁷, A. Lavorato¹¹⁸, W. Lavrijesen¹⁴, P. Laycock⁷³, A.B. Lazarev⁶⁵, A. Lazzaro^{89a,89b}, O. Le Dertz⁷⁸, E. Le Guiriec⁸³, C. Le Maner¹⁵⁸, E. Le Menedeu¹³⁶, M. Leahu²⁹, A. Lebedev⁶⁴, C. Lebel⁹³, M. Lechowski¹¹⁵, T. LeCompte⁵, F. Ledroit-Guillon⁵⁵, H. Lee¹⁰⁵, J.S.H. Lee¹⁵⁰, S.C. Lee¹⁵¹, L. Lee¹⁷⁵, M. Lefebvre¹⁶⁹, M. Legendre¹³⁶, A. Leger⁴⁹, B.C. LeGeyt¹²⁰, F. Legger⁹⁸, C. Leggett¹⁴, M. Lehmacher²⁰, G. Lehmann Miotto²⁹, M. Lehto¹³⁹, X. Lei⁶, M.A.L. Leite^{23b}, R. Leitner¹²⁶, D. Lellouch¹⁷¹, J. Lellouch⁷⁸, M. Leltchouk³⁴, V. Lendermann^{58a}, K.J.C. Leney^{145b}, T. Lenz¹⁷⁴, G. Lenzen¹⁷⁴, B. Lenzi¹³⁶, K. Leonhardt⁴³, S. Leontsinis⁹, J. Lepidis¹⁷⁴, C. Leroy⁹³, J.-R. Lessard¹⁶⁹, J. Lesser^{146a}, C.G. Lester²⁷,

- A. Leung Fook Cheong¹⁷², J. Levêque⁸³, D. Levin⁸⁷, L.J. Levinson¹⁷¹, M.S. Levitski¹²⁸, M. Lewandowska²¹, M. Leyton¹⁵, B. Li⁸³, H. Li¹⁷², S. Li^{32b}, X. Li⁸⁷, Z. Liang³⁹, Z. Liang^{118,r}, B. Liberti^{133a}, P. Lichard²⁹, M. Lichtnecker⁹⁸, K. Lie¹⁶⁵, W. Liebig¹³, R. Lifshitz¹⁵², J.N. Lilley¹⁷, H. Lim⁵, A. Limosani⁸⁶, M. Limper⁶³, S.C. Lin^{151,s}, F. Linde¹⁰⁵, J.T. Linnemann⁸⁸, E. Lipeles¹²⁰, L. Lipinsky¹²⁵, A. Lipniacka¹³, T.M. Liss¹⁶⁵, A. Lister⁴⁹, A.M. Litke¹³⁷, C. Liu²⁸, D. Liu^{151,t}, H. Liu⁸⁷, J.B. Liu⁸⁷, M. Liu^{32b}, S. Liu², Y. Liu^{32b}, M. Livan^{119a,119b}, S.S.A. Livermore¹¹⁸, A. Lleres⁵⁵, S.L. Lloyd⁷⁵, E. Lobodzinska⁴¹, P. Loch⁶, W.S. Lockman¹³⁷, S. Lockwitz¹⁷⁵, T. Loddenkoetter²⁰, F.K. Loebinger⁸², A. Loginov¹⁷⁵, C.W. Loh¹⁶⁸, T. Lohse¹⁵, K. Lohwasser⁴⁸, M. Lokajicek¹²⁵, J. Loken¹¹⁸, V.P. Lombardo^{89a,89b}, R.E. Long⁷¹, L. Lopes^{124a,b}, D. Lopez Mateos^{34,m}, M. Losada¹⁶², P. Loscutoff¹⁴, F. Lo Sterzo^{132a,132b}, M.J. Losty^{159a}, X. Lou⁴⁰, A. Louinis¹¹⁵, K.F. Loureiro¹⁶², J. Love²¹, P.A. Love⁷¹, A.J. Lowe¹⁴³, F. Lu^{32a}, J. Lu², L. Lu³⁹, H.J. Lubatti¹³⁸, C. Luci^{132a,132b}, A. Lucotte⁵⁵, A. Ludwig⁴³, D. Ludwig⁴¹, I. Ludwig⁴⁸, J. Ludwig⁴⁸, F. Luehring⁶¹, G. Luijckx¹⁰⁵, D. Lumb⁴⁸, L. Luminari^{132a}, E. Lund¹¹⁷, B. Lund-Jensen¹⁴⁷, B. Lundberg⁷⁹, J. Lundberg²⁹, J. Lundquist³⁵, M. Lungwitz⁸¹, A. Lupi^{122a,122b}, G. Lutz⁹⁹, D. Lynn²⁴, J. Lynn¹¹⁸, J. Lys¹⁴, E. Lytken⁷⁹, H. Ma²⁴, L.L. Ma¹⁷², M. Maaßen⁴⁸, J.A. Macana Goia⁹³, G. Maccarrone⁴⁷, A. Macchiolo⁹⁹, B. Maček⁷⁴, J. Machado Miguens^{124a,b}, D. Macina⁴⁹, R. Mackeprang³⁵, R.J. Madaras¹⁴, W.F. Mader⁴³, R. Maenner^{58c}, T. Maeno²⁴, P. Mättig¹⁷⁴, S. Mättig⁴¹, P.J. Magalhaes Martins^{124a,f}, L. Magnoni²⁹, E. Magradze⁵¹, C.A. Magrath¹⁰⁴, Y. Mahalalel¹⁵³, K. Mahboubi⁴⁸, G. Mahout¹⁷, C. Maiami^{132a,132b}, C. Maidantchik^{23a}, A. Maio^{124a,l}, S. Majewski²⁴, Y. Makida⁶⁶, N. Makovec¹¹⁵, P. Mal⁶, Pa. Malecki³⁸, P. Malecki³⁸, V.P. Maleev¹²¹, F. Malek⁵⁵, U. Mallik⁶³, D. Malon⁵, S. Maltezos⁹, V. Malyshev¹⁰⁷, S. Malyukov⁶⁵, R. Mameghani⁹⁸, J. Mamuzic^{12b}, A. Manabe⁶⁶, L. Mandelli^{89a}, I. Mandić⁷⁴, R. Mandrysch¹⁵, J. Maneira^{124a}, P.S. Mangeard⁸⁸, M. Mangin-Brinet⁴⁹, I.D. Manjavidze⁶⁵, A. Mann⁵⁴, W.A. Mann¹⁶¹, P.M. Manning¹³⁷, A. Manousakis-Katsikakis⁸, B. Mansoulie¹³⁶, A. Manz⁹⁹, A. Mapelli²⁹, L. Mapelli²⁹, L. March⁸⁰, J.F. Marchand²⁹, F. Marchese^{133a,133b}, M. Marchesotti²⁹, G. Marchiori⁷⁸, M. Marcisovsky¹²⁵, A. Marin^{21,*}, C.P. Marino⁶¹, F. Marroquin^{23a}, R. Marshall⁸², Z. Marshall^{34,m}, F.K. Martens¹⁵⁸, S. Marti-Garcia¹⁶⁷, A.J. Martin¹⁷⁵, B. Martin²⁹, B. Martin⁸⁸, F.F. Martin¹²⁰, J.P. Martin⁹³, Ph. Martin⁵⁵, T.A. Martin¹⁷, B. Martin dit Latour⁴⁹, M. Martinez¹¹, V. Martinez Outschoorn⁵⁷, A.C. Martyniuk⁸², M. Marx⁸², F. Marzano^{132a}, A. Marzin¹¹¹, L. Masetti⁸¹, T. Mashimo¹⁵⁵, R. Mashinistov⁹⁴, J. Maslik⁸², A.L. Maslennikov¹⁰⁷, M. Maß⁴², I. Massa^{19a,19b}, G. Massaro¹⁰⁵, N. Massol⁴, A. Mastroberardino^{36a,36b}, T. Masubuchi¹⁵⁵, M. Mathes²⁰, P. Matrimon¹¹⁵, H. Matsumoto¹⁵⁵, H. Matsumaga¹⁵⁵, T. Matsushita⁶⁷, C. Mattravers^{118,u}, J.M. Maugain²⁹, S.J. Maxfield⁷³, E.N. May⁵, A. Mayne¹³⁹, R. Mazini¹⁵¹, M. Mazur²⁰, M. Mazzanti^{89a}, E. Mazzoni^{122a,122b}, S.P. Mc Kee⁸⁷, A. McCarn¹⁶⁵, R.L. McCarthy¹⁴⁸, T.G. McCarthy²⁸, N.A. McCubbin¹²⁹, K.W. McFarlane⁵⁶, J.A. McFayden¹³⁹, S. McGarvie⁷⁶, H. McGlone⁵³, G. Mchedlidze⁵¹, R.A. McLaren²⁹, T. McLaughlan¹⁷, S.J. McMahon¹²⁹, T.R. McMahon⁷⁶, T.J. McMahon¹⁷, R.A. McPherson^{169,h}, A. Meade⁸⁴, J. Mechelich¹⁰⁵, M. Mechtel¹⁷⁴, M. Medinnis⁴¹, R. Meera-Lebbai¹¹¹, T. Meguro¹¹⁶, R. Mehdiyev⁹³, S. Mehlhase⁴¹, A. Mehta⁷³, K. Meier^{58a}, J. Meinhardt⁴⁸, B. Meirose⁷⁹, C. Melachrinos³⁰, B.R. Mellado Garcia¹⁷², L. Mendoza Navas¹⁶², Z. Meng^{151,t}, A. Mengarelli^{19a,19b}, S. Menke⁹⁹, C. Menot²⁹, E. Meoni¹¹, D. Merkl⁹⁸, P. Mermod¹¹⁸, L. Merola^{102a,102b}, C. Meroni^{89a}, F.S. Merritt³⁰, A. Messina²⁹, J. Metcalfe¹⁰³, A.S. Mete⁶⁴, S. Meuser²⁰, C. Meyer⁸¹, J-P. Meyer¹³⁶, J. Meyer¹⁷³, J. Meyer⁵⁴, T.C. Meyer²⁹, W.T. Meyer⁶⁴, J. Miao^{32d}, S. Michal²⁹, L. Micu^{25a}, R.P. Middleton¹²⁹, P. Miele²⁹, S. Migas⁷³, A. Migliaccio^{102a,102b}, L. Mijovic⁴¹, G. Mikenberg¹⁷¹, M. Mikestikova¹²⁵, B. Mikulec⁴⁹, M. Mikuž⁷⁴, D.W. Miller¹⁴³, R.J. Miller⁸⁸, W.J. Mills¹⁶⁸, C. Mills⁵⁷, A. Milov¹⁷¹, D.A. Milstead^{146a,146b}, D. Milstein¹⁷¹, A.A. Minaenko¹²⁸, M. Miñano¹⁶⁷, I.A. Minashvili⁶⁵, A.I. Mincer¹⁰⁸, B. Mindur³⁷, M. Mineev⁶⁵, Y. Ming¹³⁰, L.M. Mir¹¹, G. Mirabelli^{132a}, L. Miralles Verge¹¹, A. Misiejuk⁷⁶, A. Mitra¹¹⁸, J. Mitrevski¹³⁷, G.Y. Mitrofanov¹²⁸, V.A. Mitsou¹⁶⁷, S. Mitsui⁶⁶, P.S. Miyagawa⁸², K. Miyazaki⁶⁷, J.U. Mjörnmark⁷⁹, T. Moa^{146a,146b}, P. Mockett¹³⁸, S. Moed⁵⁷, V. Moeller²⁷, K. Möning⁴¹, N. Möser²⁰, S. Mohapatra¹⁴⁸, B. Mohn¹³, W. Mohr⁴⁸, S. Mohrdieck-Möck⁹⁹, A.M. Moisseev^{128,*}, R. Moles-Valls¹⁶⁷, J. Molina-Perez²⁹, L. Moneta⁴⁹, J. Monk⁷⁷, E. Monnier⁸³, S. Montesano^{89a,89b}, F. Monticelli⁷⁰, S. Monzani^{19a,19b}, R.W. Moore², G.F. Moorhead⁸⁶, C. Mora Herrera⁴⁹, A. Moraes⁵³, A. Morais^{124a,b}, N. Morange¹³⁶, J. Morel⁵⁴, G. Morello^{36a,36b}, D. Moreno⁸¹, M. Moreno Llácer¹⁶⁷, P. Morettini^{50a}, M. Morii⁵⁷, J. Morin⁷⁵, Y. Morita⁶⁶, A.K. Morley²⁹, G. Mornacchi²⁹, M-C. Morone⁴⁹, J.D. Morris⁷⁵, H.G. Moser⁹⁹, M. Mosidze⁵¹, J. Moss¹⁰⁹, R. Mount¹⁴³, E. Mountricha⁹, S.V. Mouraviev⁹⁴, T.H. Moye¹⁷, E.J.W. Moyse⁸⁴, M. Mudrinic^{12b}, F. Mueller^{58a}, J. Mueller¹²³, K. Mueller²⁰, T.A. Müller⁹⁸, D. Muenstermann⁴², A. Muijs¹⁰⁵, A. Muir¹⁶⁸, Y. Munwes¹⁵³, K. Murakami⁶⁶, W.J. Murray¹²⁹, I. Mussche¹⁰⁵, E. Musto^{102a,102b}, A.G. Myagkov¹²⁸, M. Myska¹²⁵, J. Nadal¹¹, K. Nagai¹⁶⁰, K. Nagano⁶⁶, Y. Nagasaka⁶⁰, A.M. Nairz²⁹, Y. Nakahama¹¹⁵, K. Nakamura¹⁵⁵, I. Nakano¹¹⁰, G. Nanava²⁰, A. Napier¹⁶¹, M. Nash^{77,u}, I. Nasteva⁸², N.R. Nation²¹, T. Nattermann²⁰, T. Naumann⁴¹, F. Nauyock⁸², G. Navarro¹⁶², H.A. Neal⁸⁷, E. Nebot⁸⁰, P.Yu. Nechaeva⁹⁴, A. Negri^{119a,119b}, G. Negri²⁹, S. Nektarjevic⁴⁹, A. Nelson⁶⁴, S. Nelson¹⁴³, T.K. Nelson¹⁴³, S. Nemecek¹²⁵, P. Nemethy¹⁰⁸, A.A. Nepomuceno^{23a}, M. Nessi²⁹, S.Y. Nesterov¹²¹, M.S. Neubauer¹⁶⁵, L. Neukermans⁴, A. Neusiedl⁸¹, R.M. Neves¹⁰⁸, P. Nevski²⁴, P.R. Newman¹⁷, C. Nicholson⁵³, R.B. Nickerson¹¹⁸, R. Nicolaïdou¹³⁶, L. Nicolas¹³⁹, B. Nicquevert²⁹, F. Niedercorn¹¹⁵, J. Nielsen¹³⁷, T. Niinikoski²⁹, A. Nikiforov¹⁵, V. Nikolaenko¹²⁸, K. Nikolaev⁶⁵, I. Nikolic-Audit⁷⁸, K. Nikolopoulos²⁴, H. Nilsen⁴⁸, P. Nilsson⁷, Y. Ninomiya¹⁵⁵, A. Nisati^{132a}, T. Nishiyama⁶⁷, R. Nisius⁹⁹,

- L. Nodulman⁵, M. Nomachi¹¹⁶, I. Nomidis¹⁵⁴, H. Nomoto¹⁵⁵, M. Nordberg²⁹, B. Nordkvist^{146a,146b}, O. Norniella Francisco¹¹, P.R. Norton¹²⁹, J. Novakova¹²⁶, M. Nozaki⁶⁶, M. Nožička⁴¹, I.M. Nugent^{159a}, A.-E. Nuncio-Quiroz²⁰, G. Nunes Hanninger²⁰, T. Nunnemann⁹⁸, E. Nurse⁷⁷, T. Nyman²⁹, B.J. O'Brien⁴⁵, S.W. O'Neale^{17,*}, D.C. O'Neil¹⁴², V. O'Shea⁵³, F.G. Oakham^{28,d}, H. Oberlack⁹⁹, J. Ocariz⁷⁸, A. Ochi⁶⁷, S. Oda¹⁵⁵, S. Odaka⁶⁶, J. Odier⁸³, G.A. Odino^{50a,50b}, H. Ogren⁶¹, A. Oh⁸², S.H. Oh⁴⁴, C.C. Ohm^{146a,146b}, T. Ohshima¹⁰¹, H. Ohshita¹⁴⁰, T.K. Ohska⁶⁶, T. Ohsugi⁵⁹, S. Okada⁶⁷, H. Okawa¹⁶³, Y. Okumura¹⁰¹, T. Okuyama¹⁵⁵, M. Olcese^{50a}, A.G. Olchevski⁶⁵, M. Oliveira^{124a,f}, D. Oliveira Damazio²⁴, C. Oliver⁸⁰, E. Oliver Garcia¹⁶⁷, D. Olivito¹²⁰, A. Olszewski³⁸, J. Olszowska³⁸, C. Omachi⁶⁷, A. Onofre^{124a,v}, P.U.E. Onyisi³⁰, C.J. Oram^{159a}, G. Ordonez¹⁰⁴, M.J. Oreglia³⁰, F. Orellana⁴⁹, Y. Oren¹⁵³, D. Orestano^{134a,134b}, I. Orlov¹⁰⁷, C. Oropeza Barrera⁵³, R.S. Orr¹⁵⁸, E.O. Ortega¹³⁰, B. Osculati^{50a,50b}, R. Ospanov¹²⁰, C. Osuna¹¹, G. Otero y Garzon²⁶, J.P. Ottersbach¹⁰⁵, B. Ottewell¹¹⁸, M. Ouchrif^{135c}, F. Ould-Saada¹¹⁷, A. Ouraou¹³⁶, Q. Ouyang^{32a}, M. Owen⁸², S. Owen¹³⁹, A. Oyarzun^{31b}, O.K. Øye¹³, V.E. Ozcan⁷⁷, N. Ozturk⁷, A. Pacheco Pages¹¹, C. Padilla Aranda¹¹, E. Paganis¹³⁹, F. Paige²⁴, K. Pajchel¹¹⁷, S. Palestini²⁹, D. Pallin³³, A. Palma^{124a,b}, J.D. Palmer¹⁷, M.J. Palmer²⁷, Y.B. Pan¹⁷², E. Panagiotopoulou⁹, B. Panes^{31a}, N. Panikashvili⁸⁷, S. Panitkin²⁴, D. Pantea^{25a}, M. Panuskova¹²⁵, V. Paolone¹²³, A. Paoloni^{133a,133b}, A. Papadelis^{146a}, Th.D. Papadopoulou⁹, A. Paramonov⁵, S.J. Park⁵⁴, W. Park^{24,w}, M.A. Parker²⁷, F. Parodi^{50a,50b}, J.A. Parsons³⁴, U. Parzefall⁴⁸, E. Pasqualucci^{132a}, A. Passeri^{134a}, F. Pastore^{134a,134b}, Fr. Pastore²⁹, G. Pásztor^{49,x}, S. Pataraia¹⁷², N. Patel¹⁵⁰, J.R. Pater⁸², S. Patricelli^{102a,102b}, T. Pauly²⁹, M. Pecsý^{144a}, M.I. Pedraza Morales¹⁷², S.J.M. Peeters¹⁰⁵, S.V. Peleganchuk¹⁰⁷, H. Peng¹⁷², R. Pengo²⁹, A. Penson³⁴, J. Penwell⁶¹, M. Perantoni^{23a}, K. Perez^{34,m}, T. Perez Cavalcanti⁴¹, E. Perez Codina¹¹, M.T. Pérez García-Estañ¹⁶⁷, V. Perez Reale³⁴, I. Peric²⁰, L. Perini^{89a,89b}, H. Pernegger²⁹, R. Perrino^{72a}, P. Perrodo⁴, S. Perseme^{3a}, P. Perus¹¹⁵, V.D. Peshekhanov⁶⁵, E. Petereit⁵, O. Peters¹⁰⁵, B.A. Petersen²⁹, J. Petersen²⁹, T.C. Petersen³⁵, E. Petit⁸³, A. Petridis¹⁵⁴, C. Petridou¹⁵⁴, E. Petrolo^{132a}, F. Petrucci^{134a,134b}, D. Petschull⁴¹, M. Petteni¹⁴², R. Pezoa^{31b}, A. Phan⁸⁶, A.W. Phillips²⁷, P.W. Phillips¹²⁹, G. Piacquadio²⁹, E. Piccaro⁷⁵, M. Piccinini^{19a,19b}, A. Pickford⁵³, R. Piegaia²⁶, J.E. Pilcher³⁰, A.D. Pilkington⁸², J. Pina^{124a,l}, M. Pinamonti^{164a,164c}, A. Pinder¹¹⁸, J.L. Pinfold², J. Ping^{32c}, B. Pinto^{124a,b}, O. Pirotte²⁹, C. Pizio^{89a,89b}, R. Placakyte⁴¹, M. Plamondon¹⁶⁹, W.G. Plano⁸², M.-A. Pleier²⁴, A.V. Pleskach¹²⁸, A. Poblagev²⁴, S. Poddar^{58a}, F. Podlyski³³, L. Poggioli¹¹⁵, T. Poghosyan²⁰, M. Pohl⁴⁹, F. Polci⁵⁵, G. Polesello^{119a}, A. Policicchio¹³⁸, A. Polini^{19a}, J. Poll⁷⁵, V. Polychronakos²⁴, D.M. Pomareda¹³⁶, D. Pomeroy²², K. Pommès²⁹, L. Pontecorvo^{132a}, B.G. Pope⁸⁸, G.A. Popenciu^{25a}, D.S. Popovic^{12a}, A. Poppleton²⁹, X. Portell Bueso⁴⁸, R. Porter¹⁶³, C. Posch²¹, G.E. Pospelov⁹⁹, S. Pospisil¹²⁷, I.N. Potrap⁹⁹, C.J. Potter¹⁴⁹, C.T. Potter⁸⁵, G. Poulard²⁹, J. Poveda¹⁷², R. Prabhu⁷⁷, P. Pralavorio⁸³, S. Prasad⁵⁷, R. Pravahan⁷, S. Prell⁶⁴, K. Pretzl¹⁶, L. Pribyl²⁹, D. Price⁶¹, L.E. Price⁵, M.J. Price²⁹, P.M. Prichard⁷³, D. Prieur¹²³, M. Primavera^{72a}, K. Prokofiev²⁹, F. Prokoshin^{31b}, S. Protopopescu²⁴, J. Proudfoot⁵, X. Prudent⁴³, H. Przysiezniak⁴, S. Psoroulas²⁰, E. Ptacek¹¹⁴, J. Purdham⁸⁷, M. Purohit^{24,w}, P. Puzo¹¹⁵, Y. Pylypchenko¹¹⁷, J. Qian⁸⁷, Z. Qian⁸³, Z. Qin⁴¹, A. Quadt⁵⁴, D.R. Quarrie¹⁴, W.B. Quayle¹⁷², F. Quinonez^{31a}, M. Raas¹⁰⁴, V. Radescu^{58b}, B. Radics²⁰, T. Rador^{18a}, F. Ragusa^{89a,89b}, G. Rahal¹⁷⁷, A.M. Rahimi¹⁰⁹, S. Rajagopalan²⁴, S. Rajek⁴², M. Rammensee⁴⁸, M. Rammes¹⁴¹, M. Ramstedt^{146a,146b}, K. Randrianarivony²⁸, P.N. Ratoff⁷¹, F. Rauscher⁹⁸, E. Rauter⁹⁹, M. Raymond²⁹, A.L. Read¹¹⁷, D.M. Rebuzzi^{119a,119b}, A. Redelbach¹⁷³, G. Redlinger²⁴, R. Reece¹²⁰, K. Reeves⁴⁰, A. Reichold¹⁰⁵, E. Reinherz-Aronis¹⁵³, A. Reinsch¹¹⁴, I. Reisinger⁴², D. Reljic^{12a}, C. Rembser²⁹, Z.L. Ren¹⁵¹, A. Renaud¹¹⁵, P. Renkel³⁹, B. Rensch³⁵, M. Rescigno^{132a}, S. Resconi^{89a}, B. Resende¹³⁶, P. Reznicek⁹⁸, R. Rezvani¹⁵⁸, A. Richards⁷⁷, R. Richter⁹⁹, E. Richter-Was^{38,y}, M. Ridel⁷⁸, S. Rieke⁸¹, M. Rijpstra¹⁰⁵, M. Rijssenbeek¹⁴⁸, A. Rimoldi^{119a,119b}, L. Rinaldi^{19a}, R.R. Rios³⁹, I. Riu¹¹, G. Rivoltella^{89a,89b}, F. Rizatdinova¹¹², E. Rizvi⁷⁵, S.H. Robertson^{85,h}, A. Robichaud-Veronneau⁴⁹, D. Robinson²⁷, J.E.M. Robinson⁷⁷, M. Robinson¹¹⁴, A. Robson⁵³, J.G. Rocha de Lima¹⁰⁶, C. Roda^{122a,122b}, D. Roda Dos Santos²⁹, S. Rodier⁸⁰, D. Rodriguez¹⁶², Y. Rodriguez Garcia¹⁵, A. Roe⁵⁴, S. Roe²⁹, O. Røhne¹¹⁷, V. Rojo¹, S. Rolli¹⁶¹, A. Romanouk⁹⁶, V.M. Romanov⁶⁵, G. Romeo²⁶, D. Romero Maltrana^{31a}, L. Roos⁷⁸, E. Ros¹⁶⁷, S. Rosati¹³⁸, M. Rose⁷⁶, G.A. Rosenbaum¹⁵⁸, E.I. Rosenberg⁶⁴, P.L. Rosendahl¹³, L. Rosselet⁴⁹, V. Rossetti¹¹, E. Rossi^{102a,102b}, L.P. Rossi^{50a}, L. Rossi^{89a,89b}, M. Rotaru^{25a}, I. Roth¹⁷¹, J. Rothberg¹³⁸, I. Rottländer²⁰, D. Rousseau¹¹⁵, C.R. Royon¹³⁶, A. Rozanov⁸³, Y. Rozen¹⁵², X. Ruan¹¹⁵, I. Rubinskiy⁴¹, B. Ruckert⁹⁸, N. Ruckstuhl¹⁰⁵, V.I. Rud⁹⁷, G. Rudolph⁶², F. Rühr⁶, A. Ruiz-Martinez⁶⁴, E. Rulikowska-Zarebska³⁷, V. Rumiantsev^{91,*}, L. Rumyantsev⁶⁵, K. Runge⁴⁸, O. Runolfsson²⁰, Z. Rurikova⁴⁸, N.A. Rusakovich⁶⁵, D.R. Rust⁶¹, J.P. Rutherford⁶, C. Ruwiedel¹⁴, P. Ruzicka¹²⁵, Y.F. Ryabov¹²¹, V. Ryadovikov¹²⁸, P. Ryan⁸⁸, M. Rybar¹²⁶, G. Rybkin¹¹⁵, N.C. Ryder¹¹⁸, S. Rzaeva¹⁰, A.F. Saavedra¹⁵⁰, I. Sadeh¹⁵³, H.F.-W. Sadrozinski¹³⁷, R. Sadykov⁶⁵, F. Safai Tehrani^{132a,132b}, H. Sakamoto¹⁵⁵, G. Salamanna¹⁰⁵, A. Salamon^{133a}, M. Saleem¹¹¹, D. Salihagic⁹⁹, A. Salnikov¹⁴³, J. Salt¹⁶⁷, B.M. Salvachua Ferrando⁵, D. Salvatore^{36a,36b}, F. Salvatore¹⁴⁹, A. Salzburger²⁹, D. Sampsonidis¹⁵⁴, B.H. Samset¹¹⁷, H. Sandaker¹³, H.G. Sander⁸¹, M.P. Sanders⁹⁸, M. Sandhoff¹⁷⁴, P. Sandhu¹⁵⁸, T. Sandoval²⁷, R. Sandstroem¹⁰⁵, S. Sandvoss¹⁷⁴, D.P.C. Sankey¹²⁹, A. Sansoni⁴⁷, C. Santamarina Rios⁸⁵, C. Santoni³³, R. Santonico^{133a,133b}, H. Santos^{124a}, J.G. Saraiva^{124a,l}, T. Sarangi¹⁷², E. Sarkisyan-Grinbaum⁷, F. Sarri^{122a,122b}, G. Sartisohn¹⁷⁴, O. Sasaki⁶⁶, T. Sasaki⁶⁶, N. Sasao⁶⁸, I. Satsounkevitch⁹⁰, G. Sauvage⁴, J.B. Sauvan¹¹⁵, P. Savard^{158,d},

- V. Savinov¹²³, P. Savva⁹, L. Sawyer^{24,i}, D.H. Saxon⁵³, L.P. Says³³, C. Sbarra^{19a,19b}, A. Sbrizzi^{19a,19b}, O. Scallon⁹³, D.A. Scannicchio¹⁶³, J. Schaarschmidt⁴³, P. Schacht⁹⁹, U. Schäfer⁸¹, S. Schatzel^{58b}, A.C. Schaffer¹¹⁵, D. Schaile⁹⁸, R.D. Schamberger¹⁴⁸, A.G. Schamov¹⁰⁷, V. Scharf^{58a}, V.A. Schegelsky¹²¹, D. Scheirich⁸⁷, M.I. Scherzer¹⁴, C. Schiavi^{50a,50b}, J. Schieck⁹⁸, M. Schioppa^{36a,36b}, S. Schlenker²⁹, J.L. Schlereth⁵, E. Schmidt⁴⁸, M.P. Schmidt^{175,*}, K. Schmieden²⁰, C. Schmitt⁸¹, M. Schmitz²⁰, A. Schöning^{58b}, M. Schott²⁹, D. Schouten¹⁴², J. Schovancova¹²⁵, M. Schram⁸⁵, A. Schreiner⁶³, C. Schroeder⁸¹, N. Schroer^{58c}, S. Schuh²⁹, G. Schuler²⁹, J. Schultes¹⁷⁴, H.-C. Schultz-Coulon^{58a}, H. Schulz¹⁵, J.W. Schumacher²⁰, M. Schumacher⁴⁸, B.A. Schumm¹³⁷, Ph. Schune¹³⁶, C. Schwanenberger⁸², A. Schwartzman¹⁴³, D. Schweiger²⁹, Ph. Schwemling⁷⁸, R. Schwienhorst⁸⁸, R. Schwierz⁴³, J. Schwindling¹³⁶, W.G. Scott¹²⁹, J. Searcy¹¹⁴, E. Sedykh¹²¹, E. Segura¹¹, S.C. Seidel¹⁰³, A. Seiden¹³⁷, F. Seifert⁴³, J.M. Seixas^{23a}, G. Sekhniaidze^{102a}, D.M. Seliverstov¹²¹, B. Sellden^{146a}, G. Sellers⁷³, M. Seman^{144b}, N. Semprini-Cesari^{19a,19b}, C. Serfon⁹⁸, L. Serin¹¹⁵, R. Seuster⁹⁹, H. Severini¹¹¹, M.E. Sevior⁸⁶, A. Sfyrla²⁹, E. Shabalina⁵⁴, M. Shamim¹¹⁴, L.Y. Shan^{32a}, J.T. Shank²¹, Q.T. Shao⁸⁶, M. Shapiro¹⁴, P.B. Shatalov⁹⁵, L. Shaver⁶, C. Shaw⁵³, K. Shaw^{164a,164c}, D. Sherman¹⁷⁵, P. Sherwood⁷⁷, A. Shibata¹⁰⁸, S. Shimizu²⁹, M. Shimojima¹⁰⁰, T. Shin⁵⁶, A. Shmeleva⁹⁴, M.J. Shochet³⁰, D. Short¹¹⁸, M.A. Shupe⁶, P. Sicho¹²⁵, A. Sidoti¹⁵, A. Siebel¹⁷⁴, F. Siegert⁴⁸, J. Siegrist¹⁴, Dj. Sijacki^{12a}, O. Silbert¹⁷¹, J. Silva^{124a,z}, Y. Silver¹⁵³, D. Silverstein¹⁴³, S.B. Silverstein^{146a}, V. Simak¹²⁷, Lj. Simic^{12a}, S. Simion¹¹⁵, B. Simmons⁷⁷, M. Simonyan³⁵, P. Sinervo¹⁵⁸, N.B. Sinev¹¹⁴, V. Sipica¹⁴¹, G. Siragusa⁸¹, A.N. Sisakyan⁶⁵, S.Yu. Sivoklokov⁹⁷, J. Sjölin^{146a,146b}, T.B. Sjursen¹³, L.A. Skinnari¹⁴, K. Skovpen¹⁰⁷, P. Skubic¹¹¹, N. Skvorodnev²², M. Slater¹⁷, T. Slavicek¹²⁷, K. Sliwa¹⁶¹, T.J. Sloan⁷¹, J. Sloper²⁹, V. Smakhtin¹⁷¹, S.Yu. Smirnov⁹⁶, L.N. Smirnova⁹⁷, O. Smirnova⁷⁹, B.C. Smith⁵⁷, D. Smith¹⁴³, K.M. Smith⁵³, M. Smizanska⁷¹, K. Smolek¹²⁷, A.A. Snesarev⁹⁴, S.W. Snow⁸², J. Snow¹¹¹, J. Snuverink¹⁰⁵, S. Snyder²⁴, M. Soares^{124a}, R. Sobie^{169,h}, J. Sodomka¹²⁷, A. Soffer¹⁵³, C.A. Solans¹⁶⁷, M. Solar¹²⁷, J. Solc¹²⁷, U. Soldevila¹⁶⁷, E. Solfaroli Camillocci^{132a,132b}, A.A. Solodkov¹²⁸, O.V. Solovyanov¹²⁸, J. Sondericker²⁴, N. Soni², V. Sopko¹²⁷, B. Sopko¹²⁷, M. Sorbi^{89a,89b}, M. Sosebee⁷, A. Soukharev¹⁰⁷, S. Spagnolo^{72a,72b}, F. Spanò³⁴, R. Spighi^{19a}, G. Spigo²⁹, F. Spila^{132a,132b}, E. Spiriti^{134a}, R. Spiwoks²⁹, M. Spousta¹²⁶, T. Spreitzer¹⁵⁸, B. Spurlock⁷, R.D. St. Denis⁵³, T. Stahl¹⁴¹, J. Stahlman¹²⁰, R. Stamen^{58a}, E. Stanecka²⁹, R.W. Stanek⁵, C. Stanescu^{134a}, S. Stapnes¹¹⁷, E.A. Starchenko¹²⁸, J. Stark⁵⁵, P. Staroba¹²⁵, P. Starovoitov⁹¹, A. Staude⁹⁸, P. Stavina^{144a}, G. Stavropoulos¹⁴, G. Steele⁵³, E. Stefanidis⁷⁷, P. Steinbach⁴³, P. Steinberg²⁴, I. Stekl¹²⁷, B. Stelzer¹⁴², H.J. Stelzer⁴¹, O. Stelzer-Chilton^{159a}, H. Stenzel⁵², K. Stevenson⁷⁵, G.A. Stewart⁵³, T. Stockmanns²⁰, M.C. Stockton²⁹, M. Stodulski³⁸, K. Stoerig⁴⁸, G. Stoica^{25a}, S. Stonjek⁹⁹, P. Strachota¹²⁶, A.R. Stradling⁷, A. Straessner⁴³, J. Strandberg⁸⁷, S. Strandberg^{146a,146b}, A. Strandlie¹¹⁷, M. Strang¹⁰⁹, E. Strauss¹⁴³, M. Strauss¹¹¹, P. Strizenec^{144b}, R. Ströhmer¹⁷³, D.M. Strom¹¹⁴, J.A. Strong^{76,*}, R. Stroynowski³⁹, J. Strube¹²⁹, B. Stugu¹³, I. Stumer^{24,*}, J. Stupak¹⁴⁸, P. Sturm¹⁷⁴, D.A. Soh^{151,r}, D. Su¹⁴³, S. Subramania², Y. Sugaya¹¹⁶, T. Sugimoto¹⁰¹, C. Suhr¹⁰⁶, K. Suita⁶⁷, M. Suk¹²⁶, V.V. Sulin⁹⁴, S. Sultansoy^{3d}, T. Sumida²⁹, X. Sun⁵⁵, J.E. Sundermann⁴⁸, K. Suruliz^{164a,164b}, S. Sushkov¹¹, G. Susinno^{36a,36b}, M.R. Sutton¹³⁹, Y. Suzuki⁶⁶, Yu.M. Sviridov¹²⁸, S. Swedish¹⁶⁸, I. Sykora^{144a}, T. Sykora¹²⁶, B. Szeless²⁹, J. Sánchez¹⁶⁷, D. Ta¹⁰⁵, K. Tackmann²⁹, A. Taffard¹⁶³, R. Tafirout^{159a}, A. Taga¹¹⁷, N. Taiblum¹⁵³, Y. Takahashi¹⁰¹, H. Takai²⁴, R. Takashima⁶⁹, H. Takeda⁶⁷, T. Takeshita¹⁴⁰, M. Talby⁸³, A. Talyshев¹⁰⁷, M.C. Tamsett²⁴, J. Tanaka¹⁵⁵, R. Tanaka¹¹⁵, S. Tanaka¹³¹, S. Tanaka⁶⁶, Y. Tanaka¹⁰⁰, K. Tami⁶⁷, N. Tannoury⁸³, G.P. Tappern²⁹, S. Tapprogge⁸¹, D. Tardif¹⁵⁸, S. Tarem¹⁵², F. Tarrade²⁴, G.F. Tartarelli^{89a}, P. Tas¹²⁶, M. Tasevsky¹²⁵, E. Tassi^{36a,36b}, M. Tatarkhanov¹⁴, C. Taylor⁷⁷, F.E. Taylor⁹², G. Taylor¹³⁷, G.N. Taylor⁸⁶, W. Taylor^{159b}, M. Teixeira Dias Castanheira⁷⁵, P. Teixeira-Dias⁷⁶, K.K. Temming⁴⁸, H. Ten Kate²⁹, P.K. Teng¹⁵¹, Y.D. Tennenbaum-Katan¹⁵², S. Terada⁶⁶, K. Terashi¹⁵⁵, J. Terron⁸⁰, M. Terwort^{41,p}, M. Testa⁴⁷, R.J. Teuscher^{158,h}, C.M. Tevlin⁸², J. Thadome¹⁷⁴, J. Therhaag²⁰, T. Theveneaux-Pelzer⁷⁸, M. Thiolye¹⁷⁵, S. Thoma⁴⁸, J.P. Thomas¹⁷, E.N. Thompson⁸⁴, P.D. Thompson¹⁷, P.D. Thompson¹⁵⁸, A.S. Thompson⁵³, E. Thomson¹²⁰, M. Thomson²⁷, R.P. Thun⁸⁷, T. Tic¹²⁵, V.O. Tikhomirov⁹⁴, Y.A. Tikhonov¹⁰⁷, C.J.W.P. Timmermans¹⁰⁴, P. Tipton¹⁷⁵, F.J. Tique Aires Viegas²⁹, S. Tisserant⁸³, J. Tobias⁴⁸, B. Toczek³⁷, T. Todorov⁴, S. Todorova-Nova¹⁶¹, B. Toggerson¹⁶³, J. Tojo⁶⁶, S. Tokár^{144a}, K. Tokunaga⁶⁷, K. Tokushuku⁶⁶, K. Tollefson⁸⁸, M. Tomoto¹⁰¹, L. Tompkins¹⁴, K. Toms¹⁰³, A. Tonazzo^{134a,134b}, G. Tong^{32a}, A. Tonoyan¹³, C. Topfel¹⁶, N.D. Topilin⁶⁵, I. Torchiani²⁹, E. Torrence¹¹⁴, E. Torró Pastor¹⁶⁷, J. Toth^{83,x}, F. Touchard⁸³, D.R. Tovey¹³⁹, D. Traynor⁷⁵, T. Trefzger¹⁷³, J. Treis²⁰, L. Tremblet²⁹, A. Tricoli²⁹, I.M. Trigger^{159a}, S. Trincaz-Duvold⁷⁸, T.N. Trinh⁷⁸, M.F. Tripiana⁷⁰, N. Triplett⁶⁴, W. Trischuk¹⁵⁸, A. Trivedi^{24,w}, B. Trocmé⁵⁵, C. Troncon^{89a}, M. Trottier-McDonald¹⁴², A. Trzupek³⁸, C. Tsarouchas²⁹, J.C-L. Tseng¹¹⁸, M. Tsiakiris¹⁰⁵, P.V. Tsiareshka⁹⁰, D. Tsionou⁴, G. Tsipolitis⁹, V. Tsiskaridze⁴⁸, E.G. Tskhadadze⁵¹, I.I. Tsukerman⁹⁵, V. Tsulaia¹²³, J.-W. Tsung²⁰, S. Tsuno⁶⁶, D. Tsybychev¹⁴⁸, A. Tua¹³⁹, J.M. Tuggle³⁰, M. Turala³⁸, D. Turecek¹²⁷, I. Turk Cakir^{3e}, E. Turlay¹⁰⁵, P.M. Tuts³⁴, A. Tykhonov⁷⁴, M. Tylmad^{146a,146b}, M. Tyndel¹²⁹, D. Typaldos¹⁷, H. Tyrvainen²⁹, G. Tzanakos⁸, K. Uchida²⁰, I. Ueda¹⁵⁵, R. Ueno²⁸, M. Ugland¹³, M. Uhlenbrock²⁰, M. Uhrmacher⁵⁴, F. Ukegawa¹⁶⁰, G. Unal²⁹, D.G. Underwood⁵, A. Undrus²⁴, G. Unel¹⁶³, Y. Unno⁶⁶, D. Urbaniec³⁴, E. Urkovsky¹⁵³, P. Urquijo⁴⁹, P. Urrejola^{31a}, G. Usai⁷, M. Uslenghi^{119a,119b}, L. Vacavant⁸³, V. Vacek¹²⁷, B. Vachon⁸⁵, S. Vahsen¹⁴, C. Valderanis⁹⁹, J. Valenta¹²⁵, P. Valente^{132a}, S. Valentinetto^{19a,19b}, S. Valkar¹²⁶,

E. Valladolid Gallego¹⁶⁷, S. Vallecorsa¹⁵², J.A. Valls Ferrer¹⁶⁷, H. van der Graaf¹⁰⁵, E. van der Kraaij¹⁰⁵, E. van der Poel¹⁰⁵, D. van der Ster²⁹, B. Van Eijk¹⁰⁵, N. van Eldik⁸⁴, P. van Gemmeren⁵, Z. van Kesteren¹⁰⁵, I. van Vulpen¹⁰⁵, W. Vandelli²⁹, G. Vandoni²⁹, A. Vaniachine⁵, P. Vankov⁴¹, F. Vannucci⁷⁸, F. Varela Rodriguez²⁹, R. Vari^{132a}, E.W. Varnes⁶, D. Varouchas¹⁴, A. Vartapetian⁷, K.E. Varvell¹⁵⁰, V.I. Vassilakopoulos⁵⁶, F. Vazeille³³, G. Vegni^{89a,89b}, J.J. Veillet¹¹⁵, C. Vellidis⁸, F. Veloso^{124a}, R. Veness²⁹, S. Veneziano^{132a}, A. Ventura^{72a,72b}, D. Ventura¹³⁸, S. Ventura⁴⁷, M. Venturi⁴⁸, N. Venturi¹⁶, V. Vercesi^{119a}, M. Verducci¹³⁸, W. Verkerke¹⁰⁵, J.C. Vermeulen¹⁰⁵, L. Vertogardov¹¹⁸, A. Vest⁴³, M.C. Vetterli^{142,d}, I. Vichou¹⁶⁵, T. Vickey^{145b,aa}, G.H.A. Viehhauser¹¹⁸, S. Viel¹⁶⁸, M. Villa^{19a,19b}, M. Villaplana Perez¹⁶⁷, E. Vilucchi⁴⁷, M.G. Vincter²⁸, E. Vinek²⁹, V.B. Vinogradov⁶⁵, M. Virchaux^{136,*}, S. Viret³³, J. Virzì¹⁴, A. Vitale^{19a,19b}, O. Vitells¹⁷¹, I. Vivarelli⁴⁸, F. Vives Vaque¹¹, S. Vlachos⁹, M. Vlasak¹²⁷, N. Vlasov²⁰, A. Vogel²⁰, P. Vokac¹²⁷, M. Volpi¹¹, G. Volpini^{89a}, H. von der Schmitt⁹⁹, J. von Loeben⁹⁹, H. von Radziewski⁴⁸, E. von Toerne²⁰, V. Vorobel¹²⁶, A.P. Vorobiev¹²⁸, V. Vorwerk¹¹, M. Vos¹⁶⁷, R. Voss²⁹, T.T. Voss¹⁷⁴, J.H. Vossebeld⁷³, A.S. Vovenko¹²⁸, N. Vranjes^{12a}, M. Vranjes Milosavljevic^{12a}, V. Vrba¹²⁵, M. Vreeswijk¹⁰⁵, T. Vu Anh⁸¹, R. Vuillermet²⁹, I. Vukotic¹¹⁵, W. Wagner¹⁷⁴, P. Wagner¹²⁰, H. Wahlen¹⁷⁴, J. Wakabayashi¹⁰¹, J. Walbersloh⁴², S. Walch⁸⁷, J. Walder⁷¹, R. Walker⁹⁸, W. Walkowiak¹⁴¹, R. Wall¹⁷⁵, P. Waller⁷³, C. Wang⁴⁴, H. Wang¹⁷², J. Wang^{32d}, J.C. Wang¹³⁸, S.M. Wang¹⁵¹, A. Warburton⁸⁵, C.P. Ward²⁷, M. Warsinsky⁴⁸, P.M. Watkins¹⁷, A.T. Watson¹⁷, M.F. Watson¹⁷, G. Watts¹³⁸, S. Watts⁸², A.T. Waugh¹⁵⁰, B.M. Waugh⁷⁷, J. Weber⁴², M. Weber¹²⁹, M.S. Weber¹⁶, P. Weber⁵⁴, A.R. Weidberg¹¹⁸, J. Weingarten⁵⁴, C. Weiser⁴⁸, H. Wellenstein²², P.S. Wells²⁹, M. Wen⁴⁷, T. Wenaus²⁴, S. Wendler¹²³, Z. Weng^{151,r}, T. Wengler²⁹, S. Wenig²⁹, N. Wermes²⁰, M. Werner⁴⁸, P. Werner²⁹, M. Werth¹⁶³, M. Wessels^{58a}, K. Whalen²⁸, S.J. Wheeler-Ellis¹⁶³, S.P. Whitaker²¹, A. White⁷, M.J. White⁸⁶, S. White²⁴, S.R. Whitehead¹¹⁸, D. Whiteson¹⁶³, D. Whittington⁶¹, F. Wicek¹¹⁵, D. Wicke¹⁷⁴, F.J. Wickens¹²⁹, W. Wiedenmann¹⁷², M. Wielers¹²⁹, P. Wienemann²⁰, C. Wiglesworth⁷³, L.A.M. Wiik⁴⁸, A. Wildauer¹⁶⁷, M.A. Wildt^{41,p}, I. Wilhelm¹²⁶, H.G. Wilkens²⁹, J.Z. Will⁹⁸, E. Williams³⁴, H.H. Williams¹²⁰, W. Willis³⁴, S. Willocq⁸⁴, J.A. Wilson¹⁷, M.G. Wilson¹⁴³, A. Wilson⁸⁷, I. Wingerter-Seez⁴, S. Winkelmann⁴⁸, F. Winklmeier²⁹, M. Wittgen¹⁴³, M.W. Wolter³⁸, H. Wolters^{124a,f}, G. Wooden¹¹⁸, B.K. Wosiek³⁸, J. Wotschack²⁹, M.J. Woudstra⁸⁴, K. Wraight⁵³, C. Wright⁵³, B. Wrona⁷³, S.L. Wu¹⁷², X. Wu⁴⁹, Y. Wu^{32b}, E. Wulf³⁴, R. Wunstorf⁴², B.M. Wynne⁴⁵, L. Xaplanteris⁹, S. Xella³⁵, S. Xie⁴⁸, Y. Xie^{32a}, C. Xu^{32b}, D. Xu¹³⁹, G. Xu^{32a}, B. Yabsley¹⁵⁰, M. Yamada⁶⁶, A. Yamamoto⁶⁶, K. Yamamoto⁶⁴, S. Yamamoto¹⁵⁵, T. Yamamura¹⁵⁵, J. Yamaoka⁴⁴, T. Yamazaki¹⁵⁵, Y. Yamazaki⁶⁷, Z. Yan²¹, H. Yang⁸⁷, S. Yang¹¹⁸, U.K. Yang⁸², Y. Yang⁶¹, Y. Yang^{32a}, Z. Yang^{146a,146b}, S. Yanush⁹¹, W-M. Yao¹⁴, Y. Yao¹⁴, Y. Yasu⁶⁶, J. Ye³⁹, S. Ye²⁴, M. Yilmaz^{3c}, R. Yoosoofmiya¹²³, K. Yorita¹⁷⁰, R. Yoshida⁵, C. Young¹⁴³, S. Youssef²¹, D. Yu²⁴, J. Yu⁷, J. Yu^{32c,ab}, L. Yuan^{32a,ac}, A. Yurkewicz¹⁴⁸, V.G. Zaets¹²⁸, R. Zaidan⁶³, A.M. Zaitsev¹²⁸, Z. Zajacova²⁹, Yo.K. Zalite¹²¹, L. Zanello^{132a,132b}, P. Zarzhitsky³⁹, A. Zaytsev¹⁰⁷, M. Zdrrazil¹⁴, C. Zeitnitz¹⁷⁴, M. Zeller¹⁷⁵, P.F. Zema²⁹, A. Zemla³⁸, C. Zendler²⁰, A.V. Zenin¹²⁸, O. Zenin¹²⁸, T. Ženiš^{144a}, Z. Zenonos^{122a,122b}, S. Zenz¹⁴, D. Zerwas¹¹⁵, G. Zevi della Porta⁵⁷, Z. Zhan^{32d}, D. Zhang^{32b}, H. Zhang⁸⁸, J. Zhang⁵, X. Zhang^{32d}, Z. Zhang¹¹⁵, L. Zhao¹⁰⁸, T. Zhao¹³⁸, Z. Zhao^{32b}, A. Zhemchugov⁶⁵, S. Zheng^{32a}, J. Zhong^{151,ad}, B. Zhou⁸⁷, N. Zhou¹⁶³, Y. Zhou¹⁵¹, C.G. Zhu^{32d}, H. Zhu⁴¹, Y. Zhu¹⁷², X. Zhuang⁹⁸, V. Zhuravlov⁹⁹, D. Ziemińska⁶¹, B. Zilka^{144a}, R. Zimmermann²⁰, S. Zimmermann²⁰, S. Zimmermann⁴⁸, M. Ziolkowski¹⁴¹, R. Zitoun⁴, L. Živković³⁴, V.V. Zmouchko^{128,*}, G. Zobernig¹⁷², A. Zoccoli^{19a,19b}, Y. Zolnierowski⁴, A. Zsenei²⁹, M. zur Nedden¹⁵, V. Zutshi¹⁰⁶, L. Zwalinski²⁹.

¹ University at Albany, 1400 Washington Ave, Albany, NY 12222, United States of America

² University of Alberta, Department of Physics, Centre for Particle Physics, Edmonton, AB T6G 2G7, Canada

³ Ankara University^(a), Faculty of Sciences, Department of Physics, TR 061000 Tandoğan, Ankara; Dumlupınar University^(b), Faculty of Arts and Sciences, Department of Physics, Kutahya; Gazi University^(c), Faculty of Arts and Sciences, Department of Physics, 06500, Teknikokullar, Ankara; TOBB University of Economics and Technology^(d), Faculty of Arts and Sciences, Division of Physics, 06560, Sogutozu, Ankara; Turkish Atomic Energy Authority^(e), 06530, Lodumlu, Ankara, Turkey

⁴ LAPP, Université de Savoie, CNRS/IN2P3, Annecy-le-Vieux, France

⁵ Argonne National Laboratory, High Energy Physics Division, 9700 S. Cass Avenue, Argonne IL 60439, United States of America

⁶ University of Arizona, Department of Physics, Tucson, AZ 85721, United States of America

⁷ The University of Texas at Arlington, Department of Physics, Box 19059, Arlington, TX 76019, United States of America

⁸ University of Athens, Nuclear & Particle Physics, Department of Physics, Panepistimioupoli, Zografou, GR 15771 Athens, Greece

⁹ National Technical University of Athens, Physics Department, 9-Iroon Polytechniou, GR 15780 Zografou, Greece

¹⁰ Institute of Physics, Azerbaijan Academy of Sciences, H. Javid Avenue 33, AZ 143 Baku, Azerbaijan

¹¹ Institut de Física d'Altes Energies, IFAE, Edifici Cn, Universitat Autònoma de Barcelona, ES - 08193 Bellaterra

(Barcelona), Spain

¹² University of Belgrade^(a), Institute of Physics, P.O. Box 57, 11001 Belgrade; Vinca Institute of Nuclear Sciences^(b) M. Petrovica Alasa 12-14, 11000 Belgrade, Serbia, Serbia

¹³ University of Bergen, Department for Physics and Technology, Allegaten 55, NO - 5007 Bergen, Norway

¹⁴ Lawrence Berkeley National Laboratory and University of California, Physics Division, MS50B-6227, 1 Cyclotron Road, Berkeley, CA 94720, United States of America

¹⁵ Humboldt University, Institute of Physics, Berlin, Newtonstr. 15, D-12489 Berlin, Germany

¹⁶ University of Bern, Albert Einstein Center for Fundamental Physics, Laboratory for High Energy Physics, Sidlerstrasse 5, CH - 3012 Bern, Switzerland

¹⁷ University of Birmingham, School of Physics and Astronomy, Edgbaston, Birmingham B15 2TT, United Kingdom

¹⁸ Bogazici University^(a), Faculty of Sciences, Department of Physics, TR - 80815 Bebek-Istanbul; Dogus

University^(b), Faculty of Arts and Sciences, Department of Physics, 34722, Kadikoy, Istanbul; ^(c)Gaziantep University, Faculty of Engineering, Department of Physics Engineering, 27310, Sehitkamil, Gaziantep, Turkey; Istanbul Technical University^(d), Faculty of Arts and Sciences, Department of Physics, 34469, Maslak, Istanbul, Turkey

¹⁹ INFN Sezione di Bologna^(a); Università di Bologna, Dipartimento di Fisica^(b), viale C. Berti Pichat, 6/2, IT - 40127 Bologna, Italy

²⁰ University of Bonn, Physikalisches Institut, Nussallee 12, D - 53115 Bonn, Germany

²¹ Boston University, Department of Physics, 590 Commonwealth Avenue, Boston, MA 02215, United States of America

²² Brandeis University, Department of Physics, MS057, 415 South Street, Waltham, MA 02454, United States of America

²³ Universidade Federal do Rio De Janeiro, COPPE/EE/IF^(a), Caixa Postal 68528, Ilha do Fundao, BR - 21945-970 Rio de Janeiro; ^(b)Universidade de Sao Paulo, Instituto de Fisica, R.do Matao Trav. R.187, Sao Paulo - SP, 05508 - 900, Brazil

²⁴ Brookhaven National Laboratory, Physics Department, Bldg. 510A, Upton, NY 11973, United States of America

²⁵ National Institute of Physics and Nuclear Engineering^(a)Bucharest-Magurele, Str. Atomistilor 407, P.O. Box MG-6, R-077125, Romania; University Politehnica Bucharest^(b), Rectorat - AN 001, 313 Splaiul Independentei, sector 6, 060042 Bucuresti; West University^(c) in Timisoara, Bd. Vasile Parvan 4, Timisoara, Romania

²⁶ Universidad de Buenos Aires, FCEyN, Dto. Fisica, Pab I - C. Universitaria, 1428 Buenos Aires, Argentina

²⁷ University of Cambridge, Cavendish Laboratory, J J Thomson Avenue, Cambridge CB3 0HE, United Kingdom

²⁸ Carleton University, Department of Physics, 1125 Colonel By Drive, Ottawa ON K1S 5B6, Canada

²⁹ CERN, CH - 1211 Geneva 23, Switzerland

³⁰ University of Chicago, Enrico Fermi Institute, 5640 S. Ellis Avenue, Chicago, IL 60637, United States of America

³¹ Pontificia Universidad Católica de Chile, Facultad de Fisica, Departamento de Fisica^(a), Avda. Vicuna Mackenna 4860, San Joaquin, Santiago; Universidad Técnica Federico Santa María, Departamento de Física^(b), Avda. España 1680, Casilla 110-V, Valparaíso, Chile

³² Institute of High Energy Physics, Chinese Academy of Sciences^(a), P.O. Box 918, 19 Yuquan Road, Shijing Shan District, CN - Beijing 100049; University of Science & Technology of China (USTC), Department of Modern Physics^(b), Hefei, CN - Anhui 230026; Nanjing University, Department of Physics^(c), Nanjing, CN - Jiangsu 210093; Shandong University, High Energy Physics Group^(d), Jinan, CN - Shandong 250100, China

³³ Laboratoire de Physique Corpusculaire, Clermont Université, Université Blaise Pascal, CNRS/IN2P3, FR - 63177 Aubiere Cedex, France

³⁴ Columbia University, Nevis Laboratory, 136 So. Broadway, Irvington, NY 10533, United States of America

³⁵ University of Copenhagen, Niels Bohr Institute, Blegdamsvej 17, DK - 2100 Kobenhavn 0, Denmark

³⁶ INFN Gruppo Collegato di Cosenza^(a); Università della Calabria, Dipartimento di Fisica^(b), IT-87036 Arcavacata di Rende, Italy

³⁷ Faculty of Physics and Applied Computer Science of the AGH-University of Science and Technology, (FPACS, AGH-UST), al. Mickiewicza 30, PL-30059 Cracow, Poland

³⁸ The Henryk Niewodniczanski Institute of Nuclear Physics, Polish Academy of Sciences, ul. Radzikowskiego 152, PL - 31342 Krakow, Poland

³⁹ Southern Methodist University, Physics Department, 106 Fondren Science Building, Dallas, TX 75275-0175, United States of America

⁴⁰ University of Texas at Dallas, 800 West Campbell Road, Richardson, TX 75080-3021, United States of America

⁴¹ DESY, Notkestr. 85, D-22603 Hamburg and Platanenallee 6, D-15738 Zeuthen, Germany

⁴² TU Dortmund, Experimentelle Physik IV, DE - 44221 Dortmund, Germany

⁴³ Technical University Dresden, Institut für Kern- und Teilchenphysik, Zellescher Weg 19, D-01069 Dresden, Germany

- ⁴⁴ Duke University, Department of Physics, Durham, NC 27708, United States of America
⁴⁵ University of Edinburgh, School of Physics & Astronomy, James Clerk Maxwell Building, The Kings Buildings, Mayfield Road, Edinburgh EH9 3JZ, United Kingdom
⁴⁶ Fachhochschule Wiener Neustadt; Johannes Gutenbergstrasse 3 AT - 2700 Wiener Neustadt, Austria
⁴⁷ INFN Laboratori Nazionali di Frascati, via Enrico Fermi 40, IT-00044 Frascati, Italy
⁴⁸ Albert-Ludwigs-Universität, Fakultät für Mathematik und Physik, Hermann-Herder Str. 3, D - 79104 Freiburg i.Br., Germany
⁴⁹ Université de Genève, Section de Physique, 24 rue Ernest Ansermet, CH - 1211 Geneve 4, Switzerland
⁵⁰ INFN Sezione di Genova^(a); Università di Genova, Dipartimento di Fisica^(b), via Dodecaneso 33, IT - 16146 Genova, Italy
⁵¹ Institute of Physics of the Georgian Academy of Sciences, 6 Tamarashvili St., GE - 380077 Tbilisi; Tbilisi State University, HEP Institute, University St. 9, GE - 380086 Tbilisi, Georgia
⁵² Justus-Liebig-Universität Giessen, II Physikalisches Institut, Heinrich-Buff Ring 16, D-35392 Giessen, Germany
⁵³ University of Glasgow, Department of Physics and Astronomy, Glasgow G12 8QQ, United Kingdom
⁵⁴ Georg-August-Universität, II. Physikalisches Institut, Friedrich-Hund Platz 1, D-37077 Göttingen, Germany
⁵⁵ LPSC, CNRS/IN2P3 and Univ. Joseph Fourier Grenoble, 53 avenue des Martyrs, FR-38026 Grenoble Cedex, France
⁵⁶ Hampton University, Department of Physics, Hampton, VA 23668, United States of America
⁵⁷ Harvard University, Laboratory for Particle Physics and Cosmology, 18 Hammond Street, Cambridge, MA 02138, United States of America
⁵⁸ Ruprecht-Karls-Universität Heidelberg: Kirchhoff-Institut für Physik^(a), Im Neuenheimer Feld 227, D-69120 Heidelberg; Physikalisches Institut^(b), Philosophenweg 12, D-69120 Heidelberg; ZITI Ruprecht-Karls-University Heidelberg^(c), Lehrstuhl für Informatik V, B6, 23-29, DE - 68131 Mannheim, Germany
⁵⁹ Hiroshima University, Faculty of Science, 1-3-1 Kagamiyama, Higashihiroshima-shi, JP - Hiroshima 739-8526, Japan
⁶⁰ Hiroshima Institute of Technology, Faculty of Applied Information Science, 2-1-1 Miyake Saeki-ku, Hiroshima-shi, JP - Hiroshima 731-5193, Japan
⁶¹ Indiana University, Department of Physics, Swain Hall West 117, Bloomington, IN 47405-7105, United States of America
⁶² Institut für Astro- und Teilchenphysik, Technikerstrasse 25, A - 6020 Innsbruck, Austria
⁶³ University of Iowa, 203 Van Allen Hall, Iowa City, IA 52242-1479, United States of America
⁶⁴ Iowa State University, Department of Physics and Astronomy, Ames High Energy Physics Group, Ames, IA 50011-3160, United States of America
⁶⁵ Joint Institute for Nuclear Research, JINR Dubna, RU-141980 Moscow Region, Russia, Russia
⁶⁶ KEK, High Energy Accelerator Research Organization, 1-1 Oho, Tsukuba-shi, Ibaraki-ken 305-0801, Japan
⁶⁷ Kobe University, Graduate School of Science, 1-1 Rokkodai-cho, Nada-ku, JP Kobe 657-8501, Japan
⁶⁸ Kyoto University, Faculty of Science, Oiwake-cho, Kitashirakawa, Sakyou-ku, Kyoto-shi, JP - Kyoto 606-8502, Japan
⁶⁹ Kyoto University of Education, 1 Fukakusa, Fujimori, fushimi-ku, Kyoto-shi, JP - Kyoto 612-8522, Japan
⁷⁰ Universidad Nacional de La Plata, FCE, Departamento de Física, IFLP (CONICET-UNLP), C.C. 67, 1900 La Plata, Argentina
⁷¹ Lancaster University, Physics Department, Lancaster LA1 4YB, United Kingdom
⁷² INFN Sezione di Lecce^(a); Università del Salento, Dipartimento di Fisica^(b) Via Arnesano IT - 73100 Lecce, Italy
⁷³ University of Liverpool, Oliver Lodge Laboratory, P.O. Box 147, Oxford Street, Liverpool L69 3BX, United Kingdom
⁷⁴ Jožef Stefan Institute and University of Ljubljana, Department of Physics, SI-1000 Ljubljana, Slovenia
⁷⁵ Queen Mary University of London, Department of Physics, Mile End Road, London E1 4NS, United Kingdom
⁷⁶ Royal Holloway, University of London, Department of Physics, Egham Hill, Egham, Surrey TW20 0EX, United Kingdom
⁷⁷ University College London, Department of Physics and Astronomy, Gower Street, London WC1E 6BT, United Kingdom
⁷⁸ Laboratoire de Physique Nucléaire et de Hautes Energies, Université Pierre et Marie Curie (Paris 6), Université Denis Diderot (Paris-7), CNRS/IN2P3, Tour 33, 4 place Jussieu, FR - 75252 Paris Cedex 05, France
⁷⁹ Fysiska institutionen, Lunds universitet, Box 118, SE - 221 00 Lund, Sweden
⁸⁰ Universidad Autonoma de Madrid, Facultad de Ciencias, Departamento de Fisica Teorica, ES - 28049 Madrid, Spain
⁸¹ Universität Mainz, Institut für Physik, Staudinger Weg 7, DE - 55099 Mainz, Germany
⁸² University of Manchester, School of Physics and Astronomy, Manchester M13 9PL, United Kingdom

- ⁸³ CPPM, Aix-Marseille Université, CNRS/IN2P3, Marseille, France
⁸⁴ University of Massachusetts, Department of Physics, 710 North Pleasant Street, Amherst, MA 01003, United States of America
⁸⁵ McGill University, High Energy Physics Group, 3600 University Street, Montreal, Quebec H3A 2T8, Canada
⁸⁶ University of Melbourne, School of Physics, AU - Parkville, Victoria 3010, Australia
⁸⁷ The University of Michigan, Department of Physics, 2477 Randall Laboratory, 500 East University, Ann Arbor, MI 48109-1120, United States of America
⁸⁸ Michigan State University, Department of Physics and Astronomy, High Energy Physics Group, East Lansing, MI 48824-2320, United States of America
⁸⁹ INFN Sezione di Milano^(a); Università di Milano, Dipartimento di Fisica^(b), via Celoria 16, IT - 20133 Milano, Italy
⁹⁰ B.I. Stepanov Institute of Physics, National Academy of Sciences of Belarus, Independence Avenue 68, Minsk 220072, Republic of Belarus
⁹¹ National Scientific & Educational Centre for Particle & High Energy Physics, NC PHEP BSU, M. Bogdanovich St. 153, Minsk 220040, Republic of Belarus
⁹² Massachusetts Institute of Technology, Department of Physics, Room 24-516, Cambridge, MA 02139, United States of America
⁹³ University of Montreal, Group of Particle Physics, C.P. 6128, Succursale Centre-Ville, Montreal, Quebec, H3C 3J7 , Canada
⁹⁴ P.N. Lebedev Institute of Physics, Academy of Sciences, Leninsky pr. 53, RU - 117 924 Moscow, Russia
⁹⁵ Institute for Theoretical and Experimental Physics (ITEP), B. Cheremushkinskaya ul. 25, RU 117 218 Moscow, Russia
⁹⁶ Moscow Engineering & Physics Institute (MEPhI), Kashirskoe Shosse 31, RU - 115409 Moscow, Russia
⁹⁷ Lomonosov Moscow State University Skobeltsyn Institute of Nuclear Physics (MSU SINP), 1(2), Leninskie gory, GSP-1, Moscow 119991 Russian Federation, Russia
⁹⁸ Ludwig-Maximilians-Universität München, Fakultät für Physik, Am Coulombwall 1, DE - 85748 Garching, Germany
⁹⁹ Max-Planck-Institut für Physik, (Werner-Heisenberg-Institut), Föhringer Ring 6, 80805 München, Germany
¹⁰⁰ Nagasaki Institute of Applied Science, 536 Aba-machi, JP Nagasaki 851-0193, Japan
¹⁰¹ Nagoya University, Graduate School of Science, Furo-Cho, Chikusa-ku, Nagoya, 464-8602, Japan
¹⁰² INFN Sezione di Napoli^(a); Università di Napoli, Dipartimento di Scienze Fisiche^(b), Complesso Universitario di Monte Sant'Angelo, via Cinthia, IT - 80126 Napoli, Italy
¹⁰³ University of New Mexico, Department of Physics and Astronomy, MSC07 4220, Albuquerque, NM 87131 USA, United States of America
¹⁰⁴ Radboud University Nijmegen/NIKHEF, Department of Experimental High Energy Physics, Heyendaalseweg 135, NL-6525 AJ, Nijmegen, Netherlands
¹⁰⁵ Nikhef National Institute for Subatomic Physics, and University of Amsterdam, Science Park 105, 1098 XG Amsterdam, Netherlands
¹⁰⁶ Department of Physics, Northern Illinois University, LaTourette Hall Normal Road, DeKalb, IL 60115, United States of America
¹⁰⁷ Budker Institute of Nuclear Physics (BINP), RU - Novosibirsk 630 090, Russia
¹⁰⁸ New York University, Department of Physics, 4 Washington Place, New York NY 10003, USA, United States of America
¹⁰⁹ Ohio State University, 191 West Woodruff Ave, Columbus, OH 43210-1117, United States of America
¹¹⁰ Okayama University, Faculty of Science, Tsushima-naka 3-1-1, Okayama 700-8530, Japan
¹¹¹ University of Oklahoma, Homer L. Dodge Department of Physics and Astronomy, 440 West Brooks, Room 100, Norman, OK 73019-0225, United States of America
¹¹² Oklahoma State University, Department of Physics, 145 Physical Sciences Building, Stillwater, OK 74078-3072, United States of America
¹¹³ Palacký University, 17.listopadu 50a, 772 07 Olomouc, Czech Republic
¹¹⁴ University of Oregon, Center for High Energy Physics, Eugene, OR 97403-1274, United States of America
¹¹⁵ LAL, Univ. Paris-Sud, IN2P3/CNRS, Orsay, France
¹¹⁶ Osaka University, Graduate School of Science, Machikaneyama-machi 1-1, Toyonaka, Osaka 560-0043, Japan
¹¹⁷ University of Oslo, Department of Physics, P.O. Box 1048, Blindern, NO - 0316 Oslo 3, Norway
¹¹⁸ Oxford University, Department of Physics, Denys Wilkinson Building, Keble Road, Oxford OX1 3RH, United Kingdom
¹¹⁹ INFN Sezione di Pavia^(a); Università di Pavia, Dipartimento di Fisica Nucleare e Teorica^(b), Via Bassi 6, IT-27100 Pavia, Italy

- ¹²⁰ University of Pennsylvania, Department of Physics, High Energy Physics Group, 209 S. 33rd Street, Philadelphia, PA 19104, United States of America
- ¹²¹ Petersburg Nuclear Physics Institute, RU - 188 300 Gatchina, Russia
- ¹²² INFN Sezione di Pisa^(a); Università di Pisa, Dipartimento di Fisica E. Fermi^(b), Largo B. Pontecorvo 3, IT - 56127 Pisa, Italy
- ¹²³ University of Pittsburgh, Department of Physics and Astronomy, 3941 O'Hara Street, Pittsburgh, PA 15260, United States of America
- ¹²⁴ Laboratorio de Instrumentacao e Fisica Experimental de Particulas - LIP^(a), Avenida Elias Garcia 14-1, PT - 1000-149 Lisboa, Portugal; Universidad de Granada, Departamento de Fisica Teorica y del Cosmos and CAFPE^(b), E-18071 Granada, Spain
- ¹²⁵ Institute of Physics, Academy of Sciences of the Czech Republic, Na Slovance 2, CZ - 18221 Praha 8, Czech Republic
- ¹²⁶ Charles University in Prague, Faculty of Mathematics and Physics, Institute of Particle and Nuclear Physics, V Holešovickach 2, CZ - 18000 Praha 8, Czech Republic
- ¹²⁷ Czech Technical University in Prague, Zikova 4, CZ - 166 35 Praha 6, Czech Republic
- ¹²⁸ State Research Center Institute for High Energy Physics, Moscow Region, 142281, Protvino, Pobeda street, 1, Russia
- ¹²⁹ Rutherford Appleton Laboratory, Science and Technology Facilities Council, Harwell Science and Innovation Campus, Didcot OX11 0QX, United Kingdom
- ¹³⁰ University of Regina, Physics Department, Canada
- ¹³¹ Ritsumeikan University, Noji Higashi 1 chome 1-1, JP - Kusatsu, Shiga 525-8577, Japan
- ¹³² INFN Sezione di Roma I^(a); Università La Sapienza, Dipartimento di Fisica^(b), Piazzale A. Moro 2, IT- 00185 Roma, Italy
- ¹³³ INFN Sezione di Roma Tor Vergata^(a); Università di Roma Tor Vergata, Dipartimento di Fisica^(b) , via della Ricerca Scientifica, IT-00133 Roma, Italy
- ¹³⁴ INFN Sezione di Roma Tre^(a); Università Roma Tre, Dipartimento di Fisica^(b), via della Vasca Navale 84, IT-00146 Roma, Italy
- ¹³⁵ Réseau Universitaire de Physique des Hautes Energies (RUPHE): Université Hassan II, Faculté des Sciences Ain Chock^(a), B.P. 5366, MA - Casablanca; Centre National de l'Energie des Sciences Techniques Nucleaires (CNESTEN)^(b), B.P. 1382 R.P. 10001 Rabat 10001; Université Mohamed Premier^(c), LPTPM, Faculté des Sciences, B.P.717. Bd. Mohamed VI, 60000, Oujda ; Université Mohammed V, Faculté des Sciences^(d)4 Avenue Ibn Battouta, BP 1014 RP, 10000 Rabat, Morocco
- ¹³⁶ CEA, DSM/IRFU, Centre d'Etudes de Saclay, FR - 91191 Gif-sur-Yvette, France
- ¹³⁷ University of California Santa Cruz, Santa Cruz Institute for Particle Physics (SCIPP), Santa Cruz, CA 95064, United States of America
- ¹³⁸ University of Washington, Seattle, Department of Physics, Box 351560, Seattle, WA 98195-1560, United States of America
- ¹³⁹ University of Sheffield, Department of Physics & Astronomy, Hounsfield Road, Sheffield S3 7RH, United Kingdom
- ¹⁴⁰ Shinshu University, Department of Physics, Faculty of Science, 3-1-1 Asahi, Matsumoto-shi, JP - Nagano 390-8621, Japan
- ¹⁴¹ Universität Siegen, Fachbereich Physik, D 57068 Siegen, Germany
- ¹⁴² Simon Fraser University, Department of Physics, 8888 University Drive, CA - Burnaby, BC V5A 1S6, Canada
- ¹⁴³ SLAC National Accelerator Laboratory, Stanford, California 94309, United States of America
- ¹⁴⁴ Comenius University, Faculty of Mathematics, Physics & Informatics^(a), Mlynska dolina F2, SK - 84248 Bratislava; Institute of Experimental Physics of the Slovak Academy of Sciences, Dept. of Subnuclear Physics^(b), Watsonova 47, SK - 04353 Kosice, Slovak Republic
- ¹⁴⁵ (a)University of Johannesburg, Department of Physics, PO Box 524, Auckland Park, Johannesburg 2006;
(b)School of Physics, University of the Witwatersrand, Private Bag 3, Wits 2050, Johannesburg, South Africa, South Africa
- ¹⁴⁶ Stockholm University: Department of Physics^(a); The Oskar Klein Centre^(b), AlbaNova, SE - 106 91 Stockholm, Sweden
- ¹⁴⁷ Royal Institute of Technology (KTH), Physics Department, SE - 106 91 Stockholm, Sweden
- ¹⁴⁸ Stony Brook University, Department of Physics and Astronomy, Nicolls Road, Stony Brook, NY 11794-3800, United States of America
- ¹⁴⁹ University of Sussex, Department of Physics and Astronomy Pevenssey 2 Building, Falmer, Brighton BN1 9QH, United Kingdom
- ¹⁵⁰ University of Sydney, School of Physics, AU - Sydney NSW 2006, Australia

- ¹⁵¹ Institute of Physics, Academia Sinica, TW - Taipei 11529, Taiwan
¹⁵² Technion, Israel Inst. of Technology, Department of Physics, Technion City, IL - Haifa 32000, Israel
¹⁵³ Tel Aviv University, Raymond and Beverly Sackler School of Physics and Astronomy, Ramat Aviv, IL - Tel Aviv 69978, Israel
¹⁵⁴ Aristotle University of Thessaloniki, Faculty of Science, Department of Physics, Division of Nuclear & Particle Physics, University Campus, GR - 54124, Thessaloniki, Greece
¹⁵⁵ The University of Tokyo, International Center for Elementary Particle Physics and Department of Physics, 7-3-1 Hongo, Bunkyo-ku, JP - Tokyo 113-0033, Japan
¹⁵⁶ Tokyo Metropolitan University, Graduate School of Science and Technology, 1-1 Minami-Osawa, Hachioji, Tokyo 192-0397, Japan
¹⁵⁷ Tokyo Institute of Technology, Department of Physics, 2-12-1 O-Okayama, Meguro, Tokyo 152-8551, Japan
¹⁵⁸ University of Toronto, Department of Physics, 60 Saint George Street, Toronto M5S 1A7, Ontario, Canada
¹⁵⁹ TRIUMF^(a), 4004 Wesbrook Mall, Vancouver, B.C. V6T 2A3; ^(b)York University, Department of Physics and Astronomy, 4700 Keele St., Toronto, Ontario, M3J 1P3, Canada
¹⁶⁰ University of Tsukuba, Institute of Pure and Applied Sciences, 1-1-1 Tennoudai, Tsukuba-shi, JP - Ibaraki 305-8571, Japan
¹⁶¹ Tufts University, Science & Technology Center, 4 Colby Street, Medford, MA 02155, United States of America
¹⁶² Universidad Antonio Narino, Centro de Investigaciones, Cra 3 Este No.47A-15, Bogota, Colombia
¹⁶³ University of California, Irvine, Department of Physics & Astronomy, CA 92697-4575, United States of America
¹⁶⁴ INFN Gruppo Collegato di Udine^(a); ICTP^(b), Strada Costiera 11, IT-34014, Trieste; Università di Udine, Dipartimento di Fisica^(c), via delle Scienze 208, IT - 33100 Udine, Italy
¹⁶⁵ University of Illinois, Department of Physics, 1110 West Green Street, Urbana, Illinois 61801, United States of America
¹⁶⁶ University of Uppsala, Department of Physics and Astronomy, P.O. Box 516, SE -751 20 Uppsala, Sweden
¹⁶⁷ Instituto de Física Corpuscular (IFIC) Centro Mixto UVEG-CSIC, Apdo. 22085 ES-46071 Valencia, Dept. Física At. Mol. y Nuclear; Dept. Ing. Electrónica; Univ. of Valencia, and Inst. de Microelectrónica de Barcelona (IMB-CNM-CSIC) 08193 Bellaterra, Spain
¹⁶⁸ University of British Columbia, Department of Physics, 6224 Agricultural Road, CA - Vancouver, B.C. V6T 1Z1, Canada
¹⁶⁹ University of Victoria, Department of Physics and Astronomy, P.O. Box 3055, Victoria B.C., V8W 3P6, Canada
¹⁷⁰ Waseda University, WISE, 3-4-1 Okubo, Shinjuku-ku, Tokyo, 169-8555, Japan
¹⁷¹ The Weizmann Institute of Science, Department of Particle Physics, P.O. Box 26, IL - 76100 Rehovot, Israel
¹⁷² University of Wisconsin, Department of Physics, 1150 University Avenue, WI 53706 Madison, Wisconsin, United States of America
¹⁷³ Julius-Maximilians-University of Würzburg, Physikalisches Institute, Am Hubland, 97074 Würzburg, Germany
¹⁷⁴ Bergische Universität, Fachbereich C, Physik, Postfach 100127, Gauss-Strasse 20, D- 42097 Wuppertal, Germany
¹⁷⁵ Yale University, Department of Physics, PO Box 208121, New Haven CT, 06520-8121, United States of America
¹⁷⁶ Yerevan Physics Institute, Alikhanian Brothers Street 2, AM - 375036 Yerevan, Armenia
¹⁷⁷ Centre de Calcul CNRS/IN2P3, Domaine scientifique de la Doua, 27 bd du 11 Novembre 1918, 69622 Villeurbanne Cedex, France
^a Also at LIP, Portugal
^b Also at Faculdade de Ciencias, Universidade de Lisboa, Lisboa, Portugal
^c Also at CPPM, Marseille, France.
^d Also at TRIUMF, Vancouver, Canada
^e Also at FPACS, AGH-UST, Cracow, Poland
^f Also at Department of Physics, University of Coimbra, Coimbra, Portugal
^g Also at Università di Napoli Parthenope, Napoli, Italy
^h Also at Institute of Particle Physics (IPP), Canada
ⁱ Also at Louisiana Tech University, Ruston, USA
^j Also at Universidade de Lisboa, Lisboa, Portugal
^k At California State University, Fresno, USA
^l Also at Faculdade de Ciencias, Universidade de Lisboa and at Centro de Fisica Nuclear da Universidade de Lisboa, Lisboa, Portugal
^m Also at California Institute of Technology, Pasadena, USA
ⁿ Also at University of Montreal, Montreal, Canada
^o Also at Baku Institute of Physics, Baku, Azerbaijan
^p Also at Institut für Experimentalphysik, Universität Hamburg, Hamburg, Germany
^q Also at Manhattan College, New York, USA

- ^r Also at School of Physics and Engineering, Sun Yat-sen University, Guangzhou, China
^s Also at Taiwan Tier-1, ASGC, Academia Sinica, Taipei, Taiwan
^t Also at School of Physics, Shandong University, Jinan, China
^u Also at Rutherford Appleton Laboratory, Didcot, UK
^v Also at Departamento de Fisica, Universidade de Minho, Braga, Portugal
^w Also at Department of Physics and Astronomy, University of South Carolina, Columbia, USA
^x Also at KFKI Research Institute for Particle and Nuclear Physics, Budapest, Hungary
^y Also at Institute of Physics, Jagiellonian University, Cracow, Poland
^z Also at Centro de Fisica Nuclear da Universidade de Lisboa, Lisboa, Portugal
^{aa} Also at Department of Physics, Oxford University, Oxford, UK
^{ab} Also at CEA, Gif sur Yvette, France
^{ac} Also at LPNHE, Paris, France
^{ad} Also at Nanjing University, Nanjing Jiangsu, China
* Deceased